Threshold dependence of central amygdala CRF in fear behaviors

Christina Akiko Akers

A dissertation
submitted in partial fulfillment of the
requirements for the degree of

Doctor of Philosophy

University of Washington

2016

Reading Committee:
Larry S. Zweifel (Chair)
Charles Chavkin
Paul E. M. Phillips

Program Authorized to Offer Degree:
Pharmacology

University of Washington

Abstract

Threshold dependence of central amygdala CRF in fear behaviors

Christina Akiko Akers

Chair of the Supervisory Committee:
Larry S. Zweifel
Department of Pharmacology

The central nucleus of the amygdala (CeA) is critical for threat association and defensive behavior. Distinct populations of neurons in the CeA are known to express an array of neuropeptides, but the role of these different neurons and their cognate neuropeptides in the modulation of fear is only beginning to be discerned. The neuropeptide corticotropin-releasing factor (CRF) is robustly produced in the CeA, yet whether CRF neurons represent a subset of neurons that modulate threat association is unknown. In the present study, we used a combination of molecular, physiological, and behavioral strategies to determine how CRF neurons contribute to adaptive fear processes.

Using immunohistochemistry and gene expression analyses, we found that CRF neurons represent a population of neurons distinct from other previously characterized cell types. Electrophysiological experiments demonstrate CRF neurons, like other defined populations in the CeA, undergo synaptic plasticity in a fear-dependent manner. *In vivo* fiber optic imaging of calcium activity revealed stimulus-specific responses of CRF neurons following cued fear conditioning. We further showed, using a number of behavioral assays coupled with cell-selective silencing and conditional gene inactivation, that CRF neuronal activity is required for the acquisition of cued fear to sub-generalization threat levels and that the CRF peptide produced by the CeA is the principal mediator during this process.

CRF neurons in the CeA engage in complex local and long range circuitry, and may thus regulate different aspects of fear through distinct pathways. Determining the function of downstream neurons is critical for understanding how CRF-dependent fear learning is processed. We therefore generated a novel mouse line expressing Cre-recombinase under the endogenous promoter of the gene expressing the primary receptor for CRF, CRFR1 (*Crhr1*$^{IRES\text{-}Cre}$*).* This targeted knock-in mutation allows for cell-selective manipulation and labeling of neurons directly downstream of CRF neurons. We found that a significant portion of Sst neurons express Crhr1, likely representing the primary target of locally projecting CRF neurons.

The results describing CRF neuronal function in cued fear behaviors, together with the *Crhr1*$^{IRES\text{-}Cre}$ mouse line, have provided a detailed report of the intricate circuitry underlying specific fear behaviors. Furthermore, the work presented here highlights how complex emotional states can be regulated at multiple levels, with distinct biochemical signaling and anatomical arrangements.

Table of Contents

Title..... 1
Abstract..... 3
Table of Contents..... 5
List of Figures 6
Glossary..... 8

Chapter 1- Introduction..... 11
Adaptive Fear..... 11
Fear Circuitry..... 12
Neuromodulation..... 15

Chapter 2- Characterization of Corticotropin-Releasing Factor Neurons in the CeA..... 19
Results
Localization within the CeA..... 20
Enrichment with other previously identified genes..... 21
Projection patterns..... 23
Electrophysiological properties..... 24
Behaviorally-evoked response properties..... 28
Discussion..... 29

Chapter 3- Role of CeA CRF neurons in cognitive behaviors..... 32
Results
CRF neurons are required for discriminative fear learning..... 33
CRF from CeA_L neurons regulate conditioned threat responses at low US intensities..... 38
Discussion..... 42

Chapter 4- Generation and characterization of the *Crhr1*$^{IRES\text{-}Cre}$ mouse..... 45
Results
Targeting strategy 46
ESC screening, breeding and genotyping..... 47
Anatomical characterization..... 48
Discussion..... 49

Chapter 5- Conclusions and future directions..... 51

Experimental Methods..... 57

Supplemental..... 69

References..... 83

List of Figures

Chapter 1:

1. Pavlovian assessment of fear
2. Fear circuitry in the amygdala

Chapter 2:

3. Immunohistochemical analysis of CeA neuronal populations
4. Gene expression analysis of CRF-producing neurons in the CeA
5. Projection patterns of CeA cell types
6. Electrophysiological analysis of CRF neurons to fear-inducing stimuli
7. Electrophysiological responses following neuronal silencing
8. Response profiles of CRF neurons to fear-predicting stimuli
9. Activity response profiles of CRF neurons obtained *ex vivo* in response to LA stimulation

Chapter 3:

10. Discriminative delayed cued fear conditioning paradigm
11. Cell-selective silencing strategy
12. Average reactivity to increasing shock amplitudes during CRF neuronal silencing
13. Baseline anxiety measures during CRF neuronal silencing
14. Silencing of CRF neurons during cued fear conditioning
15. Silencing of CRF neurons during fear recall
16. Conditional *Crh* inactivation
17. Average reactivity to increasing shock amplitudes following *Crh inactivation*
18. Baseline anxiety measures during *Crh inactivation*
19. *Crh* inactivation during cued fear conditioning
20. Appetitive learning
21. Distribution of control and *Crh* inactivation (KO) mice displaying no fear, low or high fear to increasing threat intensities
22. Comparisons of Crh:CeA:TeTx and Crh:CeA:KO freezing levels

Chapter 4:

23. Targeting strategy of *IRES-CreGFP* to endogenous *Crhr1* locus.
24. Screening of ESC clones and genotyping
25. Immunohistochemical analysis of Crhr1 neurons in the CeA

Chapter 5:

26. Updated fear circuitry schematic
27. Gain control hypothesis with neuromodulators and fear circuitry

Glossary

Abbreviation:	Term:
CRF	Corticotropin-releasing factor
CeA	Central nucleus of the amygdala
CS+	Conditioned stimulus (paired)
CS-	Conditioned stimulus (unpaired)
US	Unconditioned stimulus (shock)
BLA	Basolateral amygdala
BMA	Basomedial amygdala
LA	Lateral amygdala
BNST	Bed nucleus of the stria terminalis
LC	Locus coeruleus
PBN	Parabrachial nucleus
ITCs	Intercalated cell clusters
LTP	Long-term potentiation
EPSC	Excitatory postsynaptic potential
Sst	Somatostatin
Nts	Neurotensin
PKCδ	Protein kinase C- delta isoform
Pdyn	Prodynorphin
Cnp	2',3'-Cyclic-nucleotide 3'-phosphodiesterase
DIO	Double-floxed inverted open reading frame
IRES	Internal ribosomal entry site
AAV	Adeno-associated viral vector

TeTx	Tetanus toxin light chain
GFP	Green fluorescent protein
YFP	Yellow fluorescent protein
hM4Di	human muscarinic receptor 4 – G_i- coupled
CNO	Clozapine-N-oxide
ΔF	Change in fluorescence
Rpl22	Ribosomal protein 22
HA	Hemagglutinin
IP	Immunoprecipitate
ESC	Embryonic stem cell
I	Current
pA	Picoamp
ms	Millisecond
μM	Micromolar
mM	Millimolar
mA	Milliamp
mg	Milligram
kg	Kilogram
bp	Base pairs
kb	kilobases

Acknowledgements

I would first like to thank Dr. Larry Zweifel for all of his guidance and mentorship throughout my graduate studies, and for giving me the opportunity to conduct such an exciting project. The countless hours, advice, expertise, and patience has allowed me to become a much more thoughtful, well-rounded and independent scientist. I will always be grateful for the enriching and motivating environment you have provided. I would like to thank my committee members, Drs. Paul Phillips, Charles Chavkin, Susan Ferguson, and Horacio de la Iglesia, for all of their time and support throughout this process. Your advice and guidance has been invaluable as I move forward with my career. I would also like to thank Dr. Richard Palmiter for training me in mouse transgenics and all of the advice during lab meetings over the years.

To my fellow lab members and classmates, thank you for the years of help and encouragement. I owe much of my successes to the amazing support system in the lab. A special acknowledgment goes to Dr. Marta Soden and Madison Baird, who have both made significant contributions to this project. I would also like to thank my former lab, specifically Drs. Paul Phillips and Jeremy Clark, for providing me with a great learning environment early on and continuing to support me as a graduate student.

To my parents and amazing family, thank you for so many years of encouragement. All of my successes would not have been realized without your endless support. Finally, I would like to thank my husband, Jeff Sanford, for being by my side throughout this entire process. You were there to share every moment of success (and disappointment) from the day I decided to apply, to when I had power through the GRE, to the night I celebrated passing my general exam. Thank you for going on this journey with me.

CHAPTER 1

INTRODUCTION

Emotions are defined as affective states triggered by both extrinsic and intrinsic stimuli. Different states are associated with a particular valence and intensity, or arousal level, with the goal to direct behaviors towards achieving more favorable outcomes. Fear is a basic emotional state associated with a variety of defensive responses to threats. Observable changes in behavioral, physiological, hormonal, and autonomic measures are well conserved across species, and can be evoked by innately fearful stimuli or stimuli that have acquired fearful properties through associative processes[1].

Adaptive Fear

While humans and many animals have innate sensitivities to specific threats, the ability to adapt, anticipate and learn during hazardous situations is critical for survival. Fear conditioning studies have provided useful information regarding how threats are processed at the molecular, cellular, and systems levels with Pavlovian fear conditioning serving as the most common procedure used to study adaptive fear. In this paradigm, a neutral stimulus (i.e.

conditioned stimulus or CS) is paired with an aversive outcome (unconditioned stimulus or US) and comes to acquire negative properties, such that future presentations of the CS alone are sufficient to drive defensive responding. Pavlovian fear conditioning is not only useful for investigating fear learning to contextual and discrete cues, but is also a valuable tool for evaluating short-term and long-term learning processes. Following the acquisition phase in which fear responding to the CS gradually increases, retrieval of fear memories can be measured during re-exposure to the CS alone hours to days after the final CS-US pairing.

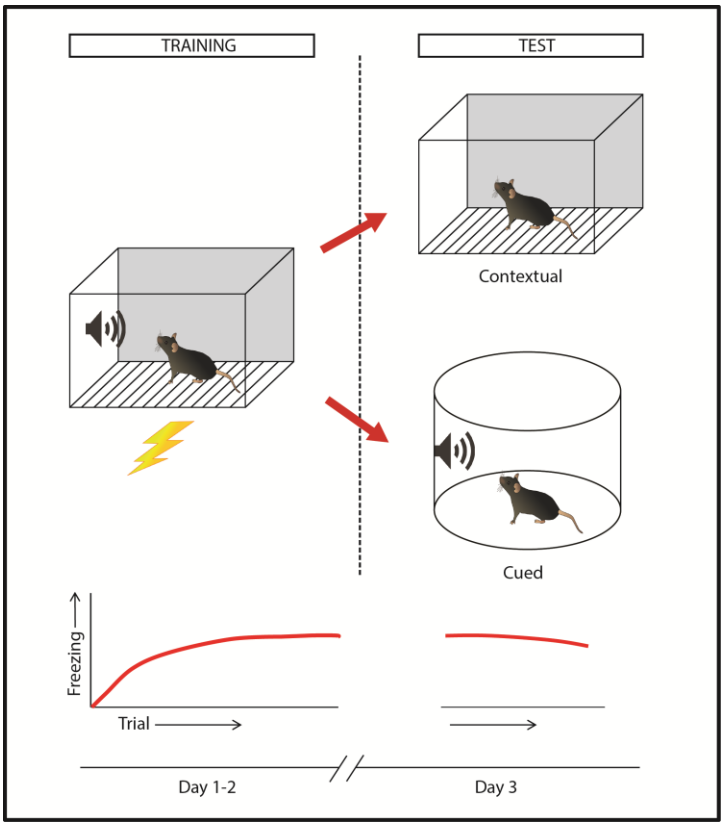

Figure 1. Pavlovian Assessment of Fear. During training (days 1-2) an animal is exposed to a neutral stimulus (conditioned stimulus or CS), such as a tone. The tone is paired with noxious stimulus (unconditioned stimulus or US), such as footshock, over multiple sessions. With repeated pairings, the neutral stimulus and context comes to acquire aversive properties, resulting in an increase in defensive behaviors (e.g. freezing). Animals are reintroduced to either the context or the neutral stimulus in the absence of the noxious stimulus during the test phase (day 3). Intact fear learning results in elevated defensive responding during the CS presentations alone.

Fear Circuitry

Numerous studies evaluating both contextual and cue-dependent fear memories have revealed a highly interconnected network of specialized cell types and brain regions important for mediating different aspects of fear[2,3]. Most of the focus has been directed towards the amygdala, a limbic structure regarded as a major integration point for sensory and affective

information[2,4-6]. Early lesioning studies in primates revealed substantial shifts in the expression of emotional behaviors, with observations of diminished aggression and defensive behaviors[7]. Decades of research thus ensued to determine the precise organization of fear-associated neural circuitry. Located in the temporal lobe, the amygdala consists of distinct nuclei with the basolateral complex (BLA) and central nucleus (CeA) representing the two main subregions.

The BLA is a cortical-like structure consisting primarily of glutamatergic projection neurons under complex regulatory control of distinct GABAergic interneuron populations[8,9]. It can be further separated into three main subdivisions including the lateral (LA), basal (BA), and basomedial (BMA) amygdala. The LA receives input of every sensory modality from a variety of extra-amygdalar brain regions, including the thalamus, sensory and association cortices, hippocampus, and brainstem nuclei, conveying information about conditioned and unconditioned stimuli[10]. Long-term potentiation (LTP) has been well characterized in the LA[5], and Hebbian plasticity mechanisms have been proposed to underlie the observed experience dependent modifications[11], supporting a critical role of the LA for the formation of stimulus-outcome associations. LA efferents project within the BLA to the BA, which also receives input from upstream cortical areas and the hippocampus, as well as outward to the intercalated cell masses (ITCs) and CeA[12].

The ITCs form a dense cluster of GABAergic cells residing between the BLA and CeA that regulate amygdala output[13,14]. The dorsal most cluster, known as the medial paracapsular ITCs (mpITCs), not only receives input from the LA, but also the thalamus and cortex[15]. Interestingly, the mpITCs make reciprocal connections with the BLA, in addition to targeting the CeA[15]. mpITCs also send inhibitory projections to the ventral cluster or main ITCs[16]. While the mpITCs are largely involved in fear expression, main ITCs are preferentially recruited during the extinction of fear and directly control output activity of the CeA to prevent defensive responding[17].

Downstream of the ITCs is the CeA. Once considered to be merely a passive relay station or fear behaviors, the CeA has recently emerged as a critical site for fear acquisition, consolidation, and expression[18]. Functionally and anatomically, the CeA can be separated into

two main subdivisions: lateral (CeA_L) and medial (CeA_M). The CeA_M is under direct inhibitory control of the CeA_L and serves as the main output of the CeA, sending efferents to distant structures such as the periaqueductal gray and brainstem[19]. The CeA_L, however, is far more complex as it is comprised of diverse cell types forming both local inhibitory networks[20,21] and long-range projections[22]. Like the BLA, the CeA_L also receives input from thalamic structures[23] and demonstrates synaptic strengthening in response to fear exposure[24]. In addition to their distinct connectivity and activity patterns, the CeA_L and CeA_M also display unique operational properties with the former implicated in fear acquisition and the latter in expression[20].

Electrophysiological recordings in the CeA_L during presentations of threat-associated stimuli have revealed two primary response profiles of "fear-on" and "fear-off" neurons[21]. Fear-inducing stimuli activate "fear-on" neurons while concomitantly inhibiting "fear-off" neurons. Genetic and functional analyses of cells within the CeA_L indicate that a proportion of "fear-on" neurons are somatostatin (Sst) positive[24], whereas "fear-off" neurons express the delta type of a calcium activated protein kinase (PKCδ)[21]. Sst neurons receive direct innervation from thalamic nuclei[23] and exhibit excitatory postsynaptic potentials in response to LA stimulation[24]. As PKCδ and Sst do not overlap, and PKCδ negative cells within the CeA inhibit PKCδ positive neurons[21], it is inferred that a significant portion of PKCδ negative neurons are Sst. Together with anatomical tracing studies, these prior results indicate PKCδ neurons project to the CeA_M and maintain a tonic firing rate to suppress CeA_M driven fear expression under basal conditions. Optogenetic and chemogenetic manipulations further suggest fear- specific activation of Sst neurons inhibit PKCδ[24], thus relieving inhibition on the CeA_M to promote defensive responding.

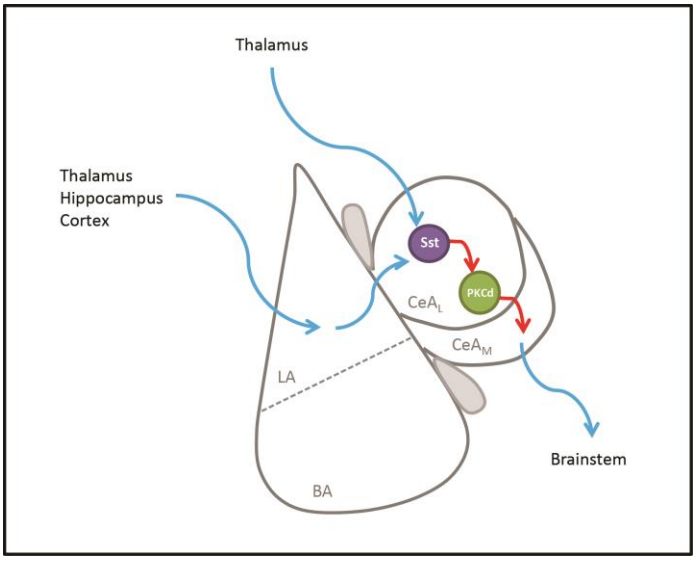

Figure 2. Fear circuitry in the amygdala. Sensory information from thalamic, hippocampal, and cortical brain regions converge at the levels of the lateral amygdala (LA) and lateral subdivision of the central nucleus (CeA$_L$). Thalamic and LA excitatory drive on Sst neurons in the CeA$_L$ inhibit PKCδ neurons that normally suppress CeA$_M$ output and fear expression. The disinhibition of the CeA$_M$ ultimately drive defensive responding during the presence of threatening stimuli.

In summary, the processing of fear-associated stimuli employs a composite of parallel and integrated circuits within the amygdala conveying sensory and affective information. This includes pathways utilizing a serial flow of information through the BLA to the CeA directly and via the ITCs, as well as those bypassing the BLA altogether and channeled through the CeA.

Neuromodulation of Fear

A variety of different signaling molecules and transmitter systems have been identified for their roles in specific aspects of fear processing. In addition to classical neurotransmitters (GABA and glutamate), the amygdala is rich in the expression of both neuropeptides and various peptide receptors[25]. Considering fear-associated behaviors include a broad repertoire of defensive responses, it is not unreasonable to suggest that select behaviors are mediated by discrete molecular mechanisms. Neuromodulatory systems, in particular, are becoming progressively more appreciated for their distinct contributions to fear processing. Additionally, because most neuromodulators act through G-protein coupled receptors, they are becoming increasingly more popular targets for pharmacotherapeutic intervention as they allow for finer control over neuronal activity. As such, neuropeptides may function as a gain control mechanism in the development and expression of fear behaviors through their actions in the CeA.

Several peptide systems within the CeA_L have been described, including cholecystokinin (CCK)[26], neuropeptide Y (NPY)[27], corticotropin-releasing factor (CRF)[28], and endogenous opioids such as dynorphin[29] and enkephalin[25]. While all of the cognate receptors for each of these neuropeptides are expressed in the CeA, distinct cell populations also express the peptide. CRF, dynorphin, endorphin, and enkephalin transcripts or protein have been reported in cell bodies, whereas only NPY and CCK fibers have been identified in the CeA. Each peptide also contributes to distinct aspects of fear, allowing for complex bidirectional control over a variety of defensive responses to threats[30,31].

Peptidergic modulation occurs at various levels, and thus provides multiple points of regulation within the amygdala fear circuit. Of note are the peptides specifically acting on the $CeA_L \rightarrow CeA_M$ pathway as they differentially impact unique responses. CCK administration, for example, promotes fear behaviors, and it is expressed by BLA GABAergic neurons that control excitatory drive onto CeA_L neurons. Direct infusions of CCK recapitulate the effects of stress induced anxiety, causing panic attacks in human subjects[32] and increasing fear in rodent models[33]. In support of those findings, single nucleotide polymorphisms in the CCK-B gene (the predominant receptor in the brain) have been linked clinically to panic disorders[34], and infusion of CCK-B antagonists have been reported to attenuate a variety of fear-associated behaviors[35]. In contrast, NPY is robustly produced by cells within the main ITCs that target CeA_M populations[36] and is largely associated with anxiolytic behavioral phenotypes[37]. This effect is thought to be primarily driven through coactivation of Y1 and Y2 receptors[38], both $G_{i/o}$-coupled, to inhibit CeA_M output and reduce fear expression.

Of all of the neuropeptides, CRF is the most studied and often associated with fear behaviors, particularly due to its robust expression within the CeA_L and broad implications in fear related disorders. CRF is 41-amino acid neuropeptide first characterized for its role in the activation of the hypothalamic-pituitary-adrenal axis[39]. As such, early studies attributed the function of CRF to a physiological stress response. Animal models with augmented CRF signaling exhibit behavioral phenotypes symptomatic of stress exposure[40,41]. This was further supported by clinical findings linking elevated CRF levels with mood and anxiety disorders[42], both

pathophysiologically sensitive to stressors. Moreover, single-nucleotide polymorphisms in the *Crhr1* gene, which encodes the primary receptor for CRF, have been identified in patients with anxious depression and panic disorders[43].

While hypothalamic CRF has been well documented for its role in stress reactivity, extrahypothalamic CRF has become increasingly more appreciated for its diverse effects on multiple behavioral modalities. Discrete brain regions outside of the hypothalamus that robustly produce CRF include the bed nucleus of the stria terminalis (BNST), parabrachial nucleus (PBN), and CeA[44]. Collectively, these brain regions regulate a broad spectrum of behaviors ranging from affective and motivational states to gustatory and pain processing. Thus, the actions of CRF are postulated to be largely dependent on the downstream circuitry and source structure. Cell-type specific knockouts of CRFR1[45] and site selective manipulation of *Crh* gene expression corroborate this hypothesis[40]. CRF acting within extended amygdala structures, such as the BNST and CeA, are particularly intriguing because of the complexity of CRF circuitry. With the CeA heavily implicated in adaptive fear, understanding the utility of CRF signaling in this area could provide valuable information regarding the intricate regulation of defensive behaviors.

Prior studies targeting CeA CRF have all suggested a critical role for CRF in fear processing, though they fail to agree on the specific aspect CeA CRF contributes to. Initial studies using pharmacological strategies to block CRF receptors throughout the CNS suggested that centrally acting CRF is necessary for cued fear learning as measured through a fear-potentiated startle assay[46]. Later studies using the same strategy, however, revealed CRF had no effect on cued fear, but rather selectively participates in the modulation of anxiety states. These findings were further supported by CRF knockdown manipulations in the CeA, where the authors were able to recapitulate the effects on stress-induced anxiety observed during pharmacological CRF receptor blockade. The key factor reconciling the differences observed between each of the studies regarding cued fear is the intensity of the fear-inducing stimulus used. In the first case that suggested a necessity for CRF in cued fear, a weak US was used, whereas a stronger US was used in the two later studies. This led to the hypothesis that CRF

from the CeA may be preferentially involved in facilitating fear learning under weak threat conditions and is unnecessary beyond a certain threshold.

CHAPTER 2

CHARACTERIZATION OF CORTICOTROPIN-RELEASING FACTOR NEURONS IN THE CEA

Introduction

The CeA is comprised of a heterogeneous population of neurons forming a complex local inhibitory network gating amygdala output and fear expression[4]. Recent studies have identified particular cell types within the CeA_L that are differentially involved in cued fear learning, including those with response profiles corresponding to putative "fear-on" and "fear-off" neurons[20]. Genetic analysis of these subpopulations revealed that many "fear-on" neurons are Sst-producing[24] and "fear-off" neurons express the delta isoform of protein kinase (PKCδ)[21]. Within this circuit, threatening stimuli activate "fear-on" GABAergic neurons, inhibiting "fear-off" neurons, leading to overall disinhibition of amygdala output to promote fear expression[21]. Beyond complex local connectivity, the CeA_L is also highly enriched in CRF as well as other neuropeptides such as dynorphin and neurotensin[25]. A thorough characterization of neurons producing these neuropeptides, however, has not been completed and whether these neurons represent multiple populations, or distribute across previously identified Sst and PKCδ neurons, is not known. Because CRF has been broadly implicated in fear behaviors and the CeA serves as one of the primary sources of centrally acting CRF, it is of particular interest to determine the organization of CRF circuitry within the amygdala. The following experiments provide

comprehensive view of CRF CeA neurons, describing their localization within the amygdala, overlap with other neuronal populations, projection patterns, and response profiles to aversive stimuli.

Localization within the CeA

To determine whether CRF-producing neurons represent a composite of previously identified cell types within the CeA_L, or form a distinct cell group, we performed immunostaining for PKCδ, Sst, and neurotensin (Nts) in tissue sections obtained from a *Crh* reporter mouse line ($Crh^{IRES\text{-}Cre}$;$Ai14^{TdTomato}$). Qualitative analyis of PKCδ immunoreactivity, which robustly labeled cell bodies, and TdTomato across the rostral-caudal axis revealed very little overlap between PKCδ and CRF neuronal populations. Similarly, Nts and Sst immunoreactivity, which largely labeled nerve terminals, did not significantly overlap with the distribution of CRF neurons, nor did they overlap with TdTomato-positive fibers. Results from all three immunostaining experiments revealed that CRF neurons are predominantly localized

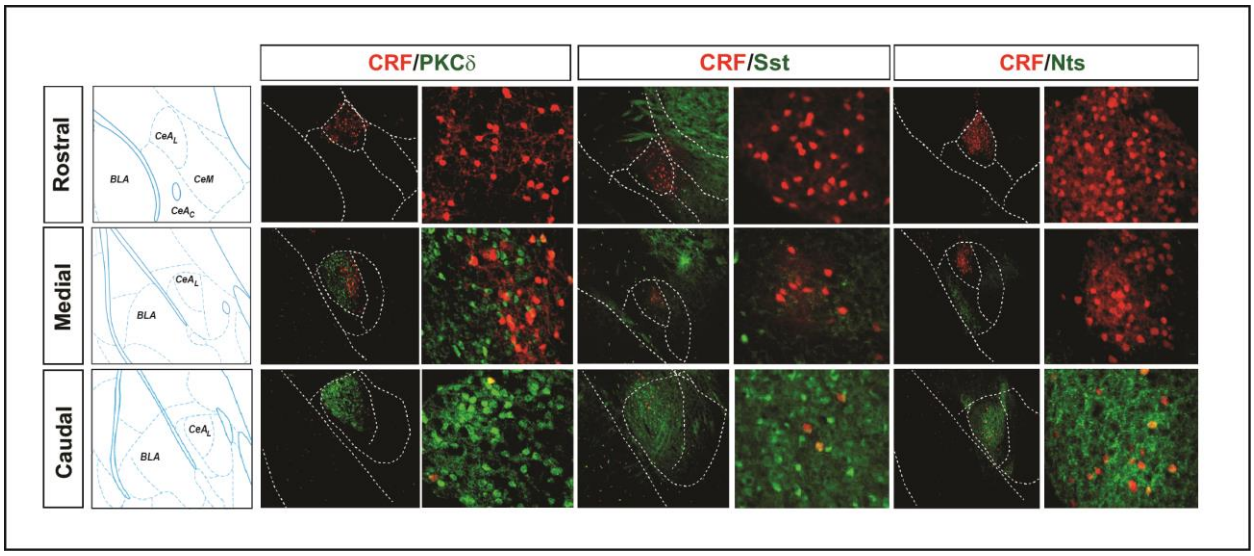

Figure 3. Immunohistochemical analysis of CeA neuronal populations. Rostral (top), medial (middle), and caudal (bottom) sections obtained from CRF reporter mouse $Crh^{IRES\text{-}Cre}$;$Ai14^{TdTomato}$ stained for PKCδ (left), Sst (middle), and Nts (right). Immunostaining reveals minimal colocalization of CRF with other cell types. Dense CRF expression is largely restricted to the rostral portion of the CeA, while other cell markers are predominantly located in the caudal CeA.

to the rostral regions of the CeA_L, diminishing significantly within the caudal most aspect. PKCδ, Sst, and Nts localized prominently within the caudal aspect of the CeA_L with a small number of CRF neurons showing partial overlap with these markers (Figure 3).

Enrichment with other previously identified genes

The immunostaining results suggest CRF neurons represent a neuronal population independent of other notable cell types. To confirm the findings of our immunohistochemistry analysis, as well as screen for the enrichment of other previously identified genetic markers, we utilized the RiboTag[47] strategy to selectively isolate actively translated mRNA from genetically defined CRF neurons (Figure 4). This approach allows for the identification of genetic markers with enriched expression within specific cell populations. Selective expression of the HA-tagged ribosomal protein L22 (Rpl22-HA) in CRF neurons was achieved by injecting an adeno-associated viral vector (AAV1) encoding a Cre-dependent Rpl22-HA to the CeA_L of mice expressing Cre-recombinase from the endogenous *Crh* locus that encodes CRF ($Crh^{IRES\text{-}Cre}$, Figure 4a). HA-tagged polyribosomes were immunoprecipitated (IP) from homogenates of tissue punches collected from injected mice (Figure 4b). RNA isolated from the IP fraction was screened for enrichment relative to the total mRNA (input) for specific genes via qPCR (Figure 4c). The genes included those encoding CRF (*Crh*), somatostatin (*Sst*), PKCδ (*Prkcd*), as well as other neuropeptides known to be expressed in the CeA_L such as neurotensin (*Nts*) and dynorphin (*Pdyn*). Analysis of the IP versus the input mRNA revealed a significant enrichment of *Crh* message relative to all other markers. Enrichment of other markers was not significantly different than the negative control oligodendrocyte marker *Cnp*. Collectively, these results indicate that CRF neurons are largely distinct from other known populations in the CeA_L.

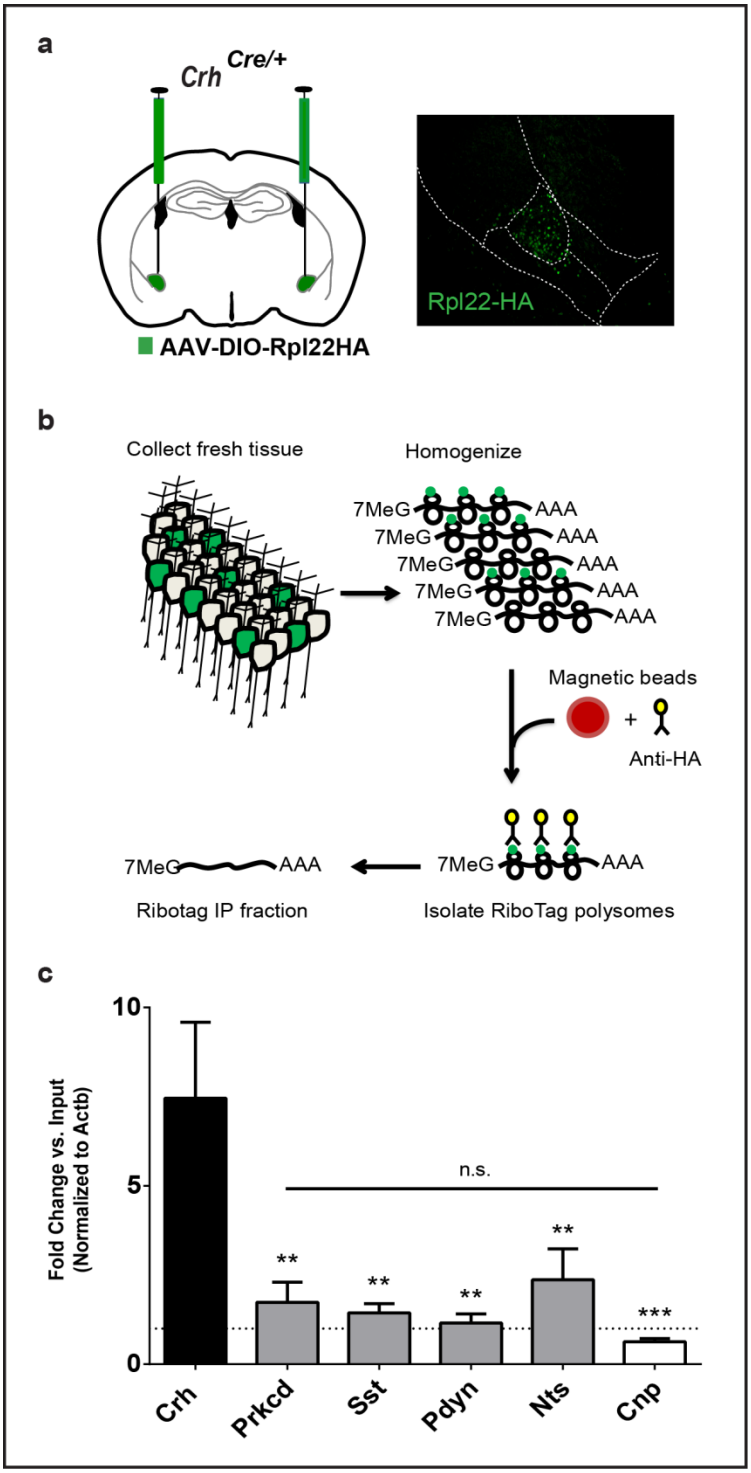

Figure 4. Gene expression analysis of CRF producing neurons in the CeA. a) Viral targeting strategy of HA-tagged Rpl22 in CRF neurons of the CeA used to isolate RNA in a cell-selective manner. b) RNA extraction procedure following RiboTag expression using magnetic bead immunoprecipitation of HA-tagged polysomes from fresh brain tissue homogenates. c) qPCR results obtained from RiboTag-expressing mice demonstrating significant enrichment for *Crh*, but no other CeA genetic marker relative to the de-enrichment gene *Cnp.* Enrichment values reflect the difference in IP versus input quantities, normalized to β-actin. Values are mean +/- SEM. Statistics: One-way ANOVA with post-hoc multiple comparisons relative to *Crh* and *Cnp. **P<0.01, ***P<0.001*

Projection patterns of CeA cell types

Individual populations of neurons are often distinguished and characterized based on gene expression. Neurons sharing the same genetic marker, however, may differ greatly in function. Alternatively, neurons with vastly different genetic profiles may share functional similarities. Another way to compare discrete subpopulations of neurons is to examine the connectivity patterns as different cell types projecting to the same areas may regulate the same phenotypic processes. Using the mouse connectivity data provided by the Allen Institute for Brain Science[48], relative connection strengths between specific CeA cell types and downstream target structures were quantified using the total pixel density in a target region and dividing it by the pixel density in the source region. The resulting values reflect the proportion of neurons from a given source region projecting to a particular target, normalizing for the volume of the target region (Figure 5a).

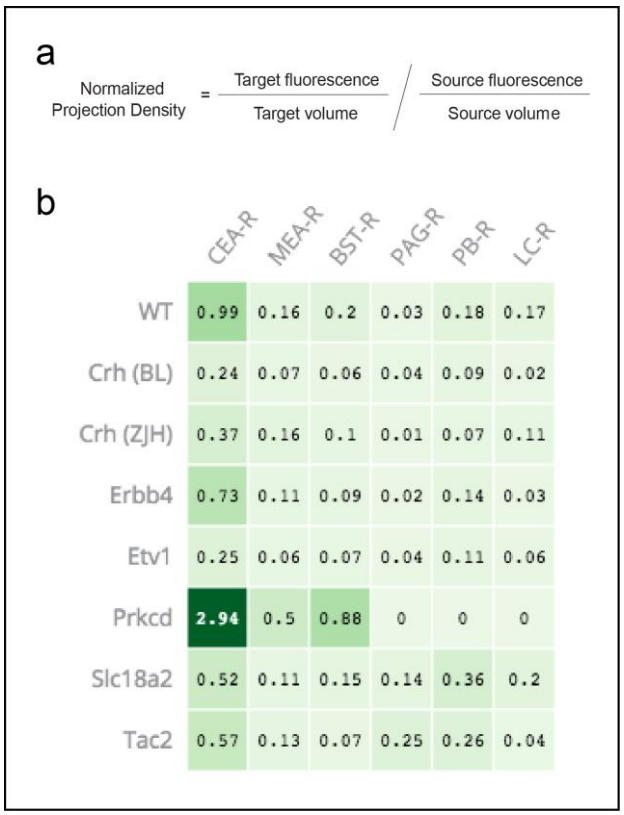

Figure 5. Projection patterns of CeA cell types. a) Calculation used to determine relative connective strengths. b) Weight matrix representing the different cell types (rows) and target structure (columns).

The connectivity analysis between the different cell types revealed that CRF neurons project mostly locally with some diffuse long range projections (Figure 5b). PKCδ neurons, however, project almost entirely locally within the CeA with some sparse innervation of the bed nucleus of the stria terminalis. Together with the immunostaining and gene expression analyses, these results support a hypothesis that CRF neurons are distinct from, but may work coordinately with, previously identified neurons (e.g. PKCδ) to regulate specific biological processes such as fear learning.

Synaptic plasticity in CRF neurons

Synapses are specialized structures that facilitate communication between neurons. The ability to change communicative strength between neurons, otherwise referred to as synaptic plasticity, is a dynamic process enabling broad adaptations to varying stimuli and is often viewed as a physiological correlate of learning and memory[49,50]. Long-term potentiation (LTP) and depression (LTD) are the two most widely studied forms synaptic plasticity, and their induction relies on a number of molecular mechanisms at both the pre- and postsynaptic levels. Additionally, different mechanisms are typically involved depending on the time point. For example, early LTP (e.g. within minutes) is thought to rely largely on the movement of existing proteins, such as trafficking of receptors to the plasma membrane in a calcium-dependent manner[51]. Late LTP, however, involves the synthesis of new proteins and upregulation of specific gene expression[52]. As a result of these biomolecular changes, cellular excitability is altered, such that subsequent stimuli produce an augmented response profile. Circuits all throughout the brain demonstrate synaptic plasticity, and this phenomenon represents a fundamental neural process driving behavioral adaptation.

Neuronal cell types within the CeA_L, such as those producing Sst, have been shown to undergo plasticity following fear conditioning that contributes to conditioned threat learning[24]. To determine whether CRF neurons also undergo synaptic plasticity at excitatory synapses, we measured the ratio of AMPAR/NMDAR[53] currents following conditioning in a differential delayed cued fear conditioning paradigm. Quantifying the change in AMPAR-mediated currents

relative NMDAR-mediated currents is a reliable procedure to gauge synaptic strengthening across samples as it normalizes for variances due to electrode distance and number of synapses activated[54]. To allow for visual identification of CRF neurons in an *ex vivo* slice preparation, we utilized *Crh*$^{IRES\text{-}Cre}$;*Ai14*^{TdTomato} reporter mice as described previously (Figure 6a). Following habituation, mice were conditioned for two consecutive days to a predictive conditioned stimulus (ten presentations of a 10-second auditory cue, CS+) that co-terminated with a 0.5-second, 0.3mA unconditioned foot shock stimulus (US). CS+ presentations were interleaved with ten presentations of a distinct auditory cue (CS-) not paired with the US. Approximately 24 hours after the last conditioning session, we isolated AMPA and NMDA receptor-mediated excitatory postsynaptic currents (EPSCs) in CeA$_L$ CRF neurons evoked by stimulation of the LA in acute brain slices (Figure 6b). Shock conditioned mice showed a significantly increased ratio of AMPA/NMDA EPSCs relative to control mice that received cue presentations but no shock

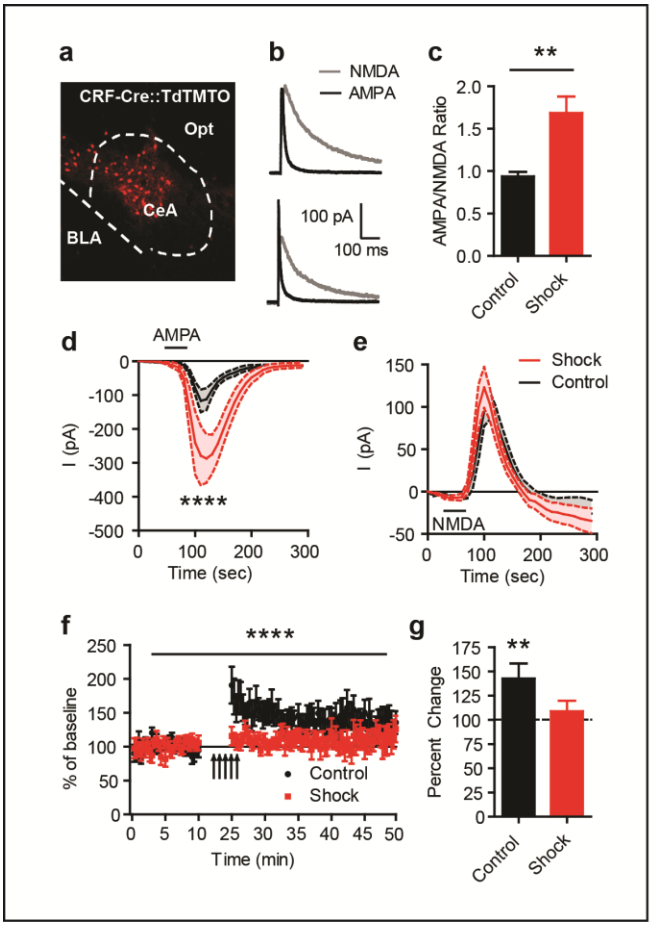

Figure 6. Electrophysiological analysis of CRF neurons to fear-inducing stimuli. a) Representative image of CeA section obtained from CRF reporter mouse used to visualize CRF neurons. b) Representative AMPA and NMDA traces from control (top) and fear conditioned (bottom) mice with shock mice. c) Quantification of the AMPA/NMDA ratios demonstrate CRF neurons from shock conditioned mice exhibit LTP. Statistics: unpaired t-test with Welch's correction, ***P<0.01.* d) Average EPSC recorded during AMPA bath application reveal a significant enhancement of postsynaptic current following fear conditioning, while e) no alterations in NMDAR-mediated current were observed. Statistics: two-way ANOVA, *****P<0.0001* time x genotype interaction. f) High frequency stimulation protocols induce LTP in control samples, but fail to do so in shock treated groups. Statistics: two-way ANOVA, *****P<0.0001* time x genotype interaction. g) Quantification of the percent change over baseline demonstrates that only control mice exhibit significant LTP induction. Statistics: one-way ANOVA relative to 100%, ***P<0.01.* All values are represented as mean +/- SEM.

(Figure 6c).

To confirm that the observed increase in AMPA/NMDA ratio is due to a selective enhancement of AMPAR-mediated currents, and not a decrease in the NMDAR-mediated current, we quantified currents evoked by bath application of either AMPA (1mM) or NMDA (10mM). AMPA-evoked currents were significantly enhanced in shocked mice relative to controls, while NMDA-evoked currents remained equivalent (Figures 6d and 6e). To further establish that fear conditioning evokes plasticity in CRF neurons, we quantified long term potentiation (LTP) induction in fluorescently identified neurons from shocked and non-shocked control mice. Under basal conditions, neurons will exhibit LTP in response to high frequency or tetanus stimulation (100 Hz for 1 second, repeated 5 times at 3 minute intervals). If a neuron has already been maximally potentiated, LTP induction will be occluded such that high frequency stimulation fails to further enhance the evoked EPSC[55]. Control mice that received only cue presentations displayed robust LTP in CRF neurons of the CeA_L following high frequency stimulation of the LA. The same stimulation pattern failed to induce LTP in shock conditioned mice, consistent with the occlusion of LTP induction by previous experience

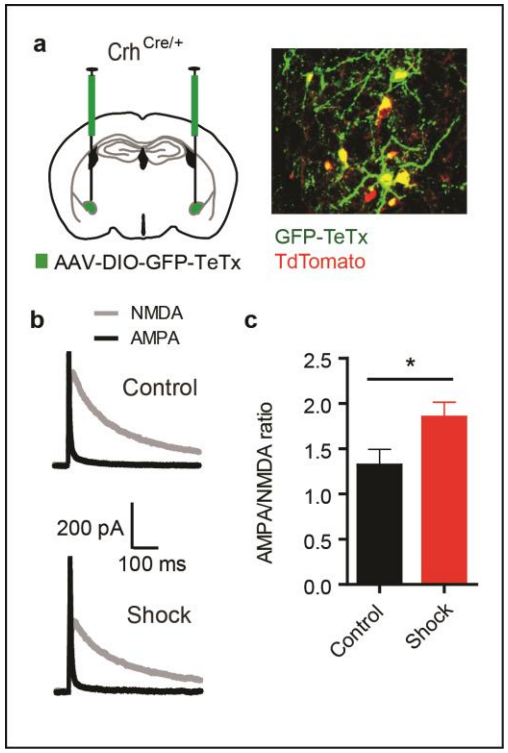

Figure 7. Electrophysiological responses during neuronal silencing. a) Viral targeting schematic for selective expression of GFP-TeTx in CeA CRF neurons. b) Representative AMPA and NMDA current traces under control (top) and shock (bottom) conditions. c) Quantitative analysis of AMPA/NMDA ratios under control and shock conditions. Values are mean +/- SEM. Statistics: unpaired t-test with Welch's correction, **P<0.05.*

dependent synaptic strengthening (Figure 6f and 6g).

It has been previously demonstrated that CRF within the CeA can enhance plasticity at excitatory synapses in the CeA through activation of the CRFR1 receptor[56]; suggesting a potential role for CRFR1 autoreceptors in the modulation of plasticity in these neurons. To test whether neurotransmitter release from CRF neurons is required for the plasticity we observed following fear conditioning, we conditionally expressed the light chain of tetanus toxin (TeTx) that has previously been demonstrated to prevent synaptic transmission[57]. A GFP-TeTx fusion protein was delivered to the CeAL of *Crh*$^{IRES\text{-}Cre}$*;Ai14*^{TdTomato} reporter mice by site-specific injection of an AAV (AAV1-DIO-GFP-TeTx; Figure 7a). Analysis of AMPA/NMDA receptor ratios in Crh:CeA:TeTx mice demonstrates that CRF neurons still undergo plasticity following fear conditioning (Figure 7b and 7c), indicating that transmitter release from these neurons is not likely to act in an autocrine fashion to modulate synaptic strength in this context.

Behaviorally-evoked response properties

Plasticity in CRF CeA_L neurons suggests that these cells may differentially respond to conditioned versus non-conditioned stimuli. Because "fear-on" neurons are preferentially activated by fearful stimuli and exhibit fear-dependent synaptic plasticity, it is possible that CRF neurons represent another "fear-on" population. In order to determine if CRF neurons are activated by distinct stimuli, we directly monitored calcium dynamics *in vivo.* With calcium serving as a ubiquitous second messenger and reliable metric for neuronal activation, calcium indicators or sensors have been a popular tool for measuring cellular activation. This strategy was first established by bulk loading synthetic indicators or dyes into neurons[58,59]. Despite relatively high spatial and temporal resolution, these early experiments presented significant limitations as targeting to intact brain tissue and specific cell types was particularly challenging and often restricted to cortical structures[60,61]. To circumvent these issues, genetically-encoded calcium indicators (GECIs) were developed[62]. GECIs consist of a circular permuted green fluorescent protein conjugated to a calmodulin (calcium binding) domain. Under calcium-deficient conditions, fluorescence is low. When the cell is activated, however, and cytosolic

calcium levels increase, the binding of calcium to the calmodulin domain induces conformational changes in the chimeric protein. This results in enhanced fluorescence that scales with increasing calcium concentration, thus reflecting an increase in neuronal activity. A number of modifications have since been made to improve the temporal resolution[63], dynamic range[64], and spectral diversity[65]. Moreover, because these sensors are genetically encoded, they can be packaged into viral vectors for site-selective expression or utilized in targeted knock-in mouse lines. This also ensures robust labeling of genetically defined neurons in intact brain tissue.

Many brain regions, including the CeA, are comprised of functionally and molecularly distinct cell populations despite sharing very similar electrophysiological profiles. Distinguishing response characteristics between unique cell types *in vivo* can therefore be challenging using conventional recording strategies, often requiring pharmacological or optical *post hoc* manipulations[66]. Assessing calcium dynamics *in vivo* with GECIs, however, eliminates the need for additional validation measures to filter signals from other cell types as only the cells of interest express the fluorescent protein and can be imaged. Furthermore, fiber optic microscopy coupled with GECIs has enabled the detection of calcium dynamics in deep brain structures of awake-behaving rodents[67]. The light-weight, thin flexible probe connected to a separate laser scanning unit allows the animal free movement while also limiting tissue damage. Images acquired at a sampling rate of 12 frames per second additionally provide adequate temporal resolution to determine stimulus-specific response properties in a cued fear conditioning paradigm. Using this strategy to reveal the specific response properties of CRF neurons to individual stimuli would therefore be extremely useful for determining the role of these neurons as they relate to known CeA fear circuitry.

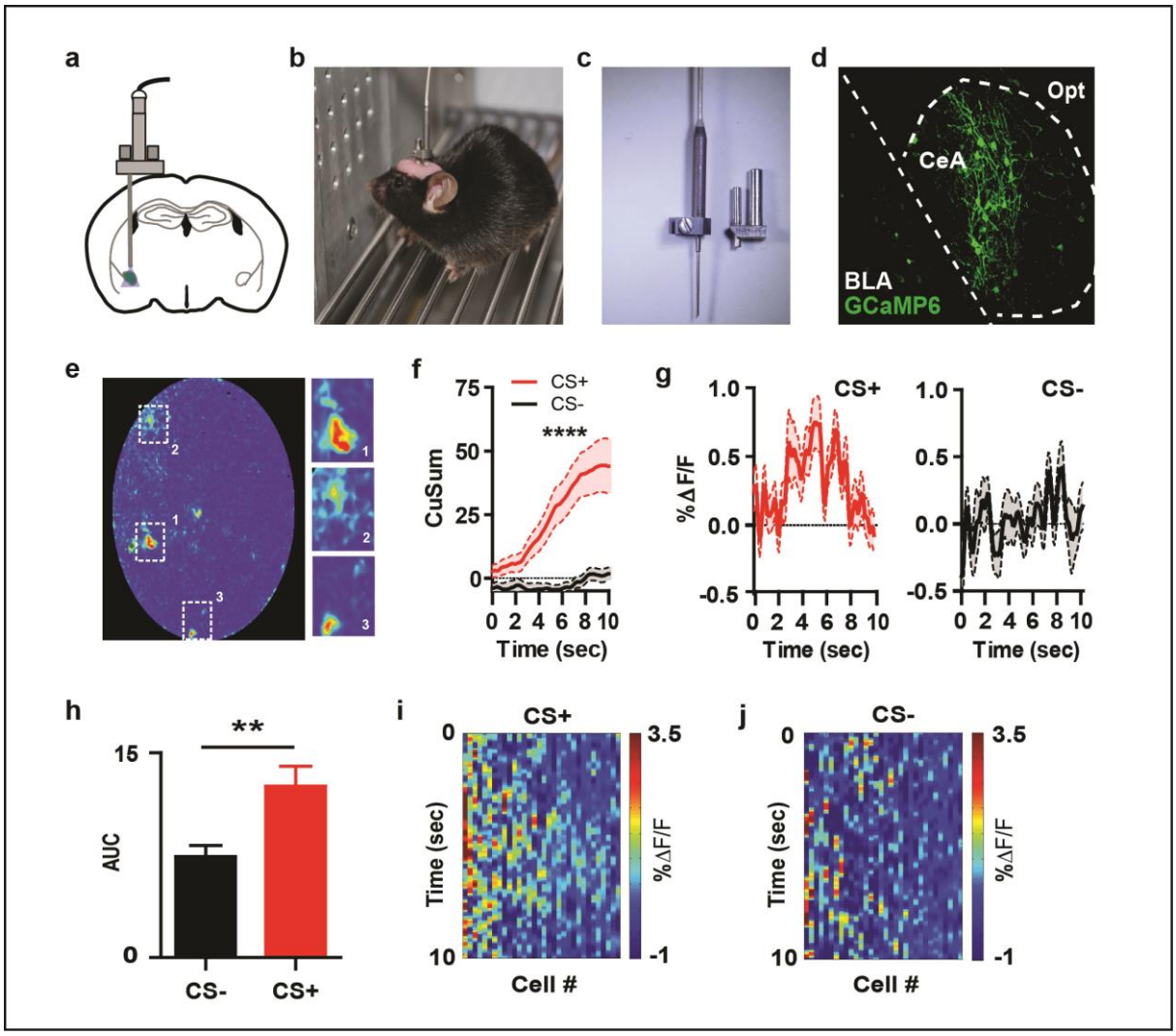

Figure 8. Response profiles of CRF neurons to fear-predictive stimuli. a) Fiber optic implant schematic. b) Image of a mouse with a chronically implanted guide cannula and anchored fiber optic probe (zoomed in image in c). d) Representative image of GCaMP6 expression in CRF neurons in the CeA. e) Pseudocolor display of imaging field obtained with the fiber optic. Individual ROIs or putative CRF neurons are circled and zoomed in on right panels. f) Cumulative summation of ΔF values over 10-second stimulus for the CS+ and CS- presentations. Statistics: two-way RM ANOVA, *****P<0.0001 time by stimulus interaction.* g) Average fluorescent traces to the CS+ (left) and CS- (right). h) Quantification of average area under the cuve (AUC) overall fluorescence reveals significantly stronger responses to the CS+ relative to the CS-. Statistics: paired t-test, ***P<0.01.* i) Individual cellular responses time aligned to stimulus onset for CS+ and j) CS-.

To establish how CRF CeA_L neurons respond to fear-predictive stimuli, we directly imaged calcium dynamics in the CeA_L using fiber-optic confocal microscopy[67,68] to detect the genetically encoded calcium indicator GCaMP6m[63] selectively expressed in CRF neurons. *Crh*$^{IRES\text{-}Cre}$ mice were injected with a conditional adeno-associated viral vector containing GCaMP6m

(AAV1-FLEX-GCaMP6) and implanted with a guide cannula targeting the CeA_L (Figure 8a-d). Two weeks following surgery, mice were fear conditioned for two days in a discriminative delayed cued fear conditioning paradigm as described above. On the third day, a fiber-optic objective was lowered into the CeA_L until fluorescence from CRF neurons was observed. Mice were returned to the conditioning chamber, and calcium-associated fluorescence signals were imaged during CS+ and CS- presentations. Putative CRF neurons were visually identified (Figure 8e) and analyzed for changes in fluorescence intensity during CS+ and CS- presentations (Figure 8f and 8g). Fluorescence signals were significantly increased in CRF neurons following CS+ deliveries relative to CS- (Figure 8h). Interestingly, we observed a delay in the onset of the calcium signal in CRF neurons in response to the CS+. To establish whether long latency calcium responses are a general feature of CRF neurons in the CeA_L, we monitored calcium dynamics of these neurons in an acute slice preparation following stimulation of the LA at stimulus frequencies consistent with firing rates previously reported for CeA_L neurons (Figure 9a-c). In accord with our *in vivo* observations, the rise in calcium signal was delayed in CRF neurons following electrical stimulation.

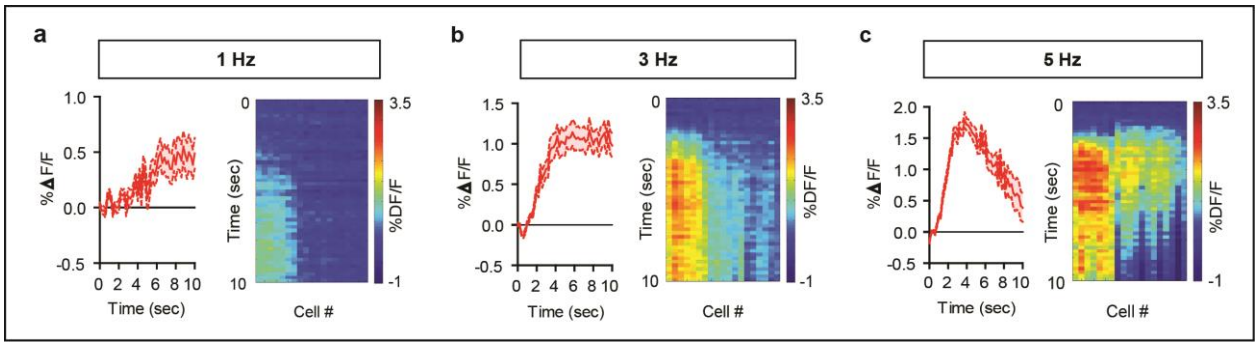

Figure 9. Activity response profiles of CRF neurons obtained *ex vivo* in response to LA stimulation. Average fluorescence trace to a) 1 Hz, b) 3 Hz, and c) 5 Hz stimulation for 10 seconds (left) and individual cellular response time aligned to stimulus onset (right).

Discussion

The findings from the immunostaining analyses suggest CRF neurons share very little, if any, overlap with the previously described Sst and PKCδ neurons. Together with the gene

expression data obtained from the Ribotag experiments and the connectivity analysis, CRF neurons also represent a population largely distinct from other proposed peptidergic cell types. We additionally find that like Sst neurons[24], CRF neurons also undergo synaptic plasticity following exposure to threatening stimuli as demonstrated by an increase in the AMPAR/NMDAR-mediated current ratios and LTP occlusion.

The synaptic strengthening of CRF neurons likely contributes to the selective responding observed *in vivo* during presentations of fear-associated stimuli. Calcium dynamics measured during a fear conditioning paradigm corresponded with calcium-dependent fluorescent traces obtained in acute slice preparations during LA stimulations. Importantly, the delay and overall magnitude of the *in vivo* imaging results aligns with those from the *ex vivo* experiments in which LA fibers were stimulated at frequencies consistent with previously reported activity profiles of CeA neurons[69]. Furthermore, the stimulation parameters used are sufficient to induce plasticity at theses synapses.

The apparent delay observed with the calcium imaging is also consistent with the firing properties of many CeA neurons in response to current injection. It has been estimated that a little over 50% of the cells in the lateral subdivision of the CeA_L display "late-firing" characteristics[70] whose activity prevails CeA_M neurons. In accordance with these early findings, the current model suggests "fear-on" neurons are first activated by excitatory input from the LA[21,24] and paraventricular nucleus of the thalamus[23], which then promotes CeA_M output through indirect, disinhibitory mechanisms[4,21]. "Fear-on" neurons also exhibit firing rates consistent with the frequencies used *ex vivo* to activate CRF neurons to the same degree that has been detected in awake-behaving mice[20]. Taken together, the findings from the current study suggest CRF neurons may comprise a novel population of "fear-on" neurons as they similar exhibit electrophysiological properties and fear-associated response profiles compared to other, non-overlapping "fear-on" neurons (i.e. Sst neurons).

**The results from this chapter will be published in the following manuscript: Sanford CA, Soden ME, Baird MA, Miller SM, Schulkin J, Clark MS, Zweifel LS. Threshold dependence of CRF in conditioned fear.*
CA performed all behavioral testing, gene expression analyses, immunohistochemistry, and calcium imaging experiments. CA and MS designed slice electrophysiology experiments and MS performed slice electrophysiology experiments. CA and SM designed and performed RiboTag experiments.

CHAPTER 3

ROLE OF CEA CRF NEURONS IN COGNITIVE BEHAVIORS

Introduction

With the CeA_L as one of the main sources of centrally acting CRF[71], and CRF levels within the CeA_L increasing in response to threats[72], CRF derived from the CeA_L has long been considered a critical component for the processing of aversive stimuli. Indeed, previous studies have shown that increasing the excitability of CRF neurons through homeostatic scaling mechanisms enhances cued fear behavior[73]. Additionally, overexpression of CRF within CeA_L potentiates defensive behavioral responses[74]. Although numerous studies point to an important role of CRF in the modulation of fear, studies evaluating the necessity of CRF signaling from the CeA_L have provided disparate results, with observations of either reduced

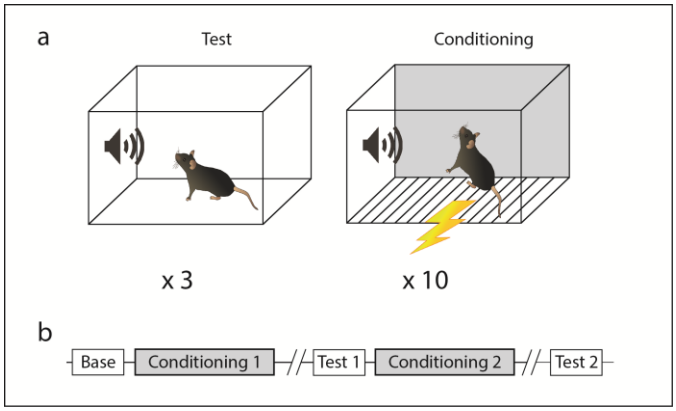

Figure 10. Discriminative delayed cued fear conditioning paradigm. a) Test context (left) and conditioning context (right). Test context consists of solid white walls and floor with acetic acid olfactory cues, and conditioning context consists of metal grid floor and metal walls. b) Behavioral timeline over three days: baseline and test sessions include 3 presentations of each cue alone, while conditioning sessions include 10 presentations of each cue with the CS+ co-terminating with a 0.3mA footshock.

conditioned threat responding[46,75] or a lack of effect of reducing CRF tone[40,76]. A major difference in these studies is the intensity of the US foot shock used to elicit conditioned fear responses. Low intensity US demonstrate a role for CRF, while high intensity stimuli show no effect. These results suggest CRF may function to modulate conditioned behavioral responses to weaker threats, but is unnecessary for the regulation of fear at higher threat levels. The following studies provide evidence that CRF neurons regulate the acquisition of conditioned fear at specific thresholds, while having no effect on chronic anxiety levels or appetitive learning processes.

CRF neurons are required for discriminative fear learning

The results demonstrating synaptic strengthening and activation by threat-associated stimuli suggests a role of CRF neurons in conditioned fear. A discriminative delayed cued fear conditioning paradigm using a 0.3 mA foot shock US was used to assess fear behaviors (Figure 10). Baseline responses to two distinct auditory stimuli were established by three interleaved presentations of the cues. Mice were then conditioned to ten CS+ presentations (10 sec auditory cue) co-terminating with the US and ten CS- presentations (distinct 10 sec auditory cue that did not co-terminate with a US). The following day mice were assessed for discriminative threat responding by monitoring freezing in response to three interleaved presentations of the CS+ or CS-. Mice were conditioned again for a second day with ten CS+/US pairings and CS- presentations, followed the next day by a second test with three interleaved presentations of each cue.

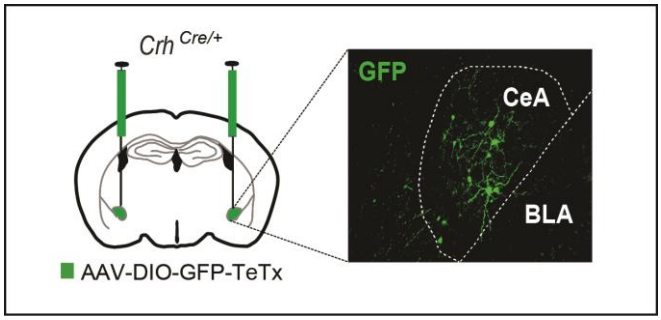

Figure 11. Cell-selective silencing strategy. Schematic of viral targeting of silencing allele consisting of the light chain of tetanus toxin (TeTx-GFP) fused to GFP (left). CeA expression of TeTx-GFP.

To test the necessity of CRF neuronal function during discriminative fear processing, we selectively silenced CRF neurons through conditional expression of GFP-TeTx[57] (AAV1-DIO-GFP-

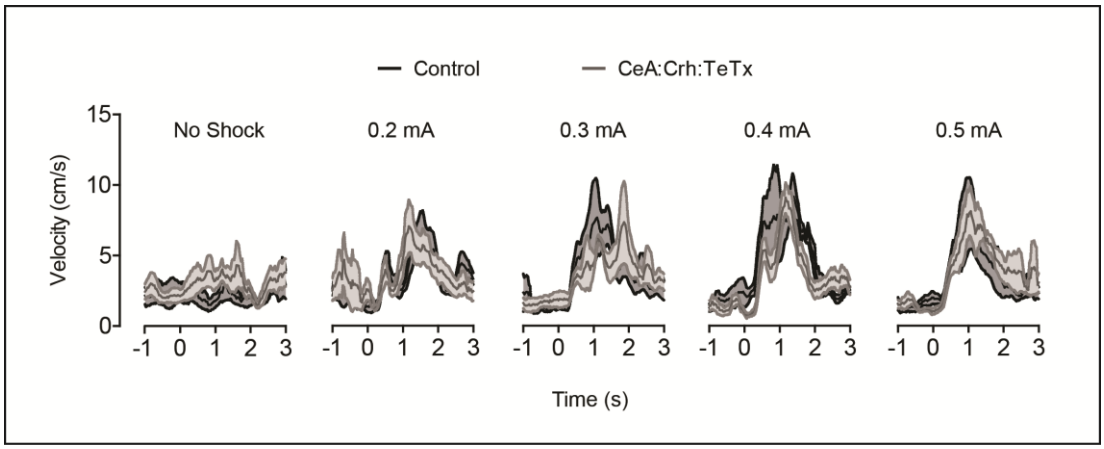

Figure 12. Average reactivity to increasing shock amplitudes during CRF neuronal silencing. Average velocities tracked during the onset of the shock at increasing intensities reveal no differences between treatment groups in unconditioned responding.

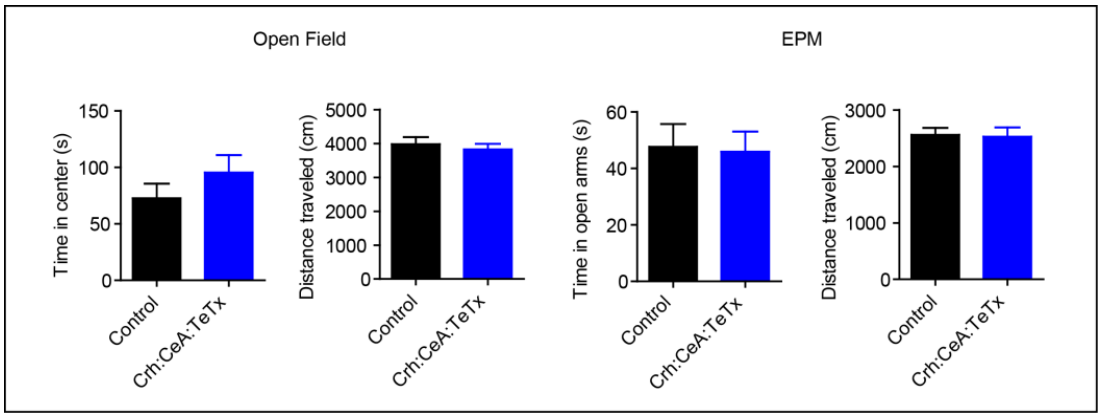

Figure 13. Baseline anxiety measures during CRF neuronal silencing. Anxiety measures in an open field assay (left two figures) and elevated plus maze (right two figures) reveal no significant differences between groups. Values are represented as mean +/- SEM.

TeTx, Figure 11) and AAV1-DIO-GFP was used as a control. Two weeks following surgery Crh:CeA:TeTx and control mice were assayed in both anxiety and cued fear conditioning paradigms. Because the CeA receives spinoparabrachial innervation and has been implicated in pain processing[77], we first assessed the shock reactivity for Crh:CeA:TeTx and control mice (Figure 12). No differences in responses to the US alone were detected between the two

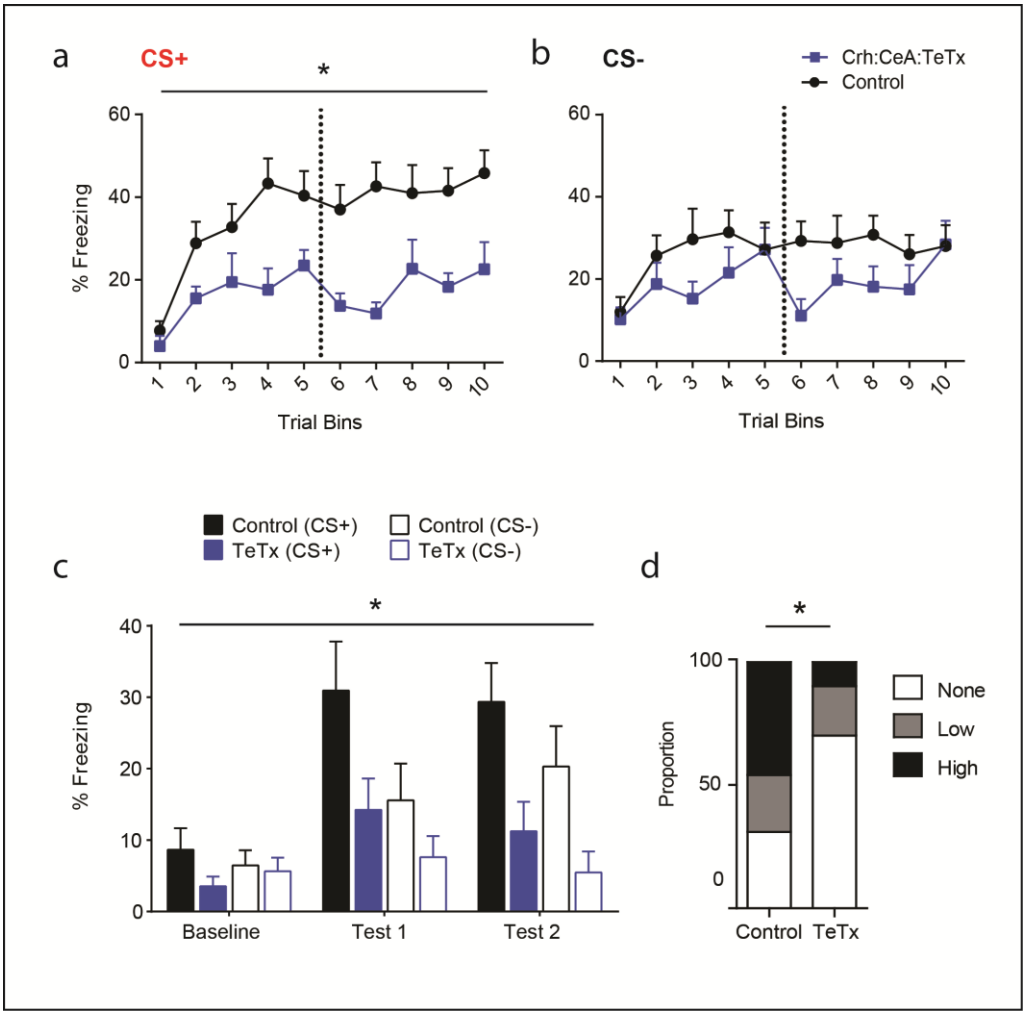

Figure 14. Silencing of CRF neurons during cued fear conditioning. a) Average percent freezing during CS+ presentations during conditioning demonstrates CRF neuronal silencing significantly impairs the acquisition of fear. Statistics: two-way RM ANOVA, *$P<0.05$ time x genotype interaction. b) Both groups show similar freezing levels to the unpaired (CS-) stimulus. c) Freezing levels are significantly reduced during recall test sessions in Crh:CeA:TeTx mice compared to GFP controls. Statistics: two-way RM ANOVA, *$P<0.05$ time x genotype interaction to the CS+. d) Proportion of mice displaying no, low or high fear. Statistics: chi-squared, *$P<0.05$.

groups, nor were any variances in baseline anxiety noted (Figure 13). Analysis of conditioned threat responses during acquisition, however, revealed that Crh:CeA:TeTx mice had significantly reduced freezing in response to CS+ presentations relative to control mice (Figure 14a), with no differences observed to the unpaired CS- (Figure 14b). Analogous to reduced freezing during acquisition, Crh:CeA:TeTx mice had reduced freezing in response to CS+ presentations relative to control mice during test days (Figure 14c). To establish whether reduced freezing behavior represents a general lack of fear, we quantified the distribution of mice that showed no fear

(<95th percentile of baseline freezing), low fear (1-2 times >95th percentile of baseline), and high fear (>2 times the 95th percentile of baseline). We observed a significant difference in the proportion of control versus Crh:CeA:TeTx mice showing high, low, or no fear (Figure 14d). Taken together, CRF neuronal silencing significantly impairs fear learning, leading to the lower probability of an animal exhibiting high fear.

Although silencing CRF neurons impairs the acquisition of conditioned fear and recall during test sessions, it is unclear whether low fear expression during test trials is a consequence of impaired acquisition. It has been previously demonstrated that inactivation of *Sst* expressing neurons in the CeA_L influences both acquisition and expression of threat memory[24], indicating

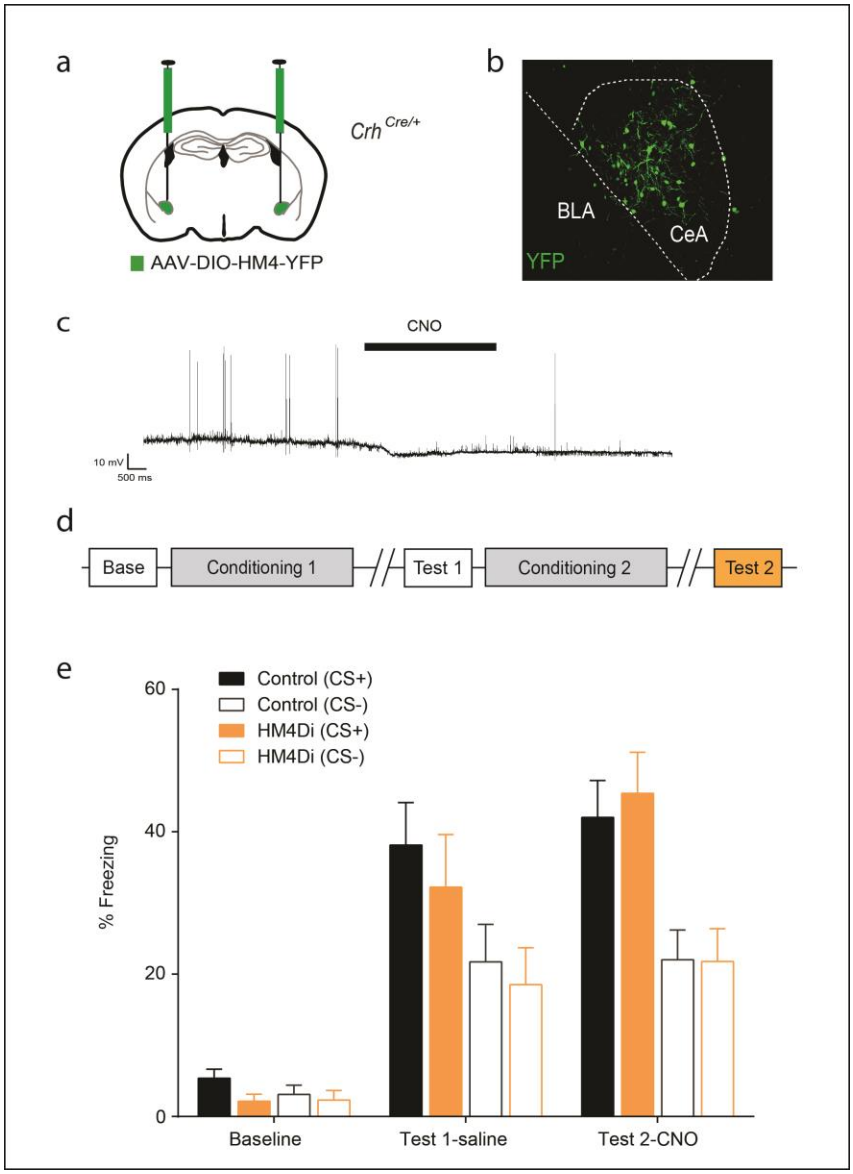

Figure 15. Silencing of CRF neurons during fear recall. a) Schematic of viral targeting of hM4Di to CRF neurons in the CeA. b) Image of hM4Di-YFP expression in CeA. c) Representative trace demonstrating hyperpolarizing state and reduced firing of a CRF neuron during CNO bath application in acute slice preparation. d) Modified behavioral strategy and timeline: saline is injected prior to baseline and first test sessions, while CNO is administered prior to the final test session on the third day. e) Freezing levels during baseline and test sessions reveal no effect of CRF neuronal silencing. Values are mean +/- SEM.

that neurons within the CeA_L can regulate both processes. To test whether CRF neurons in the CeA_L influence the expression of conditioned threat memory, we utilized the same strategy previously described for assessing the role of Sst neurons[24]. *Crh*$^{IRES\text{-}Cre}$ mice were injected with a Cre-conditional AAV containing the Designer Receptor Exclusively Activated by Designer Drug (DREADD) HM4Di fused to YFP (AAV1-DIO-HM4Di-YFP) into the CeA (Figure 15a-b). As reported for numerous other cell types[78], application of the HM4Di ligand clozapine-N-oxide (CNO, 5μM) to CRF neurons in slice hyperpolarized HM4Di-YFP expressing neurons and reduced excitability (Figure 15c). To assess the role of CRF neurons on threat memory expression, we conditioned mice as described above, except mice were injected with CNO prior to testing on the second test day (Figure 15d). CNO administration prior to testing did not affect fear expression after two days of conditioning as both control and HM4Di-expressing mice demonstrated significant freezing behavior (Figure 15e). Thus, unlike Sst neurons, CRF neurons do not appear to directly influence fear expression.

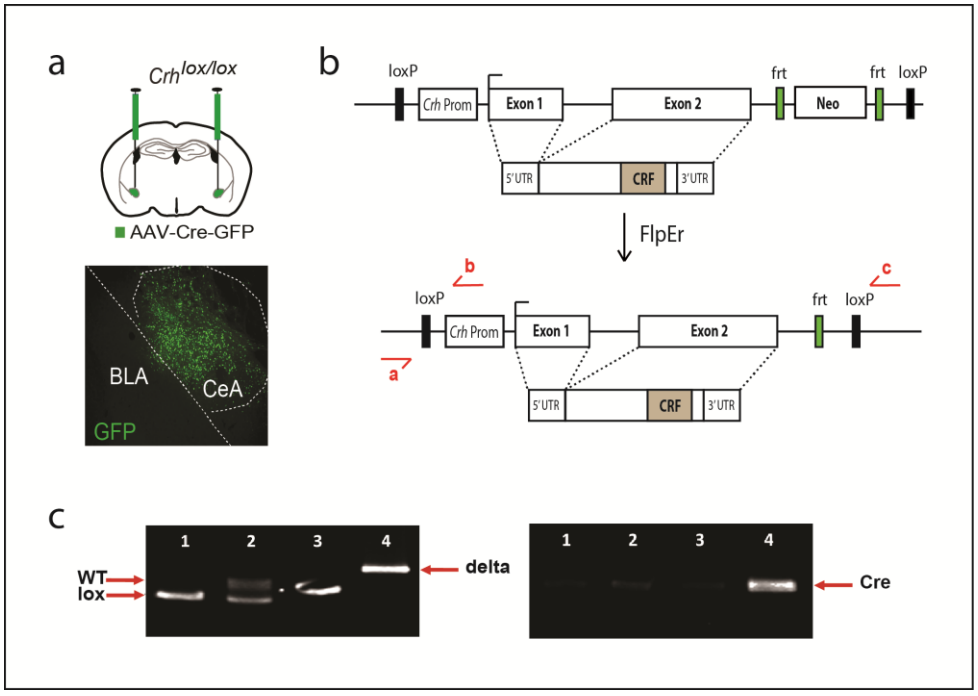

Figure 16. Conditional *Crh* inactivation. a) Viral targeting schematic of Cre-GFP delivery to the CeA of *Crh*$^{lox/lox}$ mice (top) and image of Cre-GFP expression in a coronal section of the CeA (bottom). b) Schematic of targeting construct containing *Crh* gene flanked by loxP sites followed by a frt-flanked neomycin resistance cassette. c) PCR screening strategy: primers a and b amplify 213 bp region in WT and 247 bp region with loxP sites; primers a and c amplify 320 bp region following recombination (delta). Numbered lanes contain amplicons from the following genomic DNA samples: 1. *Crh*$^{lox/lox}$, 2. *Crh*$^{lox/+}$, 3. wildtype, and 4. *Crh*$^{lox/lox}$; *Mox2-Cre.*

CRF in CeA_L neurons regulate conditioned threat responses at low US intensities

The results thus far demonstrate the necessity of CRF neurons for conditioned fear, but do not ascribe a specific role of CRF peptide function in the observed behaviors. Peptidergic neurons can express multiple different peptides[25], as well as classical neurotransmitters; thus, any phenotypical changes observed may not be due entirely to the inhibition of CRF release. To directly test the role of CRF released from cells in the CeA in conditioned fear, we genetically inactivated the gene encoding CRF, *Crh*, in the CeA_L (Crh:CeA KO) utilizing mice with a conditional floxed allele ($Crh^{lox/lox}$; Figure 16 b-c). *Crh* inactivation was anatomically restricted by site-specific injection of AAV1-CreGFP into the CeA of $Crh^{lox/lox}$ mice (Figure 16a). An AAV containing an expression cassette for a Cre-dead enzyme (AAV1-CreΔGFP) was used as a

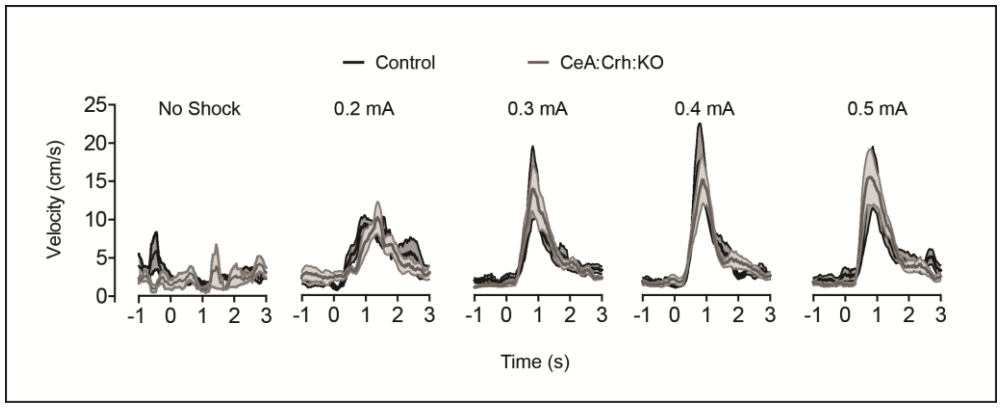

Figure 17. Average reactivity to increasing shock amplitudes following *Crh inactivation*. Average velocities tracked during the onset of the shock at increasing intensities reveal no differences between treatment groups in unconditioned responding.

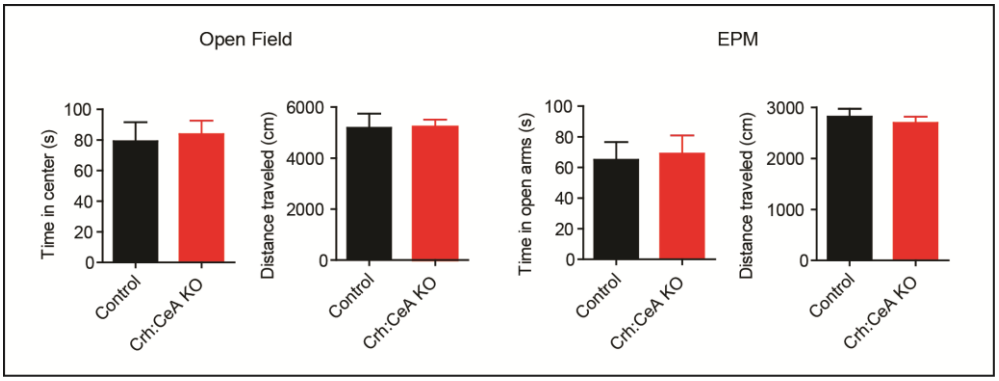

Figure 18. Baseline anxiety measures during *Crh inactivation*. Anxiety measures in an open field assay (left two figures) and elevated plus maze (right two figures) reveal no significant differences between groups. Values are represented as mean +/- SEM.

control. As with TeTx-mediated neuronal silencing, conditional inactivation of *Crh* did not affect US sensitivity as both groups exhibited similar responses to increasing shock intensities (Figure 17). Similarly, baseline anxiety states were also unaffected as measured by overall locomotor activity, time spent in the center of an open field, and time in the open arms of an elevated plus maze (Figure 18).

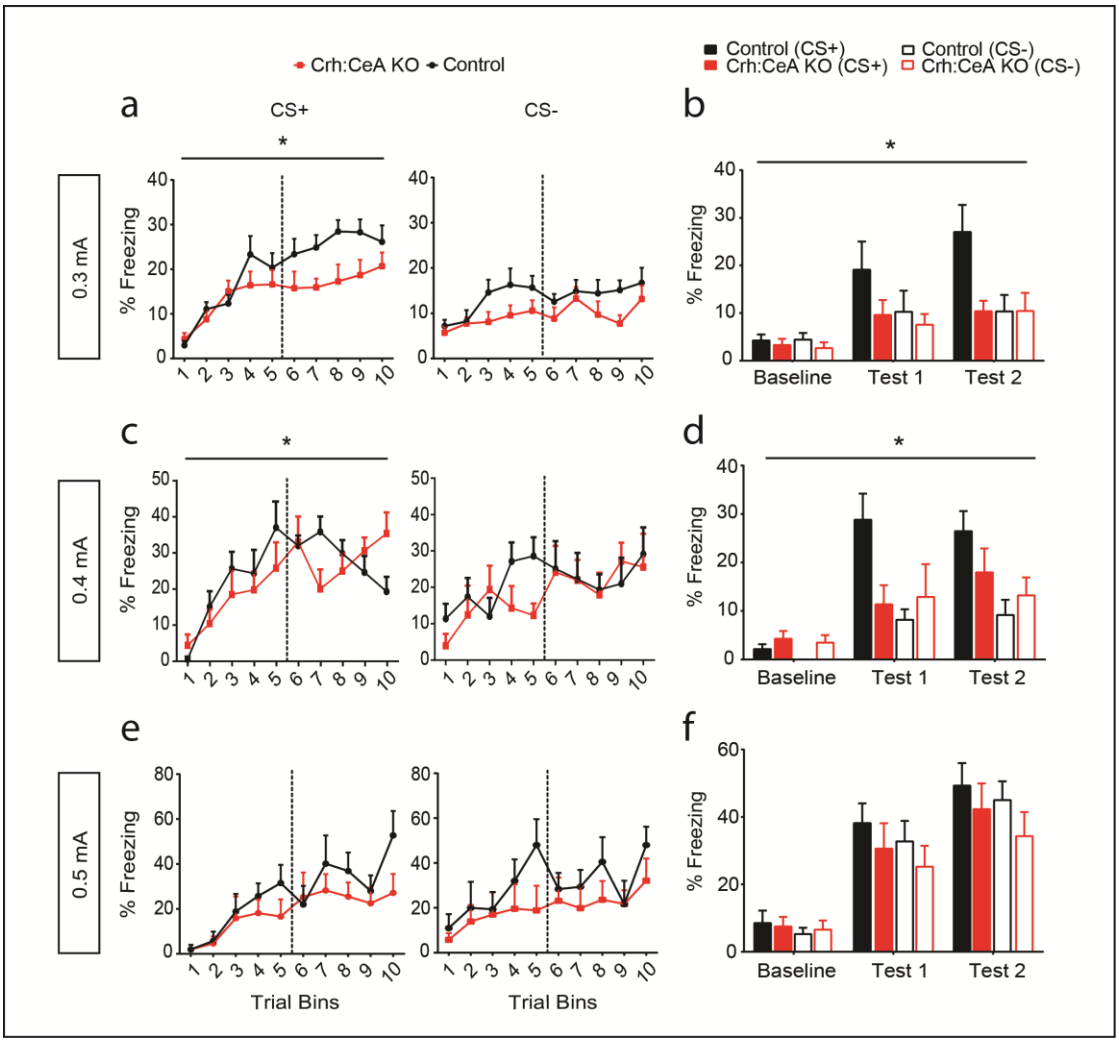

Figure 19. *Crh* inactivation during cued fear conditioning. a) Freezing during two days of conditioning to a 0.3mA footshock. Crh:CeA:KO mice exhibit significantly less freezing to the CS+ over subsequent trials compared to controls with no differences detected during the CS-. Statistics: two-way RM ANOVA, time x genotype interaction **P<0.05.* b) Freezing during recall (test) sessions following 0.3mA footshock conditioning reveals a significant difference between Crh:CeA:KO mice and controls. Statistics: two-way RM ANOVA, time x genotype interaction to the CS+ **P<0.05.* c) Freezing during conditioning to a 0.4mA footshock. Crh:CeA:KO mice exhibit significantly less freezing to the CS+. Statistics: two-way RM ANOVA, time x genotype interaction **P<0.05.* d) Freezing during recall (test) sessions following 0.4mA footshock conditioning reveals a significant difference between Crh:CeA:KO mice and controls. Statistics: two-way RM ANOVA, time x genotype interaction to the CS+ **P<0.05.* e) No differences detected between groups during conditioning to a 0.5mA footshock or f) during test sessions.

To assess cued fear, Crh:CeA KO and control mice were fear conditioned to a 0.3 mA footshock as described during the TeTx silencing experiments. During acquisition, a significant interaction of genotype (Crh:CeA KO versus control) and conditioning trial bin was observed with Crh:CeA KO mice exhibiting significantly less freezing relative to controls during the CS+ (Figure 19a). No differences in CS- responding were detected. Also in agreement with TeTx inactivation, Crh:CeA KO mice displayed less freezing to the CS+ relative to control mice during test sessions (Figure 19b).

Previous studies have reported different results concerning the necessity of CRF for the regulation of fear behaviors[40,46,75,76], leading to the hypothesis that CRF may be modulating cued fear responses at lower threat intensities. To test this, Crh:CeA KO mice were fear conditioned to a 0.4 mA US and 0.5 mA. Similar to 0.3 mA US intensity, at 0.4 mA a significant difference between Crh:CeA KO mice and control mice during acquisition was reported, though the difference was less than that observed with the 0.3 mA stimulus (Figure 19c). A significant difference between Crh:CeA KO mice and controls during testing was also observed, with Crh:CeA KO mice displaying reduced freezing (Figure 19d). Notably, Crh:CeA KO mice did begin to show conditioned freezing on the second test at 0.4 mA, though it was not different than the responses on day one. It is possible that the deficit in fear learning is due to an overall impairment in learning, including appetitive processes. Crh:CeA KO mice trained in an

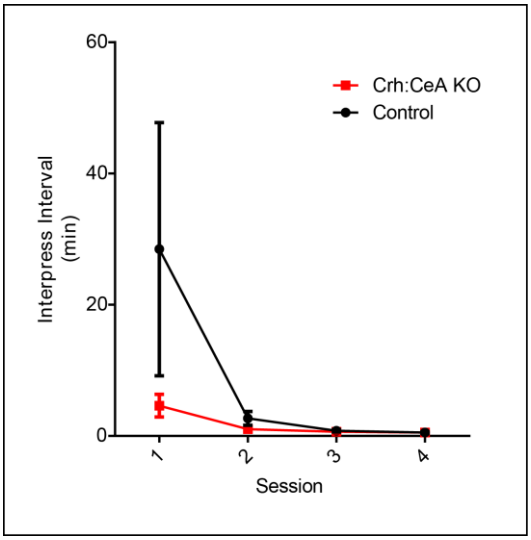

Figure 20. Instrumental learning and performance. Rate of lever pressing over 4 daily sessions consisting of 50 trials revealed no significant difference in appetitive learning. Statistics: two-way RM ANOVA time x genotype interaction *P>0.05*.

instrumental paradigm exhibited no differences relative to control mice in their ability to acquire food rewards following lever pressing (Figure 20).

In contrast to 0.3 and 0.4 mA US intensities, conditioning to a 0.5 mA US did not reveal significant differences between Crh:CeA KO mice and control mice during acquisition or testing (Figure 19e-f). Interestingly, both control and Crh:CeA KO mice showed generalized threat responses, consistent with previous reports of behavioral phenotypes observed in response to increasing US strength[79,80]. These results suggest CRF from the CeA selectively mediates conditioned fear to threats below the threshold for generalization.

The distribution of mice displaying no fear, low or high fear also scaled with increasing US intensity (Figure 21). In response to weak threats (0.3 mA), approximately half of the control mice exhibited some level of fear, while a very small percentage of KO mice displayed any fear at all. As the US increased to 0.4 mA, all control mice and a larger proportion of KO mice displayed some degree of fear (low or high). The comparative distribution, however, remained significantly different between groups. As the US increased to fear generalizing thresholds (i.e. 0.5mA), all control and KO mice exhibited fear with similar numbers displaying low and high fear.

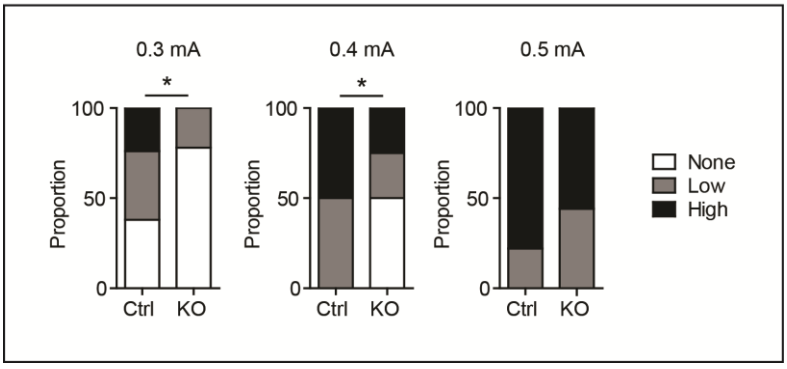

Figure 21. Distribution of control and *Crh* inactivation (KO) mice displaying no fear, low or high fear to increasing threat intensities. Significantly more control mice exhibit low and high levels of fear relative to Crh:CeA:KO mice following conditioning to 0.3 and 0.4 mA. Following conditioning to 0.5 mA, the proportion of mice displaying high and low fear levels is indistinguishable between groups. Statistics: chi-squared, **P<0.05.*

These results suggest CRF is a critical mediator for cued fear learning, but whether CRF is the exclusive facilitator from these neurons is not clear. Direct comparisons of freezing levels between CRF neuronal silenced mice (Crh:CeA:TeTx) and conditional CRF KO (Crh:CeA:KO) mice may reveal distinct differences. If CRF, for example, is only partially driving fear learning, then total silencing should result in a stronger behavioral phenotype than conditional inactivation of a single gene. Comparisons of the freezing levels of Crh:CeA:TeTx mice versus Crh:CeA:KO mice revealed no differences between treatment groups when conditioned to a 0.3mA or 0.5mA US (Figure 22). These results imply that CRF is in fact the principal mediator of conditioned fear to weaker threats.

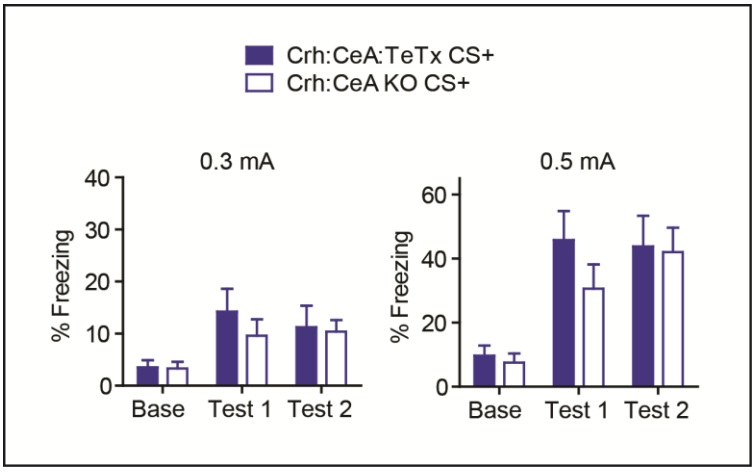

Figure 22. Comparisons of Crh:CeA:TeTx and Crh:CeA:KO freezing levels. Percent freezing to the CS+ following conditioning to 0.3 mA (left) and 0.5 mA (right). No differences were detected between treatment groups. Values are mean +/- SEM.

Discussion

The results from the current study identify CRF from the CeA as the principal mediator of conditioned threat learning. Permanent silencing of CRF neurons significantly impairs cued fear acquisition while not altering general anxiety states or threat perception. Remarkably, inactivation of *Crh* alone is sufficient to recapitulate the effects seen following total neuronal silencing. Moreover, the effect of CeA CRF appears to only be critical at sub-generalization threat levels, suggesting CRF as a critical component for discriminatory defense behaviors.

The lack of effect on general anxiety is interesting considering CRF has been broadly implicated in the clinical manifestations of anxiety[42]. These observations, which have been observed previously[40], may be explained by circuit specificity. CRF is robustly produced by other

brain regions (i.e. the BNST and LC) linked to anxiety[31], and it is therefore possible that CRF derived elsewhere is critical for basal anxiety states. Furthermore, the CeA projects to the BNST and LC, and thus activation of CeA CRF neurons is likely to engage downstream CRF circuitry required for anxiety-related behavior following a threat. Consistent with this hypothesis, shRNA-mediated knockdown of *Crh* mRNA in the CeA reduces anxiety immediately following stress[40] that has been shown to be dependent on CRF-CeA projections to the LC[81]. Alternatively, plasticity and conditioned responding of CRF neurons may facilitate higher order conditioning[82]. Consistent with this latter hypothesis, previous assessment of the role of NMDA receptor-dependent plasticity in dopamine neurons revealed that inactivation of *Grin1* (the gene encoding the essential NR1 subunit of the NMDA receptor) specifically in CRF neurons results in homeostatic synaptic scaling of AMPA receptors, increasing neural activity in these cells[73]. In the "potentiated" animals conditioned fear was found to be increased, thus cue-dependent elevations in CRF release following conditioning may enhance subsequent fear related learning.

The results using genetic inactivation of *Crh* demonstrate a key role for this peptide at low US intensities, consistent with CRF neurons modulating conditioned fear. Although the majority of experimental mice (*Crh* inactivation and conditional TeTx expression) do not show fear at low US intensities, those that do are still reduced relative to control mice and do not discriminate between predictive and non-predictive cues. This indicates that CRF is either directly facilitating this acquired discrimination, or that at lower fear levels discrimination is generally poor. As the US intensity increases beyond a threshold in which generalized fear emerges in control mice, CRF experimental mice also show equivalent fear that is equally non-discriminant. These results indicate that CRF does not promote fear generalization, but rather aids in fear discrimination at low fear levels. These findings also indicate that threat generalization is likely critically dependent on other neurotransmitters and cell types. In line with this hypothesis, it has recently been demonstrated that GABAergic mechanisms on PKCδ neurons in the CeA_L contribute to fear generalization[66]. Since we find that silencing of CRF neurons with TeTx does not affect fear at higher US intensities it is unlikely that CRF neurons are a significant source of GABA in the context of threat generalization. Furthermore, conditional inactivation of *Crh* and neuronal silencing yield the same results, indicating that

additional neurotransmitters from these neurons are not affecting fear learning. Although we do not find an attenuation of threat generalization in CRF inactivated mice or *Crh* CeA KO mice, this does not exclude the possibility that elevated CRF could drive a transition from discriminative to generalized threat responding. Consistent with this hypothesis, overexpression of CRF in the CeA augments the effects of acute stressors, leading to an enhanced anxiogenic response[40]. Whether this perturbation alters fear discrimination is not known, but does suggest that increases in excitability of CRF neurons play a positive role in fear processing. Further studies addressing the role of increased CRF signaling would address potential bidirectional control of fear by CRF-producing neurons.

**The results from this chapter will be published in the following manuscript: Sanford CA, Soden ME, Baird MA, Miller SM, Schulkin J, Clark MS, Zweifel LS. Threshold dependence of CRF in conditioned fear.*
CA performed all surgical procedures, designed and performed all behavioral testing and analysis. MB assisted with data collection and analysis.

CHAPTER 4

GENERATION OF CRHR1$^{IRES\text{-}CRE}$ MOUSE

Introduction

The previous experiments demonstrate a critical role for CRF derived from the CeA in mediating adaptive defensive responding to weaker threats. The CeA, however, contains neuronal populations sending long range projections to distant structures as well as forming local networks[2]. Thus, the precise circuit by which CRF exerts its effects on cued fear is not known. To probe the function of downstream circuits, the ability to identify and manipulate direct targets of CRF neurons is imperative. A common feature of neurons receiving input from CRF neurons is the expression of the CRF receptor. Two CRF receptors have been identified, with the CRFR1 subtype serving as the primary, high affinity receptor[83]. Neurons expressing CRFR1 would therefore be the principal target of CRF neurons. In order to assess the role of CRFR1 neurons and further elucidate the circuitry mediating CRF-dependent fear processing, a novel mouse line expressing Cre recombinase under the endogenous promoter of CRFR1 (*Crhr1*) was generated.

Targeting Strategy

In order to target Cre-recombinase to the endogenous *Crhr1* locus, a targeting vector was created containing two homology arms coinciding with the last 7 exons and 3' untranslated region (UTR) of the *Crhr1* gene flanking an internal ribosomal entry site (IRES), followed by a polyadenylated Cre-GFP sequence and neomycin resistance cassette (Figure 23). Targeted insertion of an IRES-Cre to the 3' UTR preserves expression and function of CRFR1, while limiting ectopic expression of Cre and potential breeding complications due to CRFR1 insufficiency. Using bacterial artificial chromosomes containing the *Crhr1* gene, the long homology arm corresponding to the last 7 exons of the gene (approximately 5.9 kb) and the short homology arm corresponding to the 4 kb following the termination codon were amplified

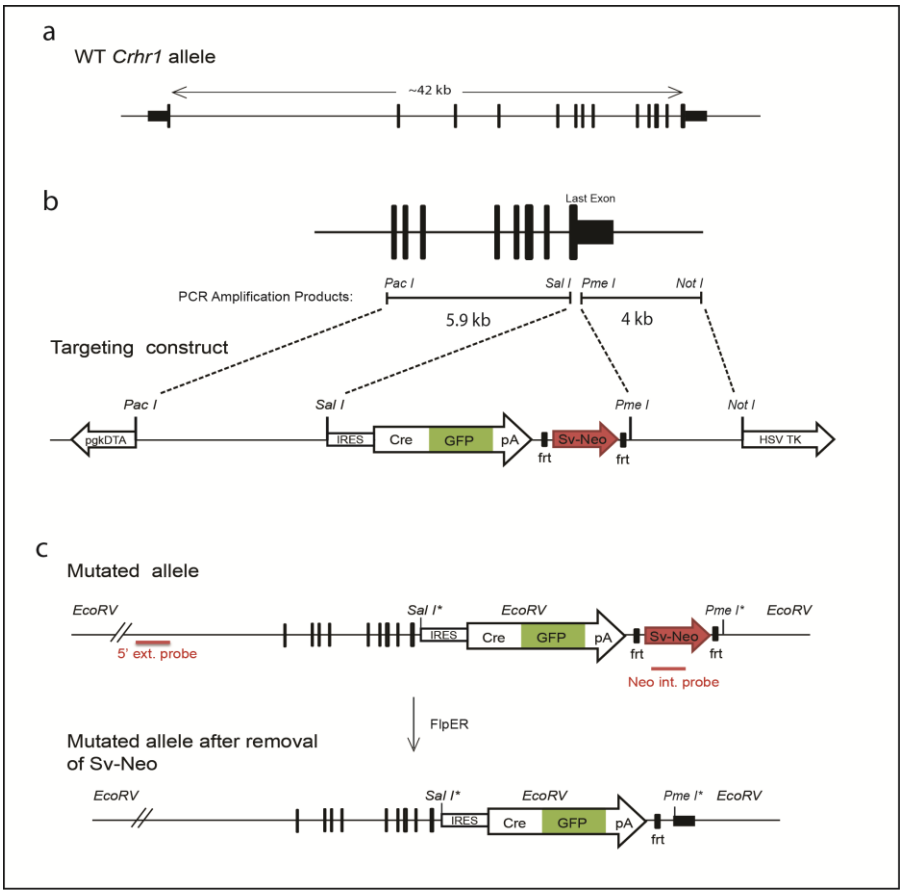

Figure 23. Targeting strategy for the generation of the *Crhr1*$^{IRES\text{-}Cre}$ mouse. a) Schematic of the wild type *Crhr1* gene. b) Schematic of the targeting construct containing two negative selection markers, and homology arms flanking the IRES-CreGFP sequence followed by a positive selection gene. c) Schematic of the mutated allele correctly incorporating the transgene and following Flp-mediated deletion of the Sv-Neo gene.

and individually subcloned into a pJet cloning vector. Restriction digests were performed on vectors containing the homology arms (5' long arm: Sal I and Pac I; 3' short arm: Pme and Not I). Digested homology arms were then purified and cloned into the targeting vector containing the IRES-CreGFP sequence. The complete targeting vector also contained two negative selection genes (pgkDTA and HSV-TK) and an frt-flanked positive selection gene (SV-Neo). The plasmids were then sent to the University of Washington Transgenic Resources core for embryonic stem cell (ESC) electroporation.

ESC colony screening, breeding and genotyping

ESC colonies were harvested upon confluency for genomic DNA extraction. DNA from each clone was then digested with EcoRV and run on 0.7% agarose gel for southern blot analysis (Figure 24a). A radiolabeled probe corresponding to a 500bp external segment 5' of the long homology arm sequence was used to identify clones harboring the correct mutated allele. Because the CreGFP sequence contains an EcoRV site, the 5' external probe should recognize an approximate 9 kb fragment from the mutated allele and 14 kb fragment from the wild type allele. Southern blots from 80 clones resulted in 17 clones heterozygous for the mutated allele. Of the 17 positive samples, 6 were selected for expansion and screened again using an internal probe recognizing the neomycin resistance gene. This secondary screening step not only

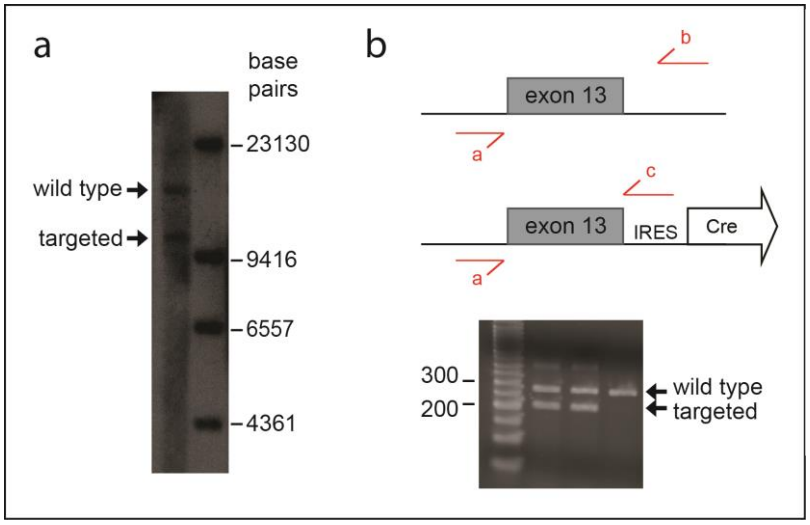

Figure 24. ESC analysis and genotyping. a) Southern blot image of positive ESC clone. Radiolabeled 5' external probe recognizing one targeted and one wild type allele. b) Genotyping strategy: common forward primer (a), wild type primer (b) and targeted primer (c). Amplification of the wildtype allele yields a band at ~290bp, while amplification of the targeted allele yields a band at ~200bp.

confirms the presence of the mutated allele, but also identifies any additional incorporation elsewhere in the genome. Positive clones were then injected into blastocysts and implanted into pseudopregnant females.

The chimeric pups were then bred with a mouse expressing Flp-recombinase to excise the neomycin resistance gene. Germline transmission of the mutant allele and Flp expression resulted in 6 pups heterozygous for CreGFP. Cre-positive males were next bred with TdTmto reporter (Ai14^{TdTmto}) and wild type (Bl6) females for further analysis. Genotyping of subsequent litters was performed using primers corresponding to sequences 3' of the termination codon (wild type) and within the IRES (Cre) sequence in combination with a common primer recognizing the last exon of the *Crhr1* gene (Figure 24b). DNA from wild type mice resulted in an amplicon of 300 bp, while amplification of the targeted allele produced a 200 bp band.

Localization of Crhr1 neurons within the CeA

Our behavioral and functional analyses highlight an important role for CRF in discriminative fear behaviors, and prior studies have described complex local circuitry within the lateral subdivision of the CeA that contain CRF neurons. Taken together, these findings suggest CRF neurons may mediate their effect through local neuronal populations expressing the primary receptor for CRF. Because a PKCδ and Sst neurons represent a significant proportion of neurons within the CeA in addition to CRF neurons, and their role in fear behaviors has been well documented[20,21,24], it is possible CRF is acting locally on one or both of these cell types. In order to determine if PKCδ and Sst neurons express Crhr1, we immunostained against PKCδ and Sst in tissue obtained from *Crhr1*$^{IRES\text{-}Cre}$; *Ai14*^{TdTmto} mice where Crhr1 neurons were robustly labeled with TdTomato (Figure 25). Crhr1 expressing neurons were located throughout the CeA along the rostral-caudal axis, with the densest localization in the rostral region. As reported previously (Chapter 2, Figure 3), PKCδ and Sst was largely located in the caudal regions. We additionally stained for Nts, and localization patterns also mirrored previous findings with strong labeling of fibers in the lateral capsule region of the CeA.

Quantification of PKCδ and Crhr1 positive cells revealed little overlap between the two populations. Approximately 15% of each cell type coexpressed the other cell marker. Because Sst and Nts label fibers and not cell bodies, we could not quantify the proportion of neurons sharing Crhr1 expression. Qualitative examination of fluorescently labeled fibers, however, did reveal overlap between Crhr1 and Sst, but not Crhr1 and Nts. These results suggest that CRF derived from the CeA may be acting locally on Sst neurons to promote the acquisition of conditioned fear to weak threats.

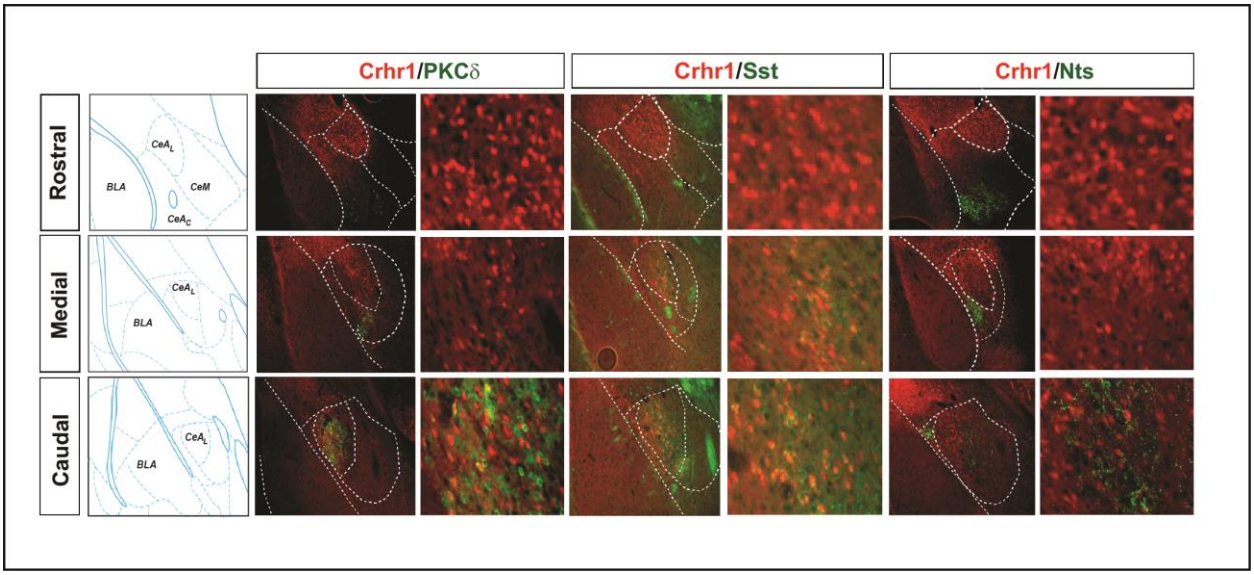

Figure 25. Immunohistochemical analysis of CeA Crhr1 neurons. Rostral (top), medial (middle), and caudal (bottom) sections obtained from Crhr1 reporter mouse *Crhr1*$^{IRES\text{-}Cre}$;*Ai14*^{TdTomato} stained for PKCδ (left), Sst (middle), and Nts (right). Immunostaining reveals minimal colocalization of CRF with PKCδ and overlapping fibers with Sst.

Discussion

Generating a novel mouse line to specifically target neural circuits downstream of CRF neurons will be instrumental in determining the biological basis of CRF-dependent adaptive fear. The present study describes such a tool and preliminary anatomical characterization has already provided some useful details regarding a potential functional circuit mechanism for CRF-dependent fear. By using selective Cre expression, robust labeling of Crhr1 neurons was achieved and used to determine potential local projection targets. Colocalization of Crhr1 with Sst fibers, but not PKCδ neurons, suggests that Sst "fear on" neurons likely represent the

principal target for locally projecting CRF neurons. This is consistent with the canonical stimulatory signaling mechanisms of Crhr1 (G_s coupled) as activation of the receptor may potentiate inhibitory transmission on to PKCδ neurons, thus amplifying threat-dependent activation of this pathway.

The higher distribution of Crhr1 neurons in the rostral CeA also suggests that CRF neurons themselves may be modulated by its own principal neurotransmitter, possibly from distant brain regions rich in CRF production such as the BNST or PBN. Viral tracing studies, however, revealed essentially no other CRF inputs to the CeA (data not shown). Thus, CRF modulation of fear through CeA circuitry is mediated by locally produced CRF acting on Sst neurons. Further studies using site-selective manipulation of Crhr1 neurons in the CeA will be essential for determining the precise function of these cells in fear behaviors.

**The results from this chapter will be published in the following manuscript: Sanford CA, Soden ME, Baird MA, Miller SM, Schulkin J, Palmiter RD, Clark MS, Zweifel LS. Threshold dependence of CRF in conditioned fear. RP designed targeting strategy. CA and RP made targeting construct, screened ES cell colonies. CA analyzed expression patterns.*

CHAPTER 5

CONCLUSIONS AND FUTURE DIRECTIONS

Summary

The findings from the present study suggest CRF neurons are a unique population of neurons located within the rostral portion of the CeA_L that are distinct from other previously described cell types. CRF neurons undergo synaptic plasticity following to threat exposure, which likely contributes to the stimulus-specific response profiles observed with the calcium imaging experiments. Furthermore, synaptic transmission from these neurons is selectively necessary for the acquisition of stimulus-threat associations at sub-generalization threat intensities, and this effect is critically dependent on CRF peptide production from these neurons. While the downstream circuit mechanisms have not been explicated, the generation of a novel transgenic mouse line will be used in future studies to advance our understanding of CRF-dependent signaling processes during fear and other behaviors.

CRF and CeA fear circuitry

Prior studies investigating the specific circuitry mediating distinct fear behaviors have revealed a highly interconnected network of specialized inhibitory neurons within the CeA. The current model states that specific threats activate Sst "fear-on" GABAergic neurons to inhibit PKCδ "fear-off" GABAergic neurons that are normally suppressing amygdala-dependent fear output[20,21,24]. Sst neurons undergo plasticity in following stimulus-threat learning[24], supporting the observation that they are necessary for fear acquisition[24]. Interestingly, activation of Sst neurons in the CeA is sufficient for fear expression as non-contingent activation induces defensive responding in fear naïve mice[24]. CRF neurons similarly undergo threat-dependent plasticity that also contributes to the necessity of CeA CRF for fear acquisition. In contrast, post-training inhibition of CRF neurons does not impair freezing, suggesting CRF neurons are not regulating fear expression as Sst neurons are. These findings are consistent with the hypothesis that CRF neurons represent a novel "fear-on" population of cells.

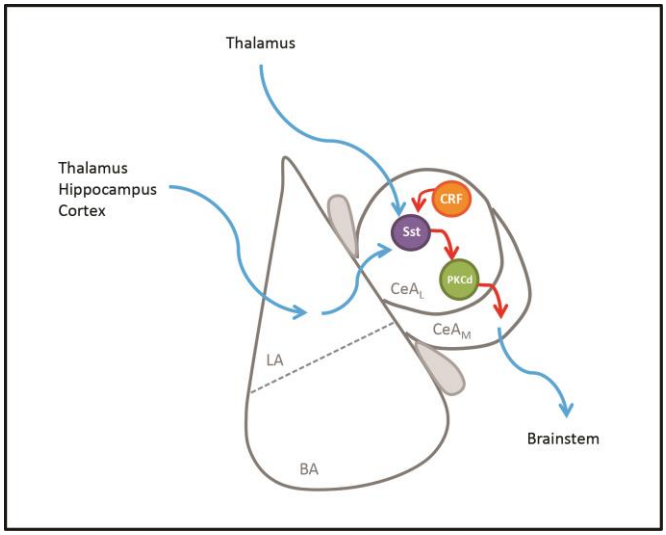

Figure 26. Updated proposed circuit diagram of CeA fear circuitry. Fear-associated stimuli activate Sst and CRF neurons, leading to CeA$_M$ disinhibition and defensive responding.

Because the necessity of CeA CRF is limited to defensive responding to weaker threats, it is possible CRF neurons act coordinately with other fear-associated networks to strengthen the Sst → PKCδ circuit in response to threatening stimuli. Considering neuronal silencing and peptide inactivation is not associated with fear suppression[21], it is more likely that the CRF population operates in parallel to the Sst or may possibly modulate Sst and PKCδ neurons directly during fear acquisition. Moreover, given that CeA CRF is particularly critical at low US

intensities and local inhibitory projections are well documented within the CeA, it is possible that CRF neurons are directly modulating the excitability of SOM or PKCδ neurons, and thus sensitizing the circuit to weaker threats[2]. This is further supported by the fact that CRF peptide functions as a neuromodulator and binds to G-protein coupled receptors (GPCRs) that are fundamentally involved in neuronal sensitivity but do not necessarily trigger action potentials.

Neuromodulatory "Gain Control"

Gain control mechanisms exist within a specific circuit to provide controlled output despite high input variability. Adjustments to the input versus output signal either amplify or dampen signals within a selective range. This process has been described in several biological systems, particularly in regard to sensory processing, and is especially critical for an organism to adapt to a broad range of external stimuli[84]. Metabotropic signaling, often through GPCRs, is one such mechanism that allows for dynamic control over neuronal communication by altering the "gain" within a circuit. Similar to other peptides and some neurotransmitters, CRF activates specific GPCRs expressed by a synaptic target or by the source cell[83]. GPCRs initiate a variety of signaling cascades to promote diverse physiological changes. These signal transduction pathways range from short term adaptations resulting in altered calcium dynamics and receptor trafficking, to long term plasticity events in response to the production of second messenger molecules (e.g. cAMP and cGMP), kinase activation, and gene expression. There are two GPCR subtypes with known affinity for CRF: CRFR1 and CRFR2[83]. While both receptors are canonically G_s-coupled, their central nervous system expression patterns and relative affinities for CRF differ with CRF binding with much higher affinity to the more broadly expressed CRFR1.

The CeA is one such area with CRFR1 expression[85], and the receptors may be located either pre- or postsynaptically similar to other brain regions[86,87]. As such, CRF is in a position to modulate circuit activity at multiple levels. Given that the CeA is comprised of local GABAergic networks, it is possible that CeA CRF is acting locally to potentiate GABAergic transmission as it does with other circuits[86,87]. Indeed, previous studies have shown that exogenous CRF administration enhances GABA release presynaptically within the CeA[88]. In line with this

hypothesis, CRF may be enhancing inhibitory control over PKCδ neurons when threat-dependent activation of Sst neurons is insufficient to produce defensive responding (e.g. at lower threat intensities). This suggests that CRF peptidergic signaling could function as a biological gain control mechanism when threats are particularly weak.

Further supporting this notion is the observation that other neuropeptides are involved in specific aspects of fear[30]. The effects of perturbing CCK signaling, for example, are only reported in cases where an intense, inescapable footshock was used[89] but not under milder conditions[90]. In the former experiments, CCK-B receptor activation is required for both acquisition and expression of fear, consistent with the phenotypes observed during photoactivation of Sst neurons. Considering CCK is expressed by the BLA[91], potentially inhibiting GABAergic projections to the CeA[92], and CCK-B activation is required for behaviors largely dependent on Sst neurons[89], it is possible that CCK potentiates Sst neuronal excitability. Moreover, Sst neuronal activation is sufficient to induce defensive responding in fear naïve animals[24] and CCK agonist administration is capable of inducing panic attacks in healthy subjects[32]. Interestingly, CCK-B antagonists do not block the effect of CRFR1 activation during fear acquisition[35], suggesting CCK signaling resides upstream of CRF and/or the two peptides are critical for fear processing at different threat levels.

While CRF and CCK are amplifying input signals in response to fearful stimuli, NPY signaling operates inversely, buffering behavioral adaptations to threats[38]. NPY is robustly expressed by the mITCs and GABAergic neurons of the BLA[37,93] which exert inhibitory control over CeA output. Thus, it is not surprising that intra-amygdala infusion of NPY is anxiolytic[94] and NPY knockout mice display anxiogenic behavioral traits[95].

Collectively, the prior studies of amygdala neuropeptides and the current investigation of CRF provide a comprehensive view of the varying degrees of neuromodulatory gain control of fear circuitry. In summary, threatening stimuli activate Sst neurons of the CeA_L to disinhibit the CeA_M via PKCδ neuronal suppression. Under weak or moderate threat conditions, CRF circuitry is activated concurrently with Sst to inhibit PKCδ neurons, relieving the inhibition of amygdala output. With stronger threats, CCK circuitry would then be recruited, leading to generalization and anxiety–like phenotypes often observed following exposure to traumatic

stimuli. CCK-dependent activation of Sst neurons would thus occlude any CRF-dependent potentiation of downstream synaptic transmission, explaining why CRF perturbation in the CeA has no effect at higher threat intensities. During extinction training, cortical inputs to the mITCs containing NPY would be engaged, suppressing CeA_M activation, and neutralizing the pro-fear effects of CRF and CCK.

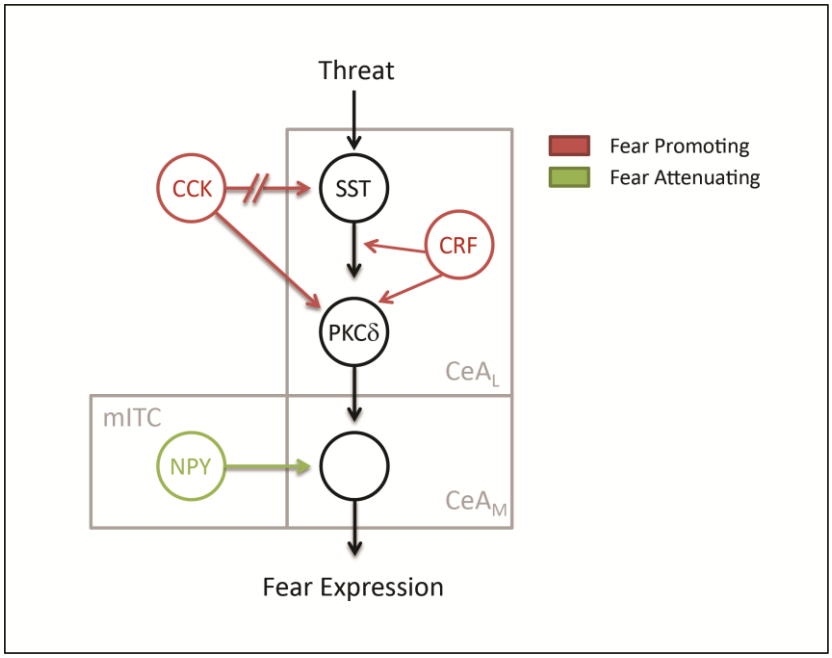

Figure 27. "Gain" control circuit. Fear promoting peptides provide amplify input signals, whereas fear attenuating peptides provide gain reduction.

Future Directions

The use of the *Crhr1*$^{IRES\text{-}Cre}$ mouse will provide critical information regarding downstream circuit mechanisms of CRF-dependent fear regulation. The precise synaptic input of CRF neurons, however, has yet to be determined. New advances in neural tracing methods now provide the ability to retrogradely label monosynaptic inputs to genetically defined neuronal populations. Complementary viral strategies using pseudotyped glycoprotein-deleted rabies virus in combination with cell-selective glycoprotein and viral envelope receptor expression[96] has been successfully used to characterize thalamic afferents to Sst neurons of the CeA[23],

demonstrating distinct connectivity patterns amongst different cell types. This same strategy can be applied to CRF circuitry to map inputs specifically to CeA CRF neurons.

Another critical question remaining involves the sufficiency of CeA CRF in fear-associated behaviors. The results from this study reveal CRF necessity in fear acquisition to weak threats; however, it does not address whether CRF signaling is sufficient to induce or enhance defensive responding. While CRF deficiency does not protect against stimulus generalization in response to intense threats, it is still possible that excessive CRF sensitizes the circuit, lowering the threshold for generalization. Furthermore, stimulus generalization is a common feature in anxiety disorders, and despite our findings failing to detect an effect of *Crh* inactivation on general anxiety levels, it is still possible CRF regulates anxiety in response to acute stressors within a limited time window. Previous studies enhancing the excitability of CRF neurons[73] and investigating the acute effects of stress exposure[40] suggest CRF from the CeA likely regulates a diverse behavioral repertoire.

Finally, identifying functionally distinct CRF subpopulations within the CeA would significantly contribute to our understanding of fear processing. CRF neurons project to several anatomically distant and functionally distinct brain regions (see chapter 2, *projection patterns)*. Defining CRF neurons not only genetically, but also anatomically, may provide important information regarding the overall organization and function of fear circuitry as it has with other systems[97,98]. The majority of CRF neurons are located in the rostral portion of the CeA where they share no overlap with Sst and PKCδ neurons. The cell bodies are relatively small with dense overlapping fibers. Progressing to more caudal regions of the CeA, CRF neurons a much fewer in number but appear to have larger cell bodies and occasionally overlap with other cell types, consistent with previous reports[99]. The structural differences alone suggest the rostral population act locally, while the large cell bodies observed in the caudal CeA support long range projection neurons, such as those regulating LC activity and anxiety in response to stress[81]. Intersectional genetic and viral targeting strategies could be particularly useful for providing greater targeting specificity in partially overlapping populations[100].

Experimental Methods

Chapter 2:

Mice

CRF reporter mice used for anatomical and electrophysiological analysis of CRF neurons in the CeA were generated by crossing *Crh*$^{IRES\text{-}Cre}$ mice[101] (stock #012704) with *Ai14*^{TdTmto} mice (stock #007914) commercially obtained from Jackson Laboratories. Mice heterozygous for both Cre and TdTmto were genotyped by PCR from tail DNA using the following primer sets:

Crh$^{IRES\text{-}Cre}$: CTT ACA CAT TTC GTC CTA GCC (common)
CAC GAC CAG GCT GCG GCT AAC (wild type)
CAA TGT ATC TTA TCA TGT CTG GAT CC (mutant)

Ai14^{TdTmto}: ATG GAA ATA CTC CGA GGC CG
GGA ACA TAC GTC ATT ATT CAC GTC
ACC TTT CTG GGA GTT CTC TGC

Mice were housed on a 12-hour light/dark cycle with *ad libitum* access to standard rodents chow and water. All experiments were conducted during the light cycle. All procedures were approved and conducted in accordance to the guidelines of the Institutional Animal Care and Use Committee of the University of Washington.

Surgery

Crh$^{IRES\text{-}Cre}$ mice (males and females 8-12 weeks for behavior and 5-3 weeks for electrophysiology) were anesthetized with isoflurane (3% induction, maintained at 1%) before bilateral stereotaxic injection with an adeno-associated virus into the central nucleus of the amygdala (from bregma in mm, A-P: -1.4, M-L: $\pm$2.9, D-V: -4.4). For *in vivo* calcium imaging, mice were implanted with guide cannulae to be fitted to the fiber optic probe. Recovery was allowed for 2 weeks prior to behavioral testing. Correct injection sites were confirmed using immunohistochemistry on brain tissue sections collected after behavioral testing. Only mice with correct bilateral targeting were included. Similarly, correct injection sites for

electrophysiology experiments were determined by examining sections under a fluorescent microscope.

Viral Vectors

AAV1-DIO-GFP-TeTx$_L$, AAV1-DIO-GCaMP6m, AAV1-DIO-Rpl22-HA were produced in house with titres of 1-3 x 10^{12} particles per mL as described[102]. TeTx$_L$GFP and Rpl22-HA plasmids were generously provided by R. Palmiter.

Histology preparation

Male and female mice were deeply anesthetized with 50 mg/kg of Beuthanasia-D and transcardially perfused with phosphate-buffered saline (PBS), followed by 4% paraformaldehyde. Whole brain tissue was dissected out and fixed overnight in 4% paraformaldehyde, and then cryoprotected by soaking in a 30% sucrose solution for 48 hours. The brains were flash frozen in OCT and stored at -80 degrees. Frozen brains were then cryosectioned at 30μm-thick sections and stored in 1x PBS with 0.1% NaAz prior to immunostaining.

Immunostaining

Coronal sections from the approximate rostral (AP:-1.0mm), medial (AP:-1.3mm), and caudal (AP:-1.6mm) were selected based on a reference atlas[103] and analyzed for protein expression. Sections were washed in 1x tris buffered saline (TBS) for 10 minutes and then blocked in 1x TBST (TBS + 0.3% TritonX 100) with 3% donkey serum for 30 minutes. Blocked sections were then incubated with the primary antibody diluted in blocking solution at the following concentrations overnight at 4 degrees:

Sst (rat, Pierce, cat. no. MA5-16987)- 1:250

PKCδ (mouse monoclonal, BD Biosciences, cat. no. 610397)- 1:500

Nts (rabbit, Immunostar, cat no. 20072)- 1:1000

HA (mouse monoclonal, ABM)- 1:1000

GFP (mouse monoclonal, Millipore, cat no. MAB3580)- 1:1000

The next day, sections were washed three times in 1x TBS for 10 minutes and then incubated in secondary antibodies conjugated to a fluorophore (AF-488, Cy3, or Cy5; Jackson Immunolabs) at a 1:200 dilution in blocking solution for 1 hour at room temperature. The sections were washed three more times in 1x TBS and mounted. The sections were subsequently imaged via wide field fluorescent microscopy (Nikon Eclipse E600) and processed with ImageJ software.

RiboTag gene expression

Crh$^{IRES\text{-}Cre}$ mice were injected with AAV1-DIO-Rpl22-HA. Following 4 weeks to allow for sufficient HA-tagged Rpl22 incorporation, brain tissue was collected. 1mm X 1.0mm punches of the CeA were homogenized and immunoprecipitation was performed as described previously[47]. Briefly, homogenized tissue was pooled from 5-7 animals and incubated with 5 μl of anti-HA antibody (Covance) coupled to 200 μl of magnetic beads (Pierce) overnight at 4°C. Following elution from magnetic beads, RNA from both immunoprecipitated (IP) samples and non-HA tagged (input) samples was obtained using the RNeasy micro kit (Qiagen) according to manufacturer's directions. Total RNA was quantified using a Ribogreen RNA assay kit (Invitrogen). cDNA was generated with Superscript IV (Invitrogen) using oligo dT primers from equal amounts of starting RNA, according to manufacturer protocol.

For qRT-PCR analysis, TaqMan (Applied Biosystems) primers were used to detect gene expression levels. Relative expression values were obtained using the comparative C_T method and normalized to *Actb* levels. Fold enrichment was calculated as the IP *versus* input ratio and represented the amount of the transcript in the targeted cell type (IP) when compared to equal amounts of RNA from the input.

Projection analysis

Imaging data obtained from the Allen Mouse Connectivity Atlas[48] was analyzed for "normalized projection density" by dividing the pixel count per volume of given source structure by the pixel count per volume of a defined target structure. The resulting weighted value was then compared across Cre-driver lines (cell types) with projections originating in the CeA. All analysis and figure generating were performed using Python scripts created during the

Summer Workshop on the Dynamic Brain 2015 with the aid of Allen Institute staff. Detailed Python scripts are represented in Supplement 1.

Behavioral training for electrophysiological and calcium imaging experiments

Crh$^{IRES\text{-}Cre}$*;Ai14*^{TdTtmto}, *Crh*$^{IRES\text{-}Cre}$ mice injected with AAV1-DIO-TeTx$_L$, or *Crh*$^{IRES\text{-}Cre}$ mice injected with AAV1-DIO-GCaMP6m were conditioned to ten 10 s auditory cues co-terminating with a 0.5 s, 0.3 mA footshock (CS+) interleaved with ten unpaired 10 s auditory cues (CS-) each day for two consecutive days in a standard operant chamber equipped with a house light, tone generator, and grid floor connected to a current generator (Med Associates). The auditory cues consisted of a pulsatile 10 kHz tone and a 20 kHz continuous pure tone, and assignments to the CS+ and CS- were counterbalanced across groups. Prior to each session, the mice were habituated for 30 minutes to the testing room.

Electrophysiology

Whole-cell recordings were made using an Axopatch 700B amplifier (Molecular Devices) with filtering at 1 KHz using 4-6 MΩ electrodes. Coronal brain slices (250 µm) were prepared from 5-8 week old *Crh*$^{IRES\text{-}Cre}$*;Ai14*^{TdTtmto}*mice or Crh*$^{IRES\text{-}Cre}$ mice injected with AAV1-DIO-TeTx$_L$. For AMPA/NMDA ratios slices were cut in an ice slush solution containing (in mM): 250 sucrose, 3 KCl, 2 $MgSO_4$, 1.2 NaH_2PO_4, 10 D-glucose, 25 $NaHCO_3$, 0.1 $CaCl_2$. Slices recovered for 1 hour at 34°C in artificial cerebral spinal fluid (ACSF) containing (in mM): 126 NaCl, 2.5 KCl, 1.2 NaH_2PO_4, 1.2 $MgCl_2$ 11 D-glucose, 18 $NaHCO_3$, 2.4 $CaCl_2$. For bath AMPA and NMDA and LTP experiments slices were cut in an ice slush solution containing (in mM): 92 NMDG, 2.5 KCl, 1.25 NaH_2PO_4, 30 $NaHCO_3$, 20 HEPES, 25 glucose, 2 thiouria, 5 Na-ascorbate, 3 Na-pyruvate, 0.5 $CaCl_2$, 10 $MgSO_4$, pH 7.3-7.4. Slices recovered for ≤12 minutes in the same solution at 32°C and then were transferred to a room temperature solution including (in mM): 92 NaCl, 2.5 KCl, 1.25 NaH_2PO_4, 30 $NaHCO_3$, 20 HEPES, 25 glucose, 2 thiouria, 5 Na-ascorbate, 3 Na-pyruvate, 2 $CaCl_2$, 2 $MgSO_4$. Slices recovered for an additional 45 minutes. All solutions were continually bubbled with O_2/CO_2, and all recordings were made in ACSF at 32°C continually perfused over slices at a rate of ~2 ml/min.

For AMPA/NMDA ratios picrotoxin (100 µM) was included in the bath and patch electrodes were filled with an internal solution containing (in mM): 120 $CsMeSO_3$, 20 HEPES, 0.4 EGTA, 2.8 NaCl, 2.5 Mg-ATP, 0.25 Na-GTP, 5 QX-314 bromide, pH 7.2-7.4, 280 mOsm.. CRF+ neurons in the CeA were identified by fluorescence and were held at +40 mV while a concentric bipolar electrode placed in the LA delivered 1 ms stimuli at 0.1 Hz to elicit an EPSC containing both AMPA and NMDA components. 15 traces were averaged per cell, followed by bath application of APV (100 µM) to isolate the AMPA component. 15 AMPA EPSC traces were averaged and digitally subtracted from the initial recording in order to generate the NMDA trace.

For bath AMPA and NMDA experiments, picrotoxin (100 µM) and tetrodotoxin (500 nM) were included in the bath and patch electrodes were filled with the same internal solution as above. For AMPA currents neurons were held at -60 mV and 50 µM cyclothiazide was perfused onto the slice for 30 seconds, followed by 1 µM AMPA (with cyclothiazide) for 30 seconds. For NMDA currents neurons were held at +40 mV and 10 µM NMDA was perfused onto the slice for 30 seconds.

For LTP experiments, picrotoxin (100 µM) was included in the bath and patch electrodes were filled with an internal solution containing (in mM): 130 K-gluconate, 10 HEPES, 5 NaCl, 1 EGTA, 5 Mg-ATP, 0.5 Na-GTP, pH 7.3, 280 mOsm. Neurons were held at -60 mV and EPSCs were evoked as described above at 0.5 Hz for a 10 min baseline period. LTP was induced with a high frequency stimulation protocol consisting of 1 ms stimuli at 100 Hz for 1 second, repeated 5 times at 3 minute intervals[55] .

Calcium imaging

For *in vivo* imaging in awake-behaving mice, a 300nm diameter fiber-optic probe (NeuroPak fiber-optic, Mauna Kea Technologies) was lowered into the CeA of $Crh^{IRES\text{-}Cre}$ mice injected with AAV1-DIO-GCaMP6m until fluorescence was detected. GCaMP6m signals were recorded using a CellVizio 488 imaging system (Mauna Kea Technologies) with laser power set to 1.35 mW. Images were acquired at a rate of 12-frames/sec for a total of 20 seconds (5 s baseline, 10 s CS, 5 s post-CS). The imaging session was triggered by a TTL pulse from the

imaging system to a Med-Associates SG-716 input connected to a DIG-716 SmartCtl. Data analyses were performed as described previously[67]. Briefly, fluorescent ROIs for individual cells were determined based on a minimal diameter of 6μm with minimal detection by four individual, adjacent fibers. Signal intensity for each ROI across trials was acquired using ImageCell software (Mauna Kea Technologies) and exported to Excel (Microsoft). Only ROIs stable across all 20 recording sessions with minimal (<1μm shift in original position) were used for further analysis. Stable images were acquired from a total of four mice of ten that were implanted. For each ROI, CS+ and CS- trials were segregated and the signal was averaged across all trials. To correct for fluorescence decay, a linear curve fit was performed using one-phase decay for the average fluorescence of each cell extrapolated from the first 5 seconds using GraphPad Prism. Change in fluorescence (%ΔF/F) was calculated by subtracting the average normalized fluorescence during the baseline 2 seconds prior to CS onset from each time point during the imaging session (20 sec total) and dividing by the fluorescence intensity at each point. Fitted curves were subtracted from both CS+ and CS- trials to generate normalized data. Data was smoothed using a 3-point sliding average. Average CuSums for each cell during 10 CS+ or 10 CS- trials were calculated for the 2 seconds following stimulus onset and compared to baseline[104] where the average of each ROI following stimulus presentation deviated greater than 3 times the standard deviation of the baseline mean.

For wide-field fluorescence detection of GCaMP6m in CRF neurons in acute slice, data were acquired using a BX51WI microscope (Olympus) with an Orca Flash 2.8 camera (Hamamatsu) and SmartShutter (Sutter) controlled by MetaFluor software (Molecular Devices). For stimulation experiments, a concentric bipolar stimulating electrode was placed in the LA as described above, and the stimulus intensity was adjusted until fluorescent signal changes were detected. Wide-field images were collected with 50 ms exposures every 200 ms, while 10 sec stimulus trains were delivered at 1, 3, and 5 Hz. Each train was delivered 3 times, separated by 10 sec intervals; fluorescence signals were averaged across three trials. Fluorescence intensity change was calculated for each cell by averaging the fluorescence intensity 1 sec before stimulus delivery (baseline) and calculating the percent change for 10 seconds following stimulus onset, relative to baseline. Three sequential stimulations for each stimulus parameter

were averaged. Following calculation of %ΔF/F, curves were fit using one-phase decay, as above and subtracted from individual cell averages; differences were smoothed using a 3-point sliding average.

Statistical analyses

All statistical tests indicated were performed using Prism (GraphPad) software. Normality assessments were performed on data where a normal distribution was assumed, followed by the appropriate parametric test and *post hoc* multiple comparisons with adjusted p-values. Variance and subjects matching are tested for each analysis. All t-tests performed are two-tailed, and unpaired t-tests where the standard deviation is not assumed to be equal between populations were performed with Welch's correction.

Chapter 3

Mice

Crh$^{IRES\text{-}Cre}$ mice (described above) were used for all neuronal silencing experiments. *Crh*$^{lox/lox}$ mice used for *Crh* inactivation were generated by Dr. Michael Clark using conventional gene targeting through homologous recombination. The 5' loxP site was inserted ~ 150 base pairs upstream of the minimal *Crh* promoter. PCR primer sequences for the detection of the 5' loxP are TTTATGGCCTTCCTCGTTAG (forward) and TCTGTCGTTACTATGGCCTG (reverse). The 3' loxP and frt-flanked neomycin resistance genes were inserted approximately 300 base pairs downstream of polyadenylation sequence. Neomycin resistance cassette was removed by crossing F1 offspring to FlpEr mice. The PCR primer sequences for detection of the delta allele is TTTATGGCCTTCCTCGTTAG (forward) and CTTTCTTAAGTGTCCTGCCAT (reverse). All mice were housed on a 12-hour light/dark cycle with *ad libitum* access to standard rodents chow and water. All experiments were conducted during the light cycle. The procedures conducted with

these mice were approved and executed in accordance to the guidelines of the Institutional Animal Care and Use Committee of the University of Washington.

Surgery

Surgical procedures for *Crh*$^{IRES\text{-}Cre}$ and *Crh*$^{lox/lox}$ mice (males and females 8-12 weeks) are identical to those described in the previous chapter. Only mice with correct bilateral targeting were included for behavioral analysis.

Viral Vectors

AAV1-DIO-GFP-TeTx$_L$, AAV1-CreGFP, and AAV1-ΔCreGFP were produced in house with titres of 1-3 x 10^{12} particles per mL as described[102]. TeTx$_L$GFP, CreGFP, and ΔCreGFP plasmids were generously provided by R. Palmiter.

Behavioral Testing

Fear Conditioning:

Behavioral sessions were performed during the light cycle in a standard operant chamber (Med Associates Inc., VT) equipped with a house light and tone generator. The first day included an initial baseline test session, followed by a conditioning session. The second day was identical to the first day in that mice received a test session followed by a conditioning session. The third and final day consisted of only a test session. The test context was comprised of solid white walls, flat floor, and 1% acetic acid olfactory cues. The conditioning context consisted of opposing transparent and metal walls, a grid floor, and cleaned with 70% ethanol. Auditory cues included a 10 kHz pulsatile tone and a 20 kHz continuous tone, each 10 seconds in duration. Assignment of the tones as the CS+ and CS- was counterbalanced across groups. Baseline and test sessions consisted of 3 presentations of each CS in the test context. Conditioning sessions consisted of 10 presentations of the CS+ co-terminating with a 0.3mA or

0.4mA footshock alternating with 10 presentations of the CS- on a 60 s intertrial interval. Conditioning sessions to the 0.5mA footshock consisted of 5 CS+ and 5 CS- presentations.

For those experiments using hM4Di-CNO to silence CRF neurons post-training, saline was administered once per day for one week prior to the behavioral training. On the first two days of behavioral training, all mice were injected with saline 3 hours prior to the test session. On the third day, all mice were injected with CNO (1 mg/kg) 3 hours prior to the test session.

All sessions were video recorded and test sessions were analyzed with Ethovision (Noldus) tracking software. For test sessions, velocities were calculated using an in house MATLAB (Mathworks) script and freezing was defined as v<0.5 cm/s normalized to baseline mobility. Because the video tracking software failed to reliably track the mouse in the conditioning context, freezing was manually scored by an experimenter blind to the group assignments. For the assessment of the proportion of mice displaying conditioned threat behavior, CS responses were average across both days of testing. Mice displaying freezing above the 95^{th} percentile of freezing for all mice during baseline testing was set as the threshold for fear expression. Assessment of discriminative fear in experimental mice that crossed this threshold was analyzed in a similar manner, taking the mean freezing responses during both testing days.

To measure shock reactivity, mice were placed in conditioning chambers and 0.5 s foot shocks were delivered. Three shocks at increasing intensities (0, 0.1, 0.2, 0.3, 0.4, 0.5 mA) were delivered at 60 s trial intervals and responses were averaged at each intensity. All sessions were video recorded and analyzed with Ethovision (Noldus) tracking software. Assessment of centerpoint velocities (cm/s) measured prior to and at the onset of the shock allowed for detection of lateral movement.

Open field assay:

Total time in the center and distance traveled in an open field (50 cm diameter tub with laminated floor designating the center of the arena) was monitored for 10 min one week prior to footshock conditioning using Ethovision (Noldus) video tracking software.

Elevated plus maze:

Total distance traveled and time spent in the open arms of an elevated plus maze (Med Associates Inc., VT) was monitored for 10 min one week prior to footshock conditioning using Ethovision (Noldus) video tracking software.

All behavioral experiments were conducted with mice from at least 2 cohorts and only those mice with correct bilateral targeting of the virus were included for analysis.

Instrumental training:

Control and Crh:CeA KO mice were food restricted and maintained to approximately 85% of their baseline body weight starting 1 week prior to training. The mice were then placed in a standard operant chamber equipped with a house light and dual levers (MedAssociates) and magazine trained to retrieve 45 mg food pellets (Bio-Serv). The mice were then trained to press either lever on fixed ratio (FR1) schedule in which a single lever press delivered a single pellet. The levers remained retracted until a head entry into the food receptacle was made. The session completed after acquiring 50 pellets or 2 hours. Lever pressing rates were calculated by dividing the number of lever presses by the total time used to complete the session. Each 50 trial or 2 hour session was repeated over 4 days.

Statistics and MATLAB code

All statistical tests indicated were performed as described in the methods for chapter 2. MATLAB scripts used to analyze freezing behavior from Ethovision-generated positional data were developed by Dr. Elliott Merriam and are described in Supplement 2.

Chapter 4

Targeting construct

The targeting construct was developed in collaboration with Dr. Richard Palmiter. Genomic sequences corresponding to the *Crhr1* gene were obtained from the UCSC genome browser. BAC clones containing the sequence were obtained (Invitrogen; #65K20 and #8N22) and screened. The 5' arm homologous to the last 5.9 kb containing exons 7-13 was PCR amplified from the BACs with new Sal I and Pac I restriction sites introduced to the 5' and 3' ends, respectively. The 3' arm homologous to the first 4 kb within the 3' UTR was PCR amplified with new Pme I and Not I restriction site introduced to the 5' and 3' ends, respectively. The arms were then subcloned into a pJet2.1 cloning vector (ThermoFisher). The arms were subsequently digested with enzymes pertaining to the newly introduced restriction sites and cloned into the targeting vector containing the IRES-Cre-GFP sequence, frt-flanked neomycin resistance gene, and two negative selection genes (pgkDTA and HSV-TK). Positive clones were linearized and submitted to the University of Washington Transgenic Resources Core for ESC electroporation.

Southern blot analysis

ESC colonies received were grown to confluency and then digested with 0.5x SDS-EDTA-Tris buffer (SET), 0.2M NaCl, and 50 μg/ml proteinase K. DNA from each colony was phenol-chloroform extracted, precipitated in 95% ethanol, and resuspended in a 10% Tris/ 0.2% EDTA buffer. Genomic DNA was digested for at least 3 hours with EcoRV and run on a 0.7% agarose gel overnight at 15 mA. The gels were stained with ethidium bromide and visualized with UV light. The gels were then denatured in 0.5M NaOH and 1.5M NaCl for 30 minutes, and neutralized in 3M NaCl and 1M Tris for additional 30 minutes. Digested DNA was transferred overnight to Zeta Probe nylon membranes (BioRad) by capillary action in 20x SSC. Membranes containing the digested DNA were UV crosslinked and incubated in hybridization solution (50 ml 7% SDS/ 0.5M $NaPO_4$, 50 ml formamide, 20 ml dextran sulfate) at 60 degrees for 30 minutes.

An external probe was generated by PCR amplification of an approximate 500 bp region 5' of the long homology arm using primers: CCTTCCCAACCAGAAAACAA (forward) and GGCAGGACATCACACTAGC (reverse). The internal probe was generated by R. Palmiter recognizing the neomycin resistance gene. Radioactive ^{32}P probes were then generated via random priming using the external and internal probe templates. The probes were then added to the pre-hybridized membranes an incubated at 45 degrees for at least 6 hours.

The membranes were then rinsed briefly with 0.5x SET, followed by three additional rinses in 0.5x SET, 10 minutes each, at 60 degrees. Membranes were dried and exposed to film at -80 degrees. The targeted allele produced a band at approximately 9.5kb and the wild type produced a band at approximately 14 kb.

Genotyping

Primer pairs flanking the termination codon of the *Crhr1* gene were designed to detect the wild type allele, amplifying a ~290 base pair region. A third primer corresponding to the IRES sequence, to be paired with the common forward primer, was generated to detect the mutated allele, resulting in a ~200 base pair amplicon.

Supplement

1. MATLAB code for freezing analysis (courtesy of E. Merriam):

a. The following script utilizes the positional data at individual time points generated by Ethovision to calculate the freezing percentage for each mouse during each CS presentation and during the inter-trial interval. Freezing thresholds are, by default, set at a minimum of 1 second of mobility defined by velocities less than 0.5 cm/s. Data from each mouse for each trial is then compiled into arrays that can be readily imported to Prism for graphical and statistical analysis. The script below is the main script defining the directory, file names, threshold, animal IDs, and session numbers. This script executes a core set of 4 separate functions described in 1b-e.

```
%%
% SECTION 1
% This section imports Excel data containing session onset times ('Onsets') and
% CS onset times ('CS Times') for a given experiment, and saves them as
% .mat files in the same directory for later retrieval. Set the current directory and file names

clear all;
cd('C:\Users\akers\Desktop\CRF CeA\CAV CeA 5mA');
Onsets=xlsread('CAV CeA 5mA.xlsx','Onsets');
save('CAV CeA 5mA Onsets.mat','Onsets');
CSTimes=xlsread('CAV CeA 5mA.xlsx','CSTimes');
save('CAV CeA 5mA CSTimes.mat','CSTimes');

%%
% SECTION 2
% This section imports Excel data generated by Ethovision, containing each animal's
% position during each frame of each video recording for a given experiment,
% and saves them as .mat files in the same directory for later retrieval.
% Note, xls files typically have 4 sheets which become 4 distinct .mat files.
% Note, importing big excel sheets in Matlab is RAM/processor intensive and takes awhile.
% For each experiment, set the correct file name to read in.

Exp = char('Raw data-CAV CeA 5mA Fear Conditioning');
Sheets={'Track-Arena 1' 'Track-Arena 2' 'Track-Arena 3' 'Track-Arena 4'}[68];
for i=1:5
    File=strcat(Exp,{'-Trial     '},num2str(i),'.xlsx'); File=File{1};
    for j=1:numel(Sheets)
        Sheet=strcat(Sheets{j},'-Subject 1');
        Arena=xlsread(File,Sheet);
        Output=strcat(File,'_',Sheet,'.mat');
        save(Output,'Arena');
    end
end

%%
% SECTION 3
% This section imports .mat files containing session onset times, CS onset times, and animal
% tracking data for an entire experiment.  Four output are datasets generated:

% FCData1a holds data for 3-trial sessions from control animals (Group 1)
% FCData2a holds data for 3-trial sessions from experimental animals (Group 2)
% FCData1b holds data for 10-trial sessions from control animals (Group 1)
% FCData2b holds data for 10-trial sessions from experimental animals (Group 2)
```

```
% These FCData datasets all have similar architecture and are referred to generically as 'FCData'
below.
% They are cell arrays holding many different pieces of data under one "umbrella".


% FCData datasets are {#animals x #sessions x 3} cell arrays.
% FCData{M,S,1}     :  Velocity data for mouse M during session S.
% FCdata{M,S,2}     :  Duration and timing of bouts of immobility for mouse M during session S.
% FCdata{M,S,3}     :  General information about the data for mouse M during session S (e.g.
sampling rate)

% Each of these is further described below...

%%%%%%%%%%%%%%%%%%%%%%%%%%%%%%%%%%%%%%%%%%%%%%%%%%%%%%%%%%%%%%%%%%%%%%%%%%%%%%%%%%%%%%%%%%%%%%%%

% FCData{M,S,1}     :
% This {4x1} cell holds velocity data (cm/second) before and during CS+ and CS- presentations for
mouse M during session S.
% FCData{M,S,1}{1}  :  Velocity data during the 30 SECONDS PRECEDING all CS+ presentations for
mouse M during session S.
% FCData{M,S,1}{2}  :  Velocity data DURING CS+ PRESENTATIONS for mouse M during session S.
% FCData{M,S,1}{3}  :  Velocity data during the 30 SECONDS PRECEDING all CS- presentations for
mouse M during session S.
% FCData{M,S,1}{4}  :  Velocity data DURING CS- PRESENTATIONS for mouse M during session S.

% All FCData{M,S,1}{k} are (#frames x #trials x 3) matrices
% FCData{M,S,1}{k}(i,j,1) : Animal CENTER-point velocity for ith frame of jth trial of condition
k for mouse M during session S.
% FCData{M,S,1}{k}(i,j,2) : Animal HEAD-point velocity for ith frame of jth trial of condition k
for mouse M during session S.
% FCData{M,S,1}{k}(i,j,3) : Animal TAIL-point velocity for ith frame of jth trial of condition k
for mouse M during session S.

%%%%%%%%%%%%%%%%%%%%%%%%%%%%%%%%%%%%%%%%%%%%%%%%%%%%%%%%%%%%%%%%%%%%%%%%%%%%%%%%%%%%%%%%%%%%%%%%

% FCData{M,S,2}     :
% This {4x1} cell contains the duration and timing of bouts of immobility before and during CS+
and CS- presentations for mouse M during session S.
% FCData{M,S,2}{1}  :  Immobility data during the 30 SECONDS PRECEDING all CS+ presentations for
mouse M during session S.
% FCData{M,S,2}{2}  :  Immobility data DURING CS+ PRESENTATIONS for mouse M during session S.
% FCData{M,S,2}{3}  :  Immobility data during the 30 SECONDS PRECEDING all CS- presentations for
mouse M during session S.
% FCData{M,S,2}{4}  :  Immobility data DURING CS- PRESENTATIONS for mouse M during session S.

% All FCData{M,S,1}{k} are (#fragments x 4) matrices
% FCData{M,S,1}{k}(:,1) holds trial number (e.g. 3 means 3rd presentation of the CS during this
session)
% FCData{M,S,1}{k}(:,2) holds which fragment of good data within the current trial this is
(1,2,...)
% FCData{M,S,1}{k}(:,3) holds durations (in seconds) of the fragments
% FCData{M,S,1}{k}(:,4) holds durations (in seconds) of bouts of immobility. Zeros mean the
animal was mobile

% This data will be used by the FCAnalysis2 function to determine what percent of time the animal
was freezing

%%%%%%%%%%%%%%%%%%%%%%%%%%%%%%%%%%%%%%%%%%%%%%%%%%%%%%%%%%%%%%%%%%%%%%%%%%%%%%%%%%%%%%%%%%%%%%%%

% FCData{M,S,3}     :
% This 1x11 cell holds miscellaneous information about mouse M, session S, and the experiment in
general:
% {sampling rate , session# , mouse ID , CSp freq(kHz) , CSm freq(kHz) , CSp duration , CSm
duration , threshold of immobility (cm/sec) , CS+ time vector , CS- time vector, # of CS+'s};

%%%%%%%%%%%%%%%%%%%%%%%%%%%%%%%%%%%%%%%%%%%%%%%%%%%%%%%%%%%%%%%%%%%%%%%%%%%%%%%%%%%%%%%%%%%%%%%%

% For each new experiment, set the current directory and file names, add animal ID numbers and
session designations.
```

```
clear all;
cd('C:\Users\akers\Desktop\CRF CeA\CAV CeA 5mA');
Exp = char('Raw data-CAV CeA 5mA Fear Conditioning');

Thresh=0.5;   % This is the threshold, in cm/second, for mobility vs. immobility
CSpDur=10;
CSmDur=10;
load('CAV CeA 5mA Onsets.mat');
load('CAV CeA 5mA CSTimes.mat');

G1=[1216 1215 1214]; % mouse ID numbers for control group
G2=[1221 1217 1220 1219 1218]; % mouse ID numbers for experimental group

N1=numel(G1);
N2=numel(G2);

% Process control animals, sessions of probe trials
SessionsA=[1 3 5];
FCData1a=cell(N1,numel(SessionsA),3);
for S=1:numel(SessionsA)
    Session=SessionsA(S);
    for M=1:N1
        Mouse1=G1(M);
        Row1=find(Onsets(:,1)==Mouse1,1);
        CSp1=Onsets(Row1,4);
        Offset1=Onsets(Row1,Session+4);
        MAtStamps1=CSTimes(:,1:3)+Offset1;
        Box1=Onsets(Row1,3);
        File=strcat(Exp,{'-Trial     '},num2str(Session),{'.xlsx_Track-Arena '},num2str(Box1),'-
Subject 1.mat');
        File=File{1};
        load(File);

        [FCData1a{M,S,1}, FCData1a{M,S,2}, FCData1a{M,S,3}] =
EthoReader3(Arena,MAtStamps1,S,Mouse1,1,Thresh,CSpDur,CSmDur,CSp1);
    end
end

% Process experimental animals, sessions of 3 trials
FCData2a=cell(N2,numel(SessionsA),3);
for S=1:numel(SessionsA)
    Session=SessionsA(S);
    for M=1:N2.
        Mouse2=G2(M);
        Row2=find(Onsets(:,1)==Mouse2,1);
        CSp2=Onsets(Row2,4);
        Offset2=Onsets(Row2,Session+4);
        MAtStamps2=CSTimes(:,1:3)+Offset2;
        Box2=Onsets(Row2,3);
        File=strcat(Exp,{'-Trial     '},num2str(Session),{'.xlsx_Track-Arena '},num2str(Box2),'-
Subject 1.mat');
        File=File{1};
        load(File);
        [FCData2a{M,S,1}, FCData2a{M,S,2}, FCData2a{M,S,3}] =
EthoReader3(Arena,MAtStamps2,S,Mouse2,1,Thresh,CSpDur,CSmDur,CSp2);
    end
end

% Process control animals, sessions of conditioning trials
SessionsB=[2 4];
FCData1b=cell(N1,numel(SessionsB),3);
for S=1:numel(SessionsB)
    Session=SessionsB(S);
    for M=1:N1
        Mouse1=G1(M);
        Row1=find(Onsets(:,1)==Mouse1,1);
        CSp1=Onsets(Row1,4);
        Offset1=Onsets(Row1,Session+4);
        MAtStamps1=CSTimes+Offset1;
        Box1=Onsets(Row1,3);
```

```
        File=strcat(Exp,{'-Trial     '},num2str(Session),{'.xlsx_Track-Arena '},num2str(Box1),'-
Subject 1.mat');
        File=File{1};
        load(File);
        [FCData1b{M,S,1}, FCData1b{M,S,2}, FCData1b{M,S,3}] =
EthoReader3(Arena,MAtStamps1,S,Mouse1,1,Thresh,CSpDur,CSmDur,CSp1);
    end
end

FCData2b=cell(N2,numel(SessionsB),3);
for S=1:numel(SessionsB)
    Session=SessionsB(S);
    for M=1:N2
        Mouse2=G2(M);
        Row2=find(Onsets(:,1)==Mouse2,1);
        CSp2=Onsets(Row2,4);
        Offset2=Onsets(Row2,Session+4);
        MAtStamps2=CSTimes+Offset2;
        Box2=Onsets(Row2,3);
        File=strcat(Exp,{'-Trial     '},num2str(Session),{'.xlsx_Track-Arena '},num2str(Box2),'-
Subject 1.mat');
        File=File{1};
        load(File);
        [FCData2b{M,S,1}, FCData2b{M,S,2}, FCData2b{M,S,3}] =
EthoReader3(Arena,MAtStamps2,S,Mouse2,1,Thresh,CSpDur,CSmDur,CSp2);
    end
end

%%
% SECTION 4
% This section calls FCAnalysis2.m, which takes FCData arrays as inputs and computes the percent
of time each animal or experimental group froze under each experimental condition for each trial
or session.

FrzDur=1; % Duration, in seconds, that a bout of immobility needs to be in order to be considered
true "freezing" behavior

[GroupDays1a GroupTrials1a MouseDays1a MouseTrials1a P1a]=FCAnalysis2(FCData1a,FrzDur); % 3-trial
sessions of control animals
[GroupDays2a GroupTrials2a MouseDays2a MouseTrials2a P2a]=FCAnalysis2(FCData2a,FrzDur); % 3-trial
sessions of experimental animals
[GroupDays1b GroupTrials1b MouseDays1b MouseTrials1b P1b]=FCAnalysis2(FCData1b,FrzDur); % 10-
trial sessions of control animals
[GroupDays2b GroupTrials2b MouseDays2b MouseTrials2b P2b]=FCAnalysis2(FCData2b,FrzDur); % 10-
trial sessions of experimental animals

% See notes about GroupDays and GroupTrials below
[GroupDays,GroupTrials] =
FCSorter(GroupDays1a,GroupDays2a,GroupDays1b,GroupDays2b,GroupTrials1a,GroupTrials2a,GroupTrials1
b,GroupTrials2b,SessionsA,SessionsB);

% GroupDays and GroupTrials hold freezing data for the CS+, CS-, and ITI (which is actually the
30 seconds before each CS+) for both control (G1) and experimental (G2) mice.  Each row of
GroupDays holds percent freezing averaged across all trials of a given session.
% Each row of GroupTrials holds percent freezing for each trial of each session.
% Columns of GroupDays and GroupTrials are organized as follows:
 [ <CS+ controls> , <CS+ experimentals> , <CS- controls> , <CS- experimentals> , <ITI controls> ,
<ITI experimentals> ]
% Each of these categories is comprised of N columns, where N is the number of mice in the larger
mouse group (control or experimental).
% Thus both GroupDays and GroupTrials will have 6*N columns in total.
% These data are ready to copy and paste into a Prism "grouped" worksheet of N replicates.
% Note, if # control animals ~= # experimental animals, the "extra" columns for the small group
will be full of NaNs.
```

b. "EthoReader3" function

This function uses the raw positional data (.mat files) called in from the script above to calculate the velocities at the defined timepoints.

```
function [VelData, FrzData, Info] = EthoReader3(Arena,MAtStamps,S,Mouse,Fig,Thresh,Dur1,Dur2,CSp)

% EthoReader3 takes the raw data and CS timestamps and CS durations for a
% given mouse in a given session and obtains the velocity and immobility
% data for the animal during relevant experimental timepoints (before and
% during CS presentations).  These are sent as outputs VelData and FrzData,
% respectively.  The 3rd output, Info, contains miscellaneous information
% about the experiment. These are sent back to Etho_MA_FC_<date>.m, which
% builds them into the FCData cell arrays (see comments in Etho_MA_FC_<date>.m).

% uncomment line below for testing only.  These are normally input variables
% Day = i; Mouse = Mice(j); Dur1=10.5; Dur2=10.5; CSp=CSp1; MAtStamps=MAtStamps1;

dArena=diff(Arena,1); % 1st order discrete derivative of the raw data
MnIFI=mean(dArena(:,1),1); % mean inter-frame interval of the raw data

% Dists=[d_center  d_head  d_tail], where d=frame to frame displacement
Dists=[sqrt(dArena(:,3).^2 + dArena(:,4).^2)   sqrt(dArena(:,5).^2 + dArena(:,6).^2)
sqrt(dArena(:,7).^2 + dArena(:,8).^2)];
% Vels=[v_center  v_head  v_tail], where v=frame-to-frame velocity
Vels=[Dists(:,1)./dArena(:,1) Dists(:,2)./dArena(:,1) Dists(:,3)./dArena(:,1)];

BW=6; % Bin-width for low-pass filter
for i=1:3
    Vels(:,i)=filter(ones(1,BW)/BW,1,Vels(:,i)); % low-pass filter the data to remove Brownian-
esque noise from Ethovision point tracking
end

tSec=Arena(:,1); % time vector in seconds
%tMin=tSec/60; % time vector in minutes, only used for figures

CSpOnTimes=MAtStamps(1, :); % CS+ Onset times
CSmOnTimes=MAtStamps(2, :); % CS- Onset times
nCSps=size(CSpOnTimes,2); % Number of CS+'s
nCSms=size(CSmOnTimes,2); % Number of CS-'s

% Define the CS+ and CS- in kHz, but with CS- as a negative number (potentially useful for making
figures)
if CSp==20
    CSm=-10;    CSpDur=Dur1;    CSmDur=Dur2;
elseif CSp==10
    CSm=-20;    CSpDur=Dur2;    CSmDur=Dur1;
end

FPS=round(1/MnIFI); % Frames per second
CSpFrames=floor(CSpDur*FPS); % Duration of CS+ in frames (seconds*frames/second=frames). floor
rounds down
CSmFrames=floor(CSmDur*FPS); % Duration of CS- in frames (seconds*frames/second=frames). floor
rounds down

CSpIndx=zeros(nCSps,1); % This will hold row #s in the time vector tSec when CS+'s start
CSmIndx=zeros(nCSms,1); % This will hold row #s in the time vector tSec when CS-'s start
tCSp=(0:CSpFrames-1)'*MnIFI; %tSec(1:CSnFrames);
tCSm=(0:CSmFrames-1)'*MnIFI; %tSec(1:CSnFrames);

ITI=3;  % this sets the pre-CS time analyzed to 3x the CS duration (e.g. 30sec for a 10sec CS)

CSpVels=nan(CSpFrames,nCSps,3);        % This will hold the velocity data DURING the CS+
presentations
preCSpVels=nan(ITI*CSpFrames,nCSps,3); % This will hold the velocity data BEFORE the CS+
presentations
CSmVels=nan(CSmFrames,nCSms,3);        % This will hold the velocity data DURING the CS-
presentations
```

```
preCSmVels=nan(ITI*CSmFrames,nCSms,3); % This will hold the velocity data BEFORE the CS-
presentations

% Loop through the CS's, identify where they occur, enter the velocity data
% into the appropriate column of the appropriate matrix.
for i=1:nCSps
    CSpIndx(i,1)=find(abs(tSec-CSpOnTimes(i))==min(abs(tSec-CSpOnTimes(i))), 1 ); % Determine the
onset time of the ith CS+
    CSpVels(:,i,:)=Vels(CSpIndx(i,1):CSpIndx(i,1)+CSpFrames-1,:);                % ith column of
CSpVels now holds velocity data for ith CS+ presentation
    preCSpVels(:,i,:)=Vels(CSpIndx(i,1)-FPS-ITI*CSpFrames+1:CSpIndx(i,1)-FPS,:);  % ith column of
preCSpVels now holds velocity data for time preceding ith CS+ presentation

    CSmIndx(i,1)=find(abs(tSec-CSmOnTimes(i))==min(abs(tSec-CSmOnTimes(i))), 1 ); % Determine the
onset time of the ith CS-
    CSmVels(:,i,:)=Vels(CSmIndx(i,1):CSmIndx(i,1)+CSmFrames-1,:);                % ith column of
CSmVels now holds velocity data for ith CS- presentation
    preCSmVels(:,i,:)=Vels(CSmIndx(i,1)-FPS-ITI*CSmFrames+1:CSmIndx(i,1)-FPS,:);  % ith column of
preCSmVels now holds velocity data for time preceding ith CS- presentation
end

% VelData holds velocity data for: {before CS+'s; during CS+'s; before CS-'s; during CS-'s}
% This becomes FCData{:,:,1} in Etho_MA_FC_<date>.m
VelData={preCSpVels; CSpVels; preCSmVels; CSmVels};

% FrzData holds immobility data for: {before CS+'s; during CS+'s; before CS-'s; during CS-'s}
% This becomes FCData{:,:,2} in Etho_MA_FC_<date>.m
FrzData=FindFreezing2(VelData,FPS,Thresh);

% Info holds: sampling rate , session# , mouse ID , CSp freq(kHz) , CSm freq(kHz) , CSp duration
, CSm duration , threshold of immobility (cm/sec) , CS+ time vector , CS- time vector, # of
CS+'s};
% This becomes FCData{:,:,3} in Etho_MA_FC_<date>.m
Info={FPS,S,Mouse,CSp,CSm,CSpDur,CSmDur,Thresh,tCSp,tCSm,nCSps};


End
```

c. "FCAnalysis2" function

This function determines the percent freezing based on the velocities calculated above.

```
function [GroupDays GroupTrials MouseDays MouseTrials P]=FCAnalysis2(FCData,tW)

% This function takes a fear conditioning dataset (FCData) and determines
% the percent freezing for each experimental condition during each session
% for each animal in the dataset.

% Freezing is defined as a bout of immobility (defined elsewhere, typically
% as velocity<0.5cm/sec) lasting a duration of tW seconds or more.

% tW is an input variable to this function, typically tW=1sec.

% There is also code in this function for plotting an animal's velocities
% across sessions and conditions.  It may have some bugs though.

% tW=1; % for testing only
nMice=size(FCData,1); % # of mice
nDays=size(FCData,2); % # of sessions (not necessarily # of days actually)
Info=FCData{1,1,3}; % General experimental information
nTrials=Info{1,11}; % number of trials per session
nCons= size(FCData{1,1,2}{1,1},2); % number of experimental conditions (typically 4 - preCSp,
CSp, preCSm, CSm)

% P is a 4D matrix that will hold all the % freezing data.
% The dimensions of P are ( # of sessions , # trials per session , # of mice , # of experimental
conditions )
P=ones(nDays,nTrials,nMice,nCons);
```

```
for j=1:nMice % loop through mice
    VelData=FCData{j,:,1};  % velocity data for this mouse
    FrzData=FCData{j,:,2}; % immobility data for this mouse

    for i=1:nDays % loop through sessions
    try
        % Unpack general information about experiment
        Info=FCData{j,i,3};       FPS=Info{1};    Day=Info{2};    Mouse=Info{3};
CSp=Info{4};    CSm=Info[105];
        CSpDur=Info{6};   CSmDur=Info{7};     Thresh=Info{8};     tCSp=Info{9};   tCSm=Info{10};

        % Unpack the immobility data for this mouse and this session
        FrzData=FCData{j,i,2};
        preCSpBouts=FrzData{1};
        CSpBouts=FrzData{2};
        preCSmBouts=FrzData{3};
        CSmBouts=FrzData{4};

        % loop to parse Freezing data by trial #
        for k=1:nTrials

            % Analyze the preCSp condition
            temp=preCSpBouts(preCSpBouts(:,1)==k,:); % temp holds immobility data for kth trial
of ith session for jth mouse
            [~, ia, ~] = unique(temp(:,2)); % ia holds indices of unique non-NaN data fragments
            Durs=temp(ia,3);  % Durs holds durations of all unique non-NaN data fragments
            % Dur holds sum of durations of all unique non-NaN data fragments >tW
            % (e.g. long enough that a bout of freezing could occur within it)
            Dur=sum(Durs(Durs>=tW));
            % P(i,k,j,1) holds the total proportion of time the animal spent freezing during the
kth trial of the ith session for the jth mouse during the preCSp condition.
            P(i,k,j,1)=sum(temp(temp(:,4)>=tW,4))/Dur; % sum all bouts of immobility >tW and
divide by total duration of non-NaN data.

            % Analyze the CSp condition, exactly as above
            temp=CSpBouts(CSpBouts(:,1)==k,:);
            [~, ia, ~] = unique(temp(:,2));
            Durs=temp(ia,3);
            Dur=sum(Durs(Durs>=tW));
            P(i,k,j,2)=sum(temp(temp(:,4)>=tW,4))/Dur;

            % Analyze the preCSm condition, exactly as above
            temp=preCSmBouts(preCSmBouts(:,1)==k,:);
            [~, ia, ~] = unique(temp(:,2));
            Durs=temp(ia,3);
            Dur=sum(Durs(Durs>=tW));
            P(i,k,j,3)=sum(temp(temp(:,4)>=tW,4))/Dur;

            % Analyze the CSm condition, exactly as above
            temp=CSmBouts(CSmBouts(:,1)==k,:);
            [~, ia, ~] = unique(temp(:,2));
            Durs=temp(ia,3);
            Dur=sum(Durs(Durs>=tW));
            P(i,k,j,4)=sum(temp(temp(:,4)>=tW,4))/Dur;

        end


        catch % catch errors arising from missing or misnamed files
            warning(strcat('data for mouse #', num2str(Mouse),' on session #', num2str(i), ' may
not be accessible'));
        end
    end
end

P=P*100; % multipy by 100 to convert proportion freezing to percent freezing

% P=(nDays,nTrials,nMice,nCons);

% The following code builds 2-dimensional arrays of data from the 4D
% dataset P, to be more suitable for statistical analysis and graphing.
```

```
GroupTrials=nan(nDays*nTrials,nMice*nCons); % For comparing the two experimental groups across
trials
GroupDays=nan(nDays,nMice*nCons); % For comparing the two experimental groups across sessions
for i=1:nDays
    for j=1:nCons
        GroupTrials((i-1)*nTrials+1:i*nTrials, (j-1)*nMice+1:j*nMice) = P(i,:,:,j);
        GroupDays(i,(j-1)*nMice+1:j*nMice) = nanmean(P(i,:,:,j),2);
    end
end

MouseDays=nan(nDays*nMice,nTrials*nCons); % For analyzing each mouse across sessions.
for i=1:nMice
    for j=1:nCons
        MouseDays((i-1)*nDays+1:i*nDays, (j-1)*nTrials+1:j*nTrials) = P(:,:,i,j);
    end
end

MouseTrials=nan(nDays*nTrials,nCons*nMice); % For analyzing each mouse across trials.
for i=1:nDays
    for j=1:nMice
        MouseTrials((i-1)*nTrials+1:i*nTrials, (j-1)*nCons+1:j*nCons) = P(i,:,j,:);
    end
end
```

d. "FCSorter" function:

This function sorts the calculated freezing data into organized arrays for direct import into Prism spreadsheets for further analysis.

```
function [GroupDays,GroupTrials] =
FCSorter(GroupDays1a,GroupDays2a,GroupDays1b,GroupDays2b,GroupTrials1a,GroupTrials2a,GroupTrials1
b,GroupTrials2b,SessionsA,SessionsB)

% This code reorganizes all the data to be amenable to graphing and analysis in Prism.
N1=size(GroupDays1a,2)/4; % size of control group
N2=size(GroupDays2a,2)/4; % size of experimental group
N=max(N1,N2); % Size of larger of two groups (if not equal).

GroupDaysA=nan(size(GroupDays1a,1), N*6); %
GroupTrialsA=nan(size(GroupTrials1a,1), N*6); %
GroupDaysB=nan(size(GroupDays1b,1), N*6); %
GroupTrialsB=nan(size(GroupTrials1b,1), N*6); %

GroupDaysA(:,0*N+1:0*N+N1)=GroupDays1a(:,1*N1+1:2*N1);
GroupDaysA(:,1*N+1:1*N+N2)=GroupDays2a(:,1*N2+1:2*N2);
GroupDaysA(:,2*N+1:2*N+N1)=GroupDays1a(:,3*N1+1:4*N1);
GroupDaysA(:,3*N+1:3*N+N2)=GroupDays2a(:,3*N2+1:4*N2);
GroupDaysA(:,4*N+1:4*N+N1)=GroupDays1a(:,0*N1+1:1*N1);
GroupDaysA(:,5*N+1:5*N+N2)=GroupDays2a(:,0*N2+1:1*N2);

GroupTrialsA(:,0*N+1:0*N+N1)=GroupTrials1a(:,1*N1+1:2*N1);
GroupTrialsA(:,1*N+1:1*N+N2)=GroupTrials2a(:,1*N2+1:2*N2);
GroupTrialsA(:,2*N+1:2*N+N1)=GroupTrials1a(:,3*N1+1:4*N1);
GroupTrialsA(:,3*N+1:3*N+N2)=GroupTrials2a(:,3*N2+1:4*N2);
GroupTrialsA(:,4*N+1:4*N+N1)=GroupTrials1a(:,0*N1+1:1*N1);
GroupTrialsA(:,5*N+1:5*N+N2)=GroupTrials2a(:,0*N2+1:1*N2);

GroupDaysB(:,0*N+1:0*N+N1)=GroupDays1b(:,1*N1+1:2*N1);
GroupDaysB(:,1*N+1:1*N+N2)=GroupDays2b(:,1*N2+1:2*N2);
GroupDaysB(:,2*N+1:2*N+N1)=GroupDays1b(:,3*N1+1:4*N1);
GroupDaysB(:,3*N+1:3*N+N2)=GroupDays2b(:,3*N2+1:4*N2);
GroupDaysB(:,4*N+1:4*N+N1)=GroupDays1b(:,0*N1+1:1*N1);
GroupDaysB(:,5*N+1:5*N+N2)=GroupDays2b(:,0*N2+1:1*N2);

GroupTrialsB(:,0*N+1:0*N+N1)=GroupTrials1b(:,1*N1+1:2*N1);
GroupTrialsB(:,1*N+1:1*N+N2)=GroupTrials2b(:,1*N2+1:2*N2);
```

```
GroupTrialsB(:,2*N+1:2*N+N1)=GroupTrials1b(:,3*N1+1:4*N1);
GroupTrialsB(:,3*N+1:3*N+N2)=GroupTrials2b(:,3*N2+1:4*N2);
GroupTrialsB(:,4*N+1:4*N+N1)=GroupTrials1b(:,0*N1+1:1*N1);
GroupTrialsB(:,5*N+1:5*N+N2)=GroupTrials2b(:,0*N2+1:1*N2);

GroupDays=nan(size(GroupDaysA,1)+size(GroupDaysB,1),N*6);
GroupTrials=[];
% GroupTrials=nan(size(GroupTrialsA,1)+size(GroupTrialsB,1),N*6);
AllSessions=sort([SessionsA SessionsB]);
nTrialsA=size(GroupTrialsA,1)/size(SessionsA,2);
nTrialsB=size(GroupTrialsB,1)/size(SessionsB,2);

for i=1:numel(AllSessions)
    S=AllSessions(i);
    if numel(find(SessionsA==S)) > 0
        Session=find(SessionsA==S);
        GroupDays(S,:)=GroupDaysA(Session,:);
        GroupTrials=[GroupTrials; GroupTrialsA((Session-1)*nTrialsA+1:Session*nTrialsA,:)];
    elseif numel(find(SessionsB==S)) > 0
        Session=find(SessionsB==S);
        GroupDays(S,:)=GroupDaysB(Session,:);
        GroupTrials=[GroupTrials; GroupTrialsB((Session-1)*nTrialsB+1:Session*nTrialsB,:)];
    else
        warning('FC data may not have sorted correctly.  Session #s for sessions of different
length must not overlap.');
    end
end
```

e. “FindFreezing2” function:

This is a secondary function executed by the “EthoReader3” function to determine the timing and duration of bouts of freezing for each mouse before and during CS presentations.

```
function FrzData=FindFreezing2(VelData,FPS,ThreshC)

% Immobility (velocity < ThreshC) determined before and during the CS+ and CS-.
% This will be used later to define the % of time the animal was freezing.
% FPS is frames per second.

% A lot of the code is dedicated to dealing with the problem of NaNs that
% occur in the data when Ethovision can't locate the animal in some frames.
% For some data this is not an issue but for other data it is.
% Bouts of continuous immobility are only assessed within "Fragments" of
% good (non-NaN) velocity data.

FragThresh=FPS*0; % minimum fragment size worth looking at (see below).  Set to 0 but could be
set to however many seconds one wants.
AllBouts=cell(size(VelData,1),1); % Initialize AllBouts to the same size as VelData (4x1
typically)

for k=1:size(VelData,1) % loop through the four experimental conditions (before/during CS+/CS-)
    Input=VelData{k}; % Velocity data for this condition (e.g. k=2 corresponds to velocity during
the CS+'s)
    dInput=(sign(Input(:,:,1)-ThreshC)); % sign of velocity - threshold ... +1 means mobile, -1
means immobile, 0 means at threshold
    for i=1:size(dInput,2) % loop through the individual trials (columns of matrix)
        temp=dInput(:,i); % velocity - threshold for the ith trial

        % The following code deals with fragmented velocity data resulting from frames in which
Ethovision did not locate the animal, resulting in NaNs
        Frags=zeros(size(temp,1),1); % Will hold Fragments of good (non-NaN) velocity data that
can be examined for bouts of immobility.
        u=1; % u is a counter
```

```
        while u<=size(temp,1) % while u is smaller than the length of the (velocity - threshold)
data vector
            v=0; % v will count up the length of this (potential) fragment
            while u+v<=size(temp,1) && ~isnan(temp(u+v,1)) % v will count up from u until u+v is
a NaN or u+v exceeds the length of the data vector
                v=v+1;
            end % when loop ends v is the length of the non-NaN fragment starting at temp(u,1),
or v is 0 if temp(u,1) was a nan in the first place
            Frags(u,1)=v; % Frags(u,1) holds the length (v) of a good (non-NaN) velocity data
fragment starting at temp(u,1).
            u=u+v+1; % bump the value of u up to the next element after u+v (recall,
temp(u:u+v,1) is the previous fragment)
        end
        % FragIndx(:,1) holds indices of the velocity - threshold data fragments.
        % FragIndx(:,2) holds their length (in samples).
        FragIndx=[find(Frags>FragThresh) Frags(Frags>FragThresh)];

        Bouts=[]; % Bouts will hold the timing and duration of bouts of immobility (velocity <
ThreshC)
        for w=1:size(FragIndx,1) % loop through the list of fragments
            Frag=temp(FragIndx(w,1):FragIndx(w,1)+FragIndx(w,2)-1,1); % Frag is the "wth"
fragment in its entirety
            u=1; % a new counter for a new while loop
            while u<=size(Frag,1) % while u is smaller than the length of the "wth" fragment
                v=0; % v will count up the length of this (potential) bout of immobility
                while u+v<=size(Frag,1) && Frag(u+v,1)<0 % v counts up from u while Frag(u+v,1)<0
(i.e. the animal is still immobile), until u+v reaches the length of Frag
                    v=v+1;
                end % when loop ends v is the length of a bout of immobility starting at
Frag(u,1), or v is 0 if the animal was moving at Frag(u,1).

                % Bouts(:,1) holds which fragment this is (1,2,...)
                % Bouts(:,2) holds the duration of this fragment in seconds
(frames/(frames/second)=seconds)
                % Bouts(:,3) holds the duration of this bout of immobility in seconds.
                Bouts=[Bouts; w size(Frag,1)/FPS v/FPS];
                u=u+v+1; % bump the value of u up to the next element after u+v
            end
        end

        % AllBouts{k}(:,1) holds trial number (e.g. 3 means 3rd presentation of the CS during
this session)
        % AllBouts{k}(:,2) holds which fragment of good data within the current trial this is
(1,2,...)
        % AllBouts{k}(:,3) holds durations (in seconds) of the fragments
        % AllBouts{k}(:,4) holds durations (in seconds) of bouts of immobility. Zeros mean the
animal was mobile
        AllBouts{k}=[AllBouts{k}; i*ones(size(Bouts,1),1) Bouts];
    end
end

FrzData=AllBouts;
```

2. Python script used to analyze projection patterns based on data from the Allen Mouse Connectivity Atlas.

```
# import pandas and NumPy functions- use Pandas to visualize and organize data tables, and NumPy
to build and calculate arrays functions for graphical analysis
# import all connectivity data in json file format

import pandas as pd
import numpy as np
import matplotlib.pyplot as plt
%matplotlib inline
from allensdk.core.mouse_connectivity_cache import MouseConnectivityCache
```

```
mcc = MouseConnectivityCache(manifest_file='/volumes/Brain2015/connectivity/manifest.json')


# open up a list of all of the experiments and ontology index

all_experiments = mcc.get_experiments(dataframe=True)
print "%d total experiments" % len(all_experiments)

ontology  = mcc.get_ontology()


# Filter by injections into the CeA of Cre-lines and display info in dataframe format

cea_id = ontology['CEA']['id']
filtered_experiments =
mcc.get_experiments(dataframe=True,cre=None,injection_structure_ids=cea_id)
print "There are %d experiments in my filtered experiment list" % len(filtered_experiments)


# Generate matrix containing filtered experiments using connectivity helper function (code below)

inj_matrix = chelp.generate_matrix( mcc, filtered_experiments, filtered_structures, [2],
                                          is_injection=True,
parameter='normalized_projection_volume')

m = inj_matrix['matrix'].copy()
m[np.isnan(m)] = 0
primary_injection_fraction = np.amax(m,1)

lab = inj_matrix['columns']['label'].values
primary_injection_label = lab[np.argmax(m,1)]

#only keep experiments above a containment threshold if desired (No containment threshold set for
CeA due to small size and restricted gene expression)

fraction_threshold = 0
experiment_mask = primary_injection_fraction > fraction_threshold
keep_experiments = filtered_experiments[experiment_mask]

print "Keeping %d experiments" % len(keep_experiments)

keep_experiments


# Filter by known CeA targets (i.e. BST, PAG, LC, CeA, MeA, PB)

from allensdk.api.queries.ontologies_api import OntologiesApi

filtered_structures = ontology['BST', 'PAG', 'LC', 'CEA', 'MEA', 'PB']
print "There are %d structures in my filtered structure list" % len(filtered_structures)


# Use connectivity helper to get values for normalized projection volumes

import connectivity_helper as chelp

data = chelp.generate_matrix( mcc, filtered_experiments, filtered_structures, [2],
                             is_injection=False, parameter='normalized_projection_volume')


# Build dataframe with filtered experiments for normalized projection volume

my_df = filtered_experiments.copy()

for row_index, row in data['columns'].iterrows():
    my_df[data['columns']['label'][row_index]] =
pd.Series(data['matrix'][:,row_index],index=my_df.index)


# Group experiments by target structure and then transgenic line
```

```
grouped = my_df.groupby(['structure-abbrev', 'transgenic-line'])
matrix = grouped.mean()
matrix_data = matrix.reset_index()
matrix_data


# Change dataframe values into an array--> need to do in order to plot with lightning function
(graphing tool developed by J. Freeman)

npv = matrix_data.iloc[:,4:].values


# Create dataframe containing all cre-lines--> did this in order to create a list of unique Cre-
lines to label columns in lightning

tl=matrix_data[['transgenic-line', 'id']]

tl_col=tl.groupby(['transgenic-line'])
tl_col1=tl_col.mean().reset_index()
tl_col1[tl_col1['transgenic-line']==''']= 'WT'
tl_col1


# Import "Lightning" graphing function and set size parameters

from lightning import Lightning
lgn = Lightning(ipython=True, local=True)
lgn.set_size('medium')


# Label rows by primary Cre-line

row_labels = ['WT', 'Crh (BL)', 'Crh (ZJH)', 'Erbb4', 'Etv1', 'Prkcd', 'Slc18a2', 'Tac2']


# Label columns by target structure acronym

column_labels = ['CEA-R', 'MEA-R', 'BST-R', 'PAG-R', 'PB-R', 'LC-R']


# Generate graph for normalized projection volumes (numbers = True will display calculated values
in figure)

matrix = npv
matrix = np.log10(matrix+1)
lgn.matrix(npv, row_labels=row_labels, column_labels=column_labels, numbers=True)


# Generate matrix of target structure volumes

tvol = chelp.generate_matrix( mcc, filtered_experiments, filtered_structures, [2],

                            is_injection=False, parameter='volume')

my_tvol = filtered_experiments.copy()

for row_index, row in tvol['columns'].iterrows():

    my_tvol[tvol['columns']['label'][row_index]] =
        pd.Series(tvol['matrix'][:,row_index],index=my_tvol.index)


# Group experiments by target structure and then trangenic line

grouped_tvol = my_tvol.groupby(['structure-abbrev', 'transgenic-line'])
matrix_tvol = grouped_tvol.mean()
matrix_data_tvol = matrix_tvol.reset_index()
matrix_data_tvol
```

```
# Generate NumPy matrix of target volumes for further calculation

tvol_arr = matrix_data_tvol.iloc[:,4:].values


# Import volumes of source structures and search for source of interest (i.e. CeA)

volumes = pd.DataFrame.from_csv('/volumes/Brain2015/connectivity/structure_volume.csv')

sources_id = [ ontology['CEA'].id.values]
sources_vol = [volumes.volume[a] for a in sources_id]
sources_vol


# Calculate normalized projection "density" by dividing the npv values by the target volumes and
multiplying the resultant values by the source volume (CeA = 0.61525 mm^3). The final array can be
directly imported to the graphing function

npd = np.divide(npv, tvol_arr)
npd_arr = npd* .61525
npd_arr


# Generate graph for npd as done for npv

matrix = npd_arr
matrix = np.log10(matrix+1)
lgn.matrix(npd_arr, row_labels=row_labels, column_labels=column_labels, numbers=True)
```

Helper function (written by L. Ng):

```
from allensdk.core.mouse_connectivity_cache import MouseConnectivityCache
import pandas as pd
import numpy as np

def generate_matrix( mcc, experiments_df, structures_df, hemisphere_ids = [2,1],
                                    is_injection=False, parameter='projection_volume') :

    # generate data matrix
    rm = get_raw_matrix( mcc, experiments_df.id.values, structures_df.id.values, hemisphere_ids,
                        is_injection, parameter )

    # make column frame
    hlabel = {1:'-L', 2:'-R', 3:''}
    tt = zip(rm['columns'][:,1], rm['columns'][:,0])
    clabels = [ structures_df.loc[s]['acronym'] + hlabel[h] for s,h in tt]

    col_df = pd.DataFrame({'structure_id':rm['columns'][:,1],
                           'hemisphere_id':rm['columns'][:,0],
                           'label': clabels} )

    output = {'matrix': rm['matrix'], 'columns':col_df }

    return output


def get_raw_matrix( mcc, experiment_ids, structure_ids, hemisphere_ids, is_injection, parameter):

    # multiple structure passing to get_structure_unionizes is not working
    # do my own filtering afterward
    su = mcc.get_structure_unionizes( experiment_ids, is_injection=is_injection )

    # structure filtering
    su = su[su['structure_id'].isin(structure_ids)]

    # hemisphere filtering
    su = su[su['hemisphere_id'].isin(hemisphere_ids)]
```

```
# create np.array
nrows = len(experiment_ids)
ncolumns = len(structure_ids) * len(hemisphere_ids)

pm = np.empty((nrows,ncolumns,))
pm[:] = np.NAN

# make lookup tables
row_lookup={}
for idx,e in enumerate(experiment_ids) :
    row_lookup[e] = idx

column_lookup={}
columns=np.empty((ncolumns,2),dtype=np.uint32)
columns[:] = np.NAN
cidx = 0
for hidx,h in enumerate(hemisphere_ids) :
    for sidx,s in enumerate(structure_ids) :
        column_lookup[(h,s)] = cidx
        columns[cidx,0] = h
        columns[cidx,1] = s
        cidx += 1

# loop through structure unionizes dataframe
for row_index, row in su.iterrows():
    rindx = row_lookup[row['experiment_id']]
    k = (row['hemisphere_id'],row['structure_id'])
    cindx = column_lookup[k]
    pm[rindx,cindx] = row[parameter]

return {'matrix':pm, 'rows':experiment_ids, 'columns':columns}
```

References:

1 Anderson, D. J. & Adolphs, R. A framework for studying emotions across species. *Cell* **157**, 187-200, doi:10.1016/j.cell.2014.03.003 (2014).

2 Tovote, P., Fadok, J. P. & Luthi, A. Neuronal circuits for fear and anxiety. *Nature reviews. Neuroscience* **16**, 317-331, doi:10.1038/nrn3945 (2015).

3 Duvarci, S. & Pare, D. Amygdala microcircuits controlling learned fear. *Neuron* **82**, 966-980, doi:10.1016/j.neuron.2014.04.042 (2014).

4 Janak, P. H. & Tye, K. M. From circuits to behaviour in the amygdala. *Nature* **517**, 284-292, doi:10.1038/nature14188 (2015).

5 Johansen, J. P., Cain, C. K., Ostroff, L. E. & LeDoux, J. E. Molecular mechanisms of fear learning and memory. *Cell* **147**, 509-524, doi:10.1016/j.cell.2011.10.009 (2011).

6 Ehrlich, I. *et al.* Amygdala inhibitory circuits and the control of fear memory. *Neuron* **62**, 757-771, doi:10.1016/j.neuron.2009.05.026 (2009).

7 Weiskrantz, L. Behavioral changes associated with ablation of the amygdaloid complex in monkeys. *Journal of comparative and physiological psychology* **49**, 381-391 (1956).

8 McDonald, A. J. Neurons of the lateral and basolateral amygdaloid nuclei: a Golgi study in the rat. *The Journal of comparative neurology* **212**, 293-312, doi:10.1002/cne.902120307 (1982).

9 McDonald, A. J. Immunohistochemical identification of gamma-aminobutyric acid-containing neurons in the rat basolateral amygdala. *Neuroscience letters* **53**, 203-207 (1985).

10 Romanski, L. M., Clugnet, M. C., Bordi, F. & LeDoux, J. E. Somatosensory and auditory convergence in the lateral nucleus of the amygdala. *Behavioral neuroscience* **107**, 444-450 (1993).

11 Rogan, M. T., Staubli, U. V. & LeDoux, J. E. Fear conditioning induces associative long-term potentiation in the amygdala. *Nature* **390**, 604-607, doi:10.1038/37601 (1997).

12 Krettek, J. E. & Price, J. L. A description of the amygdaloid complex in the rat and cat with observations on intra-amygdaloid axonal connections. *The Journal of comparative neurology* **178**, 255-280, doi:10.1002/cne.901780205 (1978).

13 Millhouse, O. E. The intercalated cells of the amygdala. *The Journal of comparative neurology* **247**, 246-271, doi:10.1002/cne.902470209 (1986).

14 Pare, D. & Smith, Y. The intercalated cell masses project to the central and medial nuclei of the amygdala in cats. *Neuroscience* **57**, 1077-1090 (1993).

15 Asede, D., Bosch, D., Luthi, A., Ferraguti, F. & Ehrlich, I. Sensory inputs to intercalated cells provide fear-learning modulated inhibition to the basolateral amygdala. *Neuron* **86**, 541-554, doi:10.1016/j.neuron.2015.03.008 (2015).

16 Busti, D. *et al.* Different fear states engage distinct networks within the intercalated cell clusters of the amygdala. *The Journal of neuroscience : the official journal of the Society for Neuroscience* **31**, 5131-5144, doi:10.1523/JNEUROSCI.6100-10.2011 (2011).

17 Likhtik, E., Popa, D., Apergis-Schoute, J., Fidacaro, G. A. & Pare, D. Amygdala intercalated neurons are required for expression of fear extinction. *Nature* **454**, 642-645, doi:10.1038/nature07167 (2008).

18 Wilensky, A. E., Schafe, G. E., Kristensen, M. P. & LeDoux, J. E. Rethinking the fear circuit: the central nucleus of the amygdala is required for the acquisition, consolidation, and expression of Pavlovian fear conditioning. *The Journal of neuroscience : the official journal of the Society for Neuroscience* **26**, 12387-12396, doi:10.1523/JNEUROSCI.4316-06.2006 (2006).

19 Keifer, O. P., Jr., Hurt, R. C., Ressler, K. J. & Marvar, P. J. The Physiology of Fear: Reconceptualizing the Role of the Central Amygdala in Fear Learning. *Physiology* **30**, 389-401, doi:10.1152/physiol.00058.2014 (2015).
20 Ciocchi, S. *et al.* Encoding of conditioned fear in central amygdala inhibitory circuits. *Nature* **468**, 277-282, doi:10.1038/nature09559 (2010).
21 Haubensak, W. *et al.* Genetic dissection of an amygdala microcircuit that gates conditioned fear. *Nature* **468**, 270-276, doi:10.1038/nature09553 (2010).
22 Penzo, M. A., Robert, V. & Li, B. Fear conditioning potentiates synaptic transmission onto long-range projection neurons in the lateral subdivision of central amygdala. *The Journal of neuroscience : the official journal of the Society for Neuroscience* **34**, 2432-2437, doi:10.1523/JNEUROSCI.4166-13.2014 (2014).
23 Penzo, M. A. *et al.* The paraventricular thalamus controls a central amygdala fear circuit. *Nature*, doi:10.1038/nature13978 (2015).
24 Li, H. *et al.* Experience-dependent modification of a central amygdala fear circuit. *Nature neuroscience* **16**, 332-339, doi:10.1038/nn.3322 (2013).
25 Cassell, M. D., Gray, T. S. & Kiss, J. Z. Neuronal architecture in the rat central nucleus of the amygdala: a cytological, hodological, and immunocytochemical study. *The Journal of comparative neurology* **246**, 478-499, doi:10.1002/cne.902460406 (1986).
26 Micevych, P., Akesson, T. & Elde, R. Distribution of cholecystokinin-immunoreactive cell bodies in the male and female rat: II. Bed nucleus of the stria terminalis and amygdala. *The Journal of comparative neurology* **269**, 381-391, doi:10.1002/cne.902690306 (1988).
27 Gustafson, E. L., Card, J. P. & Moore, R. Y. Neuropeptide Y localization in the rat amygdaloid complex. *The Journal of comparative neurology* **251**, 349-362, doi:10.1002/cne.902510306 (1986).
28 Joseph, S. A. & Knigge, K. M. Corticotropin releasing factor: immunocytochemical localization in rat brain. *Neuroscience letters* **35**, 135-141 (1983).
29 Weber, E. & Barchas, J. D. Immunohistochemical distribution of dynorphin B in rat brain: relation to dynorphin A and alpha-neo-endorphin systems. *Proceedings of the National Academy of Sciences of the United States of America* **80**, 1125-1129 (1983).
30 Bowers, M. E., Choi, D. C. & Ressler, K. J. Neuropeptide regulation of fear and anxiety: Implications of cholecystokinin, endogenous opioids, and neuropeptide Y. *Physiology & behavior* **107**, 699-710, doi:10.1016/j.physbeh.2012.03.004 (2012).
31 Davis, M., Walker, D. L., Miles, L. & Grillon, C. Phasic vs sustained fear in rats and humans: role of the extended amygdala in fear vs anxiety. *Neuropsychopharmacology : official publication of the American College of Neuropsychopharmacology* **35**, 105-135, doi:10.1038/npp.2009.109 (2010).
32 de Montigny, C. Cholecystokinin tetrapeptide induces panic-like attacks in healthy volunteers. Preliminary findings. *Archives of general psychiatry* **46**, 511-517 (1989).
33 Fekete, M., Szabo, A., Balazs, M., Penke, B. & Telegdy, G. Effects of intraventricular administration of cholecystokinin octapeptide sulfate ester and unsulfated cholecystokinin octapeptide on active avoidance and conditioned feeding behaviour of rats. *Acta physiologica Academiae Scientiarum Hungaricae* **58**, 39-45 (1981).
34 Kennedy, J. L. *et al.* Investigation of cholecystokinin system genes in panic disorder. *Molecular psychiatry* **4**, 284-285 (1999).
35 Wang, H., Wong, P. T., Spiess, J. & Zhu, Y. Z. Cholecystokinin-2 (CCK2) receptor-mediated anxiety-like behaviors in rats. *Neuroscience and biobehavioral reviews* **29**, 1361-1373, doi:10.1016/j.neubiorev.2005.05.008 (2005).

36 Wood, J. *et al.* Structure and function of the amygdaloid NPY system: NPY Y2 receptors regulate excitatory and inhibitory synaptic transmission in the centromedial amygdala. *Brain structure & function*, doi:10.1007/s00429-015-1107-7 (2015).
37 Tasan, R. O. *et al.* The role of Neuropeptide Y in fear conditioning and extinction. *Neuropeptides*, doi:10.1016/j.npep.2015.09.007 (2015).
38 Verma, D., Tasan, R. O., Herzog, H. & Sperk, G. NPY controls fear conditioning and fear extinction by combined action on Y(1) and Y(2) receptors. *British journal of pharmacology* **166**, 1461-1473, doi:10.1111/j.1476-5381.2012.01872.x (2012).
39 Vale, W., Spiess, J., Rivier, C. & Rivier, J. Characterization of a 41-residue ovine hypothalamic peptide that stimulates secretion of corticotropin and beta-endorphin. *Science* **213**, 1394-1397 (1981).
40 Regev, L., Tsoory, M., Gil, S. & Chen, A. Site-specific genetic manipulation of amygdala corticotropin-releasing factor reveals its imperative role in mediating behavioral response to challenge. *Biological psychiatry* **71**, 317-326, doi:10.1016/j.biopsych.2011.05.036 (2012).
41 Gafford, G. M. *et al.* Cell-type specific deletion of GABA(A)alpha1 in corticotropin-releasing factor-containing neurons enhances anxiety and disrupts fear extinction. *Proceedings of the National Academy of Sciences of the United States of America* **109**, 16330-16335, doi:10.1073/pnas.1119261109 (2012).
42 Nemeroff, C. B. *et al.* Elevated concentrations of CSF corticotropin-releasing factor-like immunoreactivity in depressed patients. *Science* **226**, 1342-1344 (1984).
43 Binder, E. B. & Nemeroff, C. B. The CRF system, stress, depression and anxiety-insights from human genetic studies. *Molecular psychiatry* **15**, 574-588, doi:10.1038/mp.2009.141 (2010).
44 Sawchenko, P. E. & Swanson, L. W. Localization, colocalization, and plasticity of corticotropin-releasing factor immunoreactivity in rat brain. *Federation proceedings* **44**, 221-227 (1985).
45 Refojo, D. *et al.* Glutamatergic and dopaminergic neurons mediate anxiogenic and anxiolytic effects of CRHR1. *Science* **333**, 1903-1907, doi:10.1126/science.1202107 (2011).
46 Swerdlow, N. R., Britton, K. T. & Koob, G. F. Potentiation of acoustic startle by corticotropin-releasing factor (CRF) and by fear are both reversed by alpha-helical CRF (9-41). *Neuropsychopharmacology : official publication of the American College of Neuropsychopharmacology* **2**, 285-292 (1989).
47 Sanz, E. *et al.* Cell-type-specific isolation of ribosome-associated mRNA from complex tissues. *Proceedings of the National Academy of Sciences of the United States of America* **106**, 13939-13944, doi:10.1073/pnas.0907143106 (2009).
48 Oh, S. W. *et al.* A mesoscale connectome of the mouse brain. *Nature* **508**, 207-214, doi:10.1038/nature13186 (2014).
49 Bliss, T. V. & Collingridge, G. L. A synaptic model of memory: long-term potentiation in the hippocampus. *Nature* **361**, 31-39, doi:10.1038/361031a0 (1993).
50 Citri, A. & Malenka, R. C. Synaptic plasticity: multiple forms, functions, and mechanisms. *Neuropsychopharmacology : official publication of the American College of Neuropsychopharmacology* **33**, 18-41, doi:10.1038/sj.npp.1301559 (2008).
51 Byth, L. A. Ca(2+)- and CaMKII-mediated processes in early LTP. *Annals of neurosciences* **21**, 151-153, doi:10.5214/ans.0972.7531.210408 (2014).
52 Abraham, W. C. & Williams, J. M. LTP maintenance and its protein synthesis-dependence. *Neurobiology of learning and memory* **89**, 260-268, doi:10.1016/j.nlm.2007.10.001 (2008).
53 Malinow, R. & Malenka, R. C. AMPA receptor trafficking and synaptic plasticity. *Annual review of neuroscience* **25**, 103-126, doi:10.1146/annurev.neuro.25.112701.142758 (2002).
54 Kauer, J. A. & Malenka, R. C. Synaptic plasticity and addiction. *Nature reviews. Neuroscience* **8**, 844-858, doi:10.1038/nrn2234 (2007).

55 Fu, Y. *et al.* Long-term potentiation (LTP) in the central amygdala (CeA) is enhanced after prolonged withdrawal from chronic cocaine and requires CRF1 receptors. *Journal of neurophysiology* **97**, 937-941, doi:10.1152/jn.00349.2006 (2007).

56 Pollandt, S. *et al.* Cocaine withdrawal enhances long-term potentiation induced by corticotropin-releasing factor at central amygdala glutamatergic synapses via CRF, NMDA receptors and PKA. *The European journal of neuroscience* **24**, 1733-1743, doi:10.1111/j.1460-9568.2006.05049.x (2006).

57 Kim, J. C. *et al.* Linking genetically defined neurons to behavior through a broadly applicable silencing allele. *Neuron* **63**, 305-315, doi:10.1016/j.neuron.2009.07.010 (2009).

58 Pologruto, T. A., Yasuda, R. & Svoboda, K. Monitoring neural activity and [Ca2+] with genetically encoded Ca2+ indicators. *The Journal of neuroscience : the official journal of the Society for Neuroscience* **24**, 9572-9579, doi:10.1523/JNEUROSCI.2854-04.2004 (2004).

59 Yuste, R., Peinado, A. & Katz, L. C. Neuronal domains in developing neocortex. *Science* **257**, 665-669 (1992).

60 Svoboda, K., Denk, W., Kleinfeld, D. & Tank, D. W. In vivo dendritic calcium dynamics in neocortical pyramidal neurons. *Nature* **385**, 161-165, doi:10.1038/385161a0 (1997).

61 Stosiek, C., Garaschuk, O., Holthoff, K. & Konnerth, A. In vivo two-photon calcium imaging of neuronal networks. *Proceedings of the National Academy of Sciences of the United States of America* **100**, 7319-7324, doi:10.1073/pnas.1232232100 (2003).

62 Baird, G. S., Zacharias, D. A. & Tsien, R. Y. Circular permutation and receptor insertion within green fluorescent proteins. *Proceedings of the National Academy of Sciences of the United States of America* **96**, 11241-11246 (1999).

63 Chen, T. W. *et al.* Ultrasensitive fluorescent proteins for imaging neuronal activity. *Nature* **499**, 295-300, doi:10.1038/nature12354 (2013).

64 Akerboom, J. *et al.* Optimization of a GCaMP calcium indicator for neural activity imaging. *The Journal of neuroscience : the official journal of the Society for Neuroscience* **32**, 13819-13840, doi:10.1523/JNEUROSCI.2601-12.2012 (2012).

65 Akerboom, J. *et al.* Genetically encoded calcium indicators for multi-color neural activity imaging and combination with optogenetics. *Frontiers in molecular neuroscience* **6**, 2, doi:10.3389/fnmol.2013.00002 (2013).

66 Botta, P. *et al.* Regulating anxiety with extrasynaptic inhibition. *Nature neuroscience* **18**, 1493-1500, doi:10.1038/nn.4102 (2015).

67 Gore, B. B., Soden, M. E. & Zweifel, L. S. Visualization of plasticity in fear-evoked calcium signals in midbrain dopamine neurons. *Learning & memory* **21**, 575-579, doi:10.1101/lm.036079.114 (2014).

68 Vincent, P. *et al.* Live imaging of neural structure and function by fibred fluorescence microscopy. *EMBO reports* **7**, 1154-1161, doi:10.1038/sj.embor.7400801 (2006).

69 Veinante, P. & Freund-Mercier, M. J. Intrinsic and extrinsic connections of the rat central extended amygdala: an in vivo electrophysiological study of the central amygdaloid nucleus. *Brain research* **794**, 188-198 (1998).

70 Martina, M., Royer, S. & Pare, D. Physiological properties of central medial and central lateral amygdala neurons. *Journal of neurophysiology* **82**, 1843-1854 (1999).

71 Moga, M. M. & Gray, T. S. Evidence for corticotropin-releasing factor, neurotensin, and somatostatin in the neural pathway from the central nucleus of the amygdala to the parabrachial nucleus. *The Journal of comparative neurology* **241**, 275-284, doi:10.1002/cne.902410304 (1985).

72 Makino, S., Gold, P. W. & Schulkin, J. Corticosterone effects on corticotropin-releasing hormone mRNA in the central nucleus of the amygdala and the parvocellular region of the paraventricular nucleus of the hypothalamus. *Brain research* **640**, 105-112 (1994).
73 Gafford, G., Jasnow, A. M. & Ressler, K. J. Grin1 receptor deletion within CRF neurons enhances fear memory. *PloS one* **9**, e111009, doi:10.1371/journal.pone.0111009 (2014).
74 Flandreau, E. I., Ressler, K. J., Owens, M. J. & Nemeroff, C. B. Chronic overexpression of corticotropin-releasing factor from the central amygdala produces HPA axis hyperactivity and behavioral anxiety associated with gene-expression changes in the hippocampus and paraventricular nucleus of the hypothalamus. *Psychoneuroendocrinology* **37**, 27-38, doi:10.1016/j.psyneuen.2011.04.014 (2012).
75 Pitts, M. W. & Takahashi, L. K. The central amygdala nucleus via corticotropin-releasing factor is necessary for time-limited consolidation processing but not storage of contextual fear memory. *Neurobiology of learning and memory* **95**, 86-91, doi:10.1016/j.nlm.2010.11.006 (2011).
76 de Jongh, R., Groenink, L., van der Gugten, J. & Olivier, B. Light-enhanced and fear-potentiated startle: temporal characteristics and effects of alpha-helical corticotropin-releasing hormone. *Biological psychiatry* **54**, 1041-1048 (2003).
77 Han, S., Soleiman, M. T., Soden, M. E., Zweifel, L. S. & Palmiter, R. D. Elucidating an Affective Pain Circuit that Creates a Threat Memory. *Cell* **162**, 363-374, doi:10.1016/j.cell.2015.05.057 (2015).
78 Sternson, S. M. & Roth, B. L. Chemogenetic tools to interrogate brain functions. *Annual review of neuroscience* **37**, 387-407, doi:10.1146/annurev-neuro-071013-014048 (2014).
79 Baldi, E., Lorenzini, C. A. & Bucherelli, C. Footshock intensity and generalization in contextual and auditory-cued fear conditioning in the rat. *Neurobiology of learning and memory* **81**, 162-166, doi:10.1016/j.nlm.2004.02.004 (2004).
80 Ghosh, S. & Chattarji, S. Neuronal encoding of the switch from specific to generalized fear. *Nature neuroscience* **18**, 112-120, doi:10.1038/nn.3888 (2015).
81 McCall, J. G. *et al.* CRH Engagement of the Locus Coeruleus Noradrenergic System Mediates Stress-Induced Anxiety. *Neuron* **87**, 605-620, doi:10.1016/j.neuron.2015.07.002 (2015).
82 Gewirtz, J. C. & Davis, M. Application of Pavlovian higher-order conditioning to the analysis of the neural substrates of fear conditioning. *Neuropharmacology* **37**, 453-459 (1998).
83 Bonfiglio, J. J. *et al.* The corticotropin-releasing hormone network and the hypothalamic-pituitary-adrenal axis: molecular and cellular mechanisms involved. *Neuroendocrinology* **94**, 12-20, doi:10.1159/000328226 (2011).
84 Salinas, E. & Thier, P. Gain modulation: a major computational principle of the central nervous system. *Neuron* **27**, 15-21 (2000).
85 Radulovic, J., Sydow, S. & Spiess, J. Characterization of native corticotropin-releasing factor receptor type 1 (CRFR1) in the rat and mouse central nervous system. *Journal of neuroscience research* **54**, 507-521 (1998).
86 Williams, C. L., Buchta, W. C. & Riegel, A. C. CRF-R2 and the heterosynaptic regulation of VTA glutamate during reinstatement of cocaine seeking. *The Journal of neuroscience : the official journal of the Society for Neuroscience* **34**, 10402-10414, doi:10.1523/JNEUROSCI.0911-13.2014 (2014).
87 Beckstead, M. J. *et al.* CRF enhancement of GIRK channel-mediated transmission in dopamine neurons. *Neuropsychopharmacology : official publication of the American College of Neuropsychopharmacology* **34**, 1926-1935, doi:10.1038/npp.2009.25 (2009).
88 Nie, Z. *et al.* Ethanol augments GABAergic transmission in the central amygdala via CRF1 receptors. *Science* **303**, 1512-1514, doi:10.1126/science.1092550 (2004).

89 Izumi, T. *et al.* Effect of the selective CCKB receptor antagonist LY288513 on conditioned fear stress in rats. *European journal of pharmacology* **300**, 25-31 (1996).
90 Raud, S. *et al.* Targeted invalidation of CCK2 receptor gene induces anxiolytic-like action in light-dark exploration, but not in fear conditioning test. *Psychopharmacology* **181**, 347-357, doi:10.1007/s00213-005-2255-x (2005).
91 Jasnow, A. M., Ressler, K. J., Hammack, S. E., Chhatwal, J. P. & Rainnie, D. G. Distinct subtypes of cholecystokinin (CCK)-containing interneurons of the basolateral amygdala identified using a CCK promoter-specific lentivirus. *Journal of neurophysiology* **101**, 1494-1506, doi:10.1152/jn.91149.2008 (2009).
92 Chung, L. & Moore, S. D. Cholecystokinin enhances GABAergic inhibitory transmission in basolateral amygdala. *Neuropeptides* **41**, 453-463, doi:10.1016/j.npep.2007.08.001 (2007).
93 McDonald, A. J. & Pearson, J. C. Coexistence of GABA and peptide immunoreactivity in non-pyramidal neurons of the basolateral amygdala. *Neuroscience letters* **100**, 53-58 (1989).
94 Heilig, M. Antisense inhibition of neuropeptide Y (NPY)-Y1 receptor expression blocks the anxiolytic-like action of NPY in amygdala and paradoxically increases feeding. *Regulatory peptides* **59**, 201-205 (1995).
95 Bannon, A. W. *et al.* Behavioral characterization of neuropeptide Y knockout mice. *Brain research* **868**, 79-87 (2000).
96 Callaway, E. M. & Luo, L. Monosynaptic Circuit Tracing with Glycoprotein-Deleted Rabies Viruses. *The Journal of neuroscience : the official journal of the Society for Neuroscience* **35**, 8979-8985, doi:10.1523/JNEUROSCI.0409-15.2015 (2015).
97 Lammel, S., Ion, D. I., Roeper, J. & Malenka, R. C. Projection-specific modulation of dopamine neuron synapses by aversive and rewarding stimuli. *Neuron* **70**, 855-862, doi:10.1016/j.neuron.2011.03.025 (2011).
98 Beier, K. T. *et al.* Circuit Architecture of VTA Dopamine Neurons Revealed by Systematic Input-Output Mapping. *Cell* **162**, 622-634, doi:10.1016/j.cell.2015.07.015 (2015).
99 Cai, H., Haubensak, W., Anthony, T. E. & Anderson, D. J. Central amygdala PKC-delta(+) neurons mediate the influence of multiple anorexigenic signals. *Nature neuroscience* **17**, 1240-1248, doi:10.1038/nn.3767 (2014).
100 Madisen, L. *et al.* Transgenic mice for intersectional targeting of neural sensors and effectors with high specificity and performance. *Neuron* **85**, 942-958, doi:10.1016/j.neuron.2015.02.022 (2015).
101 Taniguchi, H. *et al.* A resource of Cre driver lines for genetic targeting of GABAergic neurons in cerebral cortex. *Neuron* **71**, 995-1013, doi:10.1016/j.neuron.2011.07.026 (2011).
102 Gore, B. B., Soden, M. E. & Zweifel, L. S. Manipulating gene expression in projection-specific neuronal populations using combinatorial viral approaches. *Current protocols in neuroscience / editorial board, Jacqueline N. Crawley ... [et al.]* **4**, 4 35 31-34 35 20, doi:10.1002/0471142301.ns0435s65 (2013).
103 Franklin, K. B. J. & Paxinos, G. *Paxinos and Franklin's The mouse brain in stereotaxic coordinates*. Fourth edition. edn.
104 Davey, N. J., Ellaway, P. H. & Stein, R. B. Statistical limits for detecting change in the cumulative sum derivative of the peristimulus time histogram. *Journal of neuroscience methods* **17**, 153-166 (1986).
105 American Psychiatric Association. & American Psychiatric Association. DSM-5 Task Force. *Diagnostic and statistical manual of mental disorders : DSM-5*. 5th edn, (American Psychiatric Association, 2013).

Vita

Christina Akiko Sanford (Akers) was born and raised in Oxnard, CA. She later moved to Vancouver, WA and graduated from Fort Vancouver High School. Christina received her B.S. in Neurobiology from the University of Washington in 2006. During her undergraduate studies, she worked with Dr. Jeremy Clark in Dr. Ilene Bernstein's laboratory in the Department of Psychology studying the cross-sensitization of salt appetite and drugs of abuse. She later went on to work as a technician and manager for over four years in the laboratory of Dr. Paul Phillips in the Psychiatry and Behavioral Sciences Department at the University of Washington. Under Dr. Phillips' mentorship, Christina contributed to a number of projects examining phasic dopamine release during motivated behaviors using fast-scan cyclic voltammetry at chronically implanted carbon fiber microelectrodes. In 2011, she began her graduate studies in the Pharmacology program at the University of Washington working under the mentorship of Dr. Larry S. Zweifel. Christina received her doctorate degree in February of 2016.